POLYTECHNIC OF TURIN

Master of science program Biomedical engineering

Master Thesis in Biomedical instrumentation

Mixed-Signal Readout for Potentiometric and Potentiostatic Measurements on a Single Platform and Realization of Lactate and Li^+ sensors.

Lucia Lobello

Supervisors:
Prof. Danilo Demarchi
Prof. Sandro Carrara

Academic Year 2017-2018

A mio padre e mia madre

Abstract

This thesis presents the design and the implementation of a wearable bio-electronic system for the monitoring of athletes under physical efforts.
The realized electronic board has been printed on a flexible substrate and is interfaced with electrochemical sensors for ions and metabolites detection. The hardware combines potentiostatic and potentiometric circuitry on the same platform, enabling both amperometric and *Open Circuit Potential* (OCP). Four multiplexed sensing channels are available: two for amperometries and two for potentiometries.
Further, an investigation on sensing platforms for lactate and lithium detection in sweat has presented in the this work. Lactate and lithium have been chosen as metabolite and ion models, respectively. Indeed, they can provide important information on the athlete's health status during the training. The optimum electrochemical detection was achieved with functionalized Pt *Screen Printed Electrodes* (SPE). In case of lactate detection a Nafion membrane and Lactate Oxidase (LOD) enzyme have been deposited on the working electrode's area, while Au and Pt nanostructures have been employed for lithium sensing. The best Limits of detection for both lactate and lithium detection are $2.46mM$ and $1.28 \cdot 10^{-5}M$, respectively.
The wearability and the portability of the system are ensured by the flexibility of the substrate, the small dimensions that fit in an armband case, and the wireless transmission through *Bluetooth Low Energy* (BLE) module. A graphical interface (implemented with *Matlab 2017a*) enriches the system to allow the user to easy interact with the system. The power consumption of the system has been evaluated to be 200 mW, with a rechargeable battery coin cell, which ensure a 3.6 V power supply.

Sommario

Questa tesi presenta la progettazione e l'implementazione di un sistema elettronico indossabile per applicazioni bio, in grado di monitorare le performance di un atleta durante uno sforzo fisico.
Il circuito elettronico realizzato è stato stampato su un substrato flessibile e interfaccia sensori elettrochimici per la rilevazione di ioni e metaboliti. L'hardware combina i due circuiti per Amperometria e Potenziometria sulla medesima piattaforma, rendendo possibili misure di corrente e di potenziale contemporaneamente. Sono disponibili quattro diversi canali per effettuare le misure, due per le amperometrie e due per le potenziometrie.
Inoltre, in questo lavoro è presente anche lo studio e l'implementazione di sensori per rilevare la concentrazione di lattato e litio nel sudore, essendo questi ultimi scelti come modelli di metabolita e di ione, rispettivamente. La migliore misura elettrochimica è stata ottenuta con un elettrodo in Platino, stampato su un substrato ceramico funzionalizzato. Nel caso del lattato, è stata depositata sull'area dell'elettrodo una membrana di Nafion e successivamente l'enzima Lattato Ossidasi; mentre, per rendere tale elettrodo sensibile alle concentrazioni di litio nel sudore ,sono state depositate nanostruttute in Oro e Platino sul WE. I limiti di sensibilità ottimali per entrambe le misure sono $2.46mM$ e $1.28 \cdot 10^{-5}M$, rispettivamente per lattato e litio. L'indossabilità e la portabilità del sistema sono assicurati dalla flessibilità del substrato, dalle sue piccole dimensioni che permettono di integrarlo in un accessorio sportivo di uso comune da applicare al braccio (armband) e dalla trasmissione wireless attraverso un dispositivo Bluetooth a bassa energia. Un'interfaccia grafica (implementata con *Matlab 2017a*) completa il sistema e permette all'utente di interagire in modo semplice e immediato. Il consumo del dispositivo è stato elettricamente valutato essere di 200 mW, con una batteria ricaricabile, che assicura un'alimentazione di 3.6 V.

Contents

List of Figures

List of Tables

List of Abbreviations

WE	Working Electrode
RE	Reference Electrode
CE	Counter Electrode
CV	Cyclic Voltammetry
DPV	Differential Pulse Voltammetry
CA	ChronoAmperometry
SCE	Saturated Calomel Electrode
TIA	Trans-Impedance Amplifier
OCP	Open-Circuit Potential
ADC	Analog-to-Digital-Converter
LOD	Limit of Detection
DAC	Digital-to-Analog-Converter
FPCB	Flexible Printed Circuit Board
LPF	low-pass filter
SPI	Serial Peripheral Interface
UART	Universal Asynchronous Receiver-Transmitter
TWI	Two-Wire Interface
I2C	Inter Integrated Circuit
RISC	Reduced Instruction Set Computer
MOSI	Maste Out Slave In

MISO Master In Slave Out

SCL Serial Clock Line

SDA Serial Data Line

CPU Central Processing Unit

IC Integrated Circuit

LSB Least Significant Bit

TC Timer/Counters

CMOS Complementary Metal-Oxide Semiconductor

LDO Low Drop Regulator

BR Basic Rate

EDR Enhanced Data Rate

LE Low Energy

GUI Graphical User Interface

RF Radio Frequency

IA Instrumentation Amplifier

CMRR Common-Mode Rejection Ratio

DDA Differential Difference Amplifier

FPGA Field Programmable Gate Array

FISA Flexible Integrated Sensing Array

HPLC High Performance Liquid Chromatography

PSRR Power Supply Rejection Ratio

SPP Serial Port Profile

GATT Generic Attribute Profile

SPE Screen Printed Electrode

PBS Phosphate Buffered Saline

SNR Signal to Noise Ratio

CRC Current Reversal Chronopotentiometry

Chapter 1

Introduction

Wearable sensors have received great interest in the recent years especially in the field of personalized diagnosis and health-care tracking [4]. One of the major field where these innovative devices are employed is in sport applications [26]. This is due to the fact that some biological and physiological parameters need to be continuously monitored to evaluate fatigue and health status of the athletes undergoing physical efforts. Furthermore, since mental disorders (e.g. meticulous attention to diet, relative hyperactivity) are very common among sportive subjects, high attention has to be paid on the dosage of mood stabilizer, which are largely administered [79].
In order to realize comfort-to-use devices, in the last two decades, there have been a large investigation of engineering portable devices characterized by different geometries, sizes and materials [9].
Some important parameters that are interesting to be monitored to deduce information about the subject's health-conditions and first symptoms of a disorders are: endogenous compounds, e.g. lactate and glucose [78], [67], [93], [85], and ions, e.g. Na^+, K^+ and Cl^- ([93], [83], [87]). The endogenous compounds reveal the status of the metabolism of the organism, while ions give indication of the body hydration, heat-stress, bone mineral, etc.

All these compounds change their concentration depending on the body fluids where they are detected: (i) blood, (ii) saliva, (ii) urine or (iv) skin excretion, such as sweat. The sweat can be defined as an optimal fluid where to monitor metabolites and ions since it is non-invasive, on the contrary of blood that requires the insertion of catheters or the use of an implantable sensor [7].
In sport-science applications sweat is definitively convenient since it is naturally produced during physical exercises and trainings.

Towards this application, the endogenous metabolite lactate and the ion lithium can be chosen as target analytes to monitor not only the fatigue during the physical effort, but also to reveal the health-status of the athlete. Indeed, high attention has to be paid also on possible symptoms caused by mental disorders, which are widely spread

among sport competitors, such as meticulous attention to diet, hyperactivity or even bipolarism, manic and depressive episodes [79].

Lactate production is strictly related with the anaerobic metabolism of glucose that plays a fundamental role in human energy process. While performing physical efforts an accumulation of lactate in muscle cells happens and has to be monitored to avoid adverse consequences, such as acidosis.

On the other hand, lithium (Li^+) is a widely used mood stabilizer to treat psychiatric disorders. A constant monitor of lithium levels in sweat is of crucial importance to dose this treatment in a proper manner avoiding side effects and toxicity [34].

Considering the importance of these two compounds, a wearable device able to simultaneously detect these two concentrations in sweat can be an important step towards better and enhanced sport performances while ensuring proper health conditions of the athlete.

Main objective of this thesis is to develop a wearable system for the electrochemical detection of lithium and lactate in sweat. The system includes a flexible electronics, able to perform potentiostatic and potentiometric measurements, and optimized electrochemical sensors for lactate and lithium sensing.
The design, the realization and the in-vitro realization of all the parts of the system are presented in the following Chapters. The combination of a wireless connection (Bluetooth Low-Energy), wearability, substrate flexibility, small dimensions (to fit in commercially-available armband cases) and low-power consumption are key factors that we have considered during the device realization process.

Chapter 2

Theoretical Background

2.1 Electrochemical Biosensor

In the past two decades, biosensors have been largely improved and exploited for measuring biochemical phenomen with great influence in medical and biotechnological applications. Indeed, the main purspose of a biosensor is to convert a biological process into a quantifiable and processable signal. It detects the presence of a specific target sample in a physical system, producing a signal proportional to the specific analyte concentration. A typical biosensor comprises two main elements, as sketched in Fig. 2.1: (i) a bio-receptor and (ii) a transducer. The first is involved in the identification of the analyte through a specific chemical binding or reaction, the second converts the chemical signal into a measurable electrical signal.

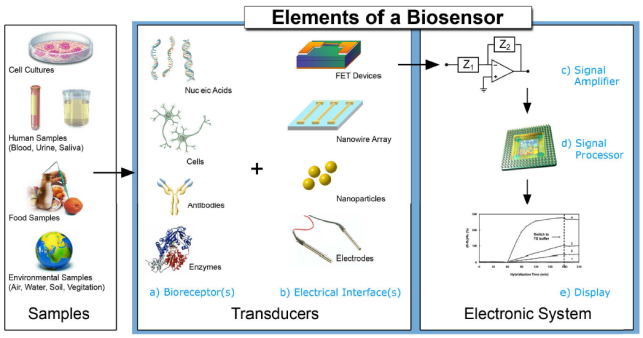

Figure 2.1: Sketch of the main elements comprising a typical biosensor. (Reprinted by [33].)

The detection process happens inside a sample solutions, which can be cell culture media, food solutions, body fluids or other environment samples. As soon as the analyte reaches the biosensor's surface, the chemical reaction happens and the detection process starts. The chemical signal is then converted in an electrical measurable signal that needs a dedicated electronic system to be read out. The read-out circuit normally amplifies the signal, processes it and then sends the resulting data to the final user.

Main features that a biosensor has to provide are [15]:

- *Specificity*: the bioreceptor has to be selective for the specific analyte to prevent the interference by other substances;
- *Stability*: the biosensor has to be stable during all its operation time;
- *Resolution*: is the smallest incremental change of input parameter that can be detected in the output signal;
- *Accuracy*: the biosensor's responce has to be accurate, this means that the measured value of the sensor has to be close to the actual values (value measured by a good standard);
- *Sensitivity*: is defined as the slope of the output characteristic curve (DY/DX in Fig. 2.2). In other words, it is defined as an output current or voltage change for a given change in input analyte's concentration;

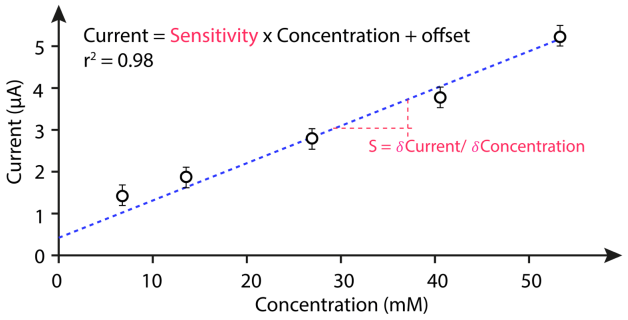

Figure 2.2: An example of calibration line for a sensor.

- *Precision*: is the degree of reproducibility of a measurement. In an ideal situation, if a measurement is repeated for several times, the output would be the same every time. A real sensor has an output values distributed in some manner relative to the actual correct value;
- *Offset*: is the error visible when, for example, under stardand condition, the output value of the sensor should be zero. For the sensitivy slope this means, infact, that it crosses the Y-axis not in zero but at different value;
- *Bio-compatibility*: a biosensor, especially if adopted for invasive monitoring, has to not produce toxic or antigenic effects [29].

In general, what makes biosensors so attractive is that they are a cheap, portable and easy-to-use solution for bio-sensing applications [33].

The bionsensors can be classified according to different parameters [10]: (i) the transduction element, or (ii) the measurement technique, (iii) or the target application, (iv) or the recognition element and its immobilization technique. Some example are schematically reported in Fig. 2.3.

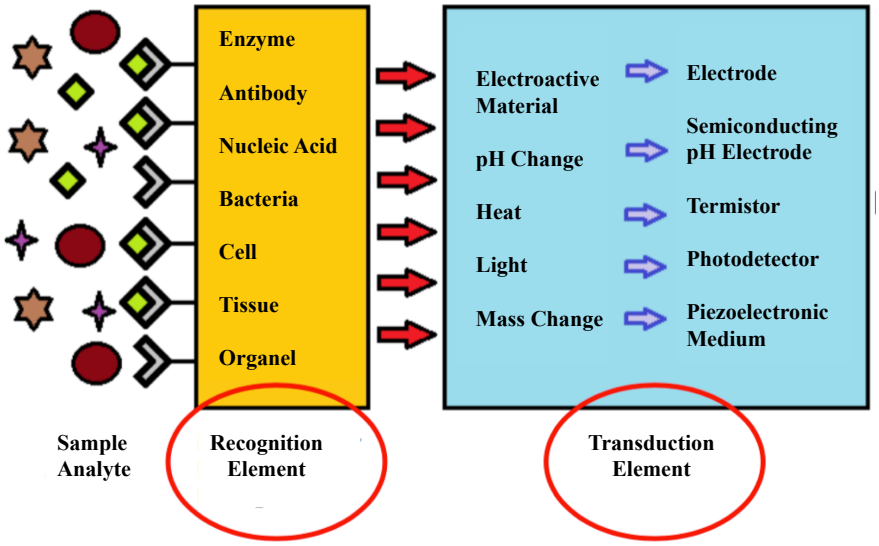

Figure 2.3: Classification of biosensors on dipending of different parameters (Reprinted by [97]).

The present thesis is focused on the electrochemical transduction method. In this kind of sensors, an oxidation/reduction occurs at the electrode, transducer, during this chemical reaction, electrodes are exchanged between the transducer and the analyte, hence the chemical event is converted in an electrical signal. It can be distinguished between *direct electrochemistry* where the analyte reacts on the electrode's surface without the need of an intermediary species, or the electrode can be functionalized with a specific recognition element [19]. In this case, a specific reagent is immobilized on the electrode's surface to improve the contact between the bioreceptor and the electrode [96].

2.1.1 Electrochemistry

Electrochemistry is the branch of chemistry which focuses on the inter-relation between a chemical reaction and an electrical signal, as a measurable and quantitative phenomenon. In other words, it comprises a wide number of analytical techniques that use a measurable signal, as potential, charge-accumulation, or current, to obtain information about a chemical analyte, *e.g.* its concentration and/or its chemical reactivity [37].
In general, when the sensor surface interfaces with a conductive solution, an inter-

face, with accumulated ions between the surface and the solution, occurs. Figure 2.4 schematically represents the phenomenon at the electrode-electrolyte interface.

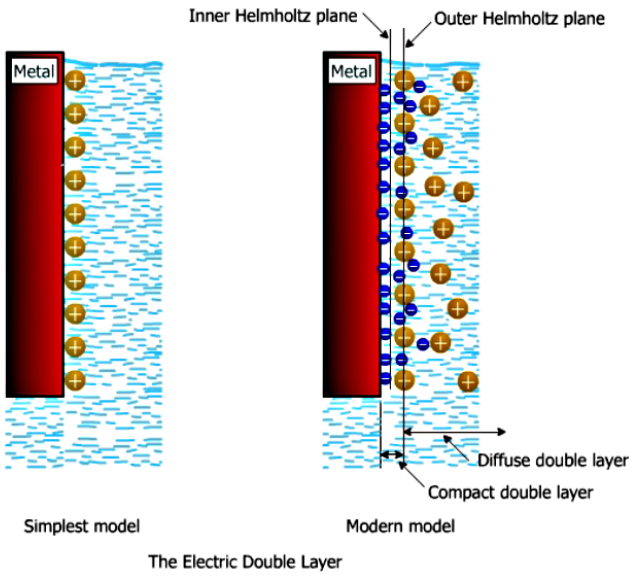

Figure 2.4: *Helmoltz planes* at the electrode surface dipped in a conductive solution Reprinted by [35]).

When an electrode is charged, it becomes an attractive source for the ions in the solution [31]: the type of binding and the attractive forces change if increasing the distance from the electrode's surface. Accordingly to the Hermann von Helmholtz theory, it is possible to recognize different layers, called *Helmoltz layers*.

- The first layer is called *inner Helmoltz layer*. It includes the ions that are very close to the electrical interface.
- Beyond the first one, the second layer is called *outer Helmoltz layer*. It contains ions that are surrounded by conductive solution's molecules and cannot stay close the electrode.
- The last region is called *diffusion double layer*. It completes the interface and includes the less interactive ions.

Once the ions interact with the polarized electrodes, then *RedOx reactions* occur. With the term *RedOx reaction* we refer to the chemical **re**duction-**ox**idation reaction characterized by an exchange of electrons from one species to the other [80]. The electrons flow is the signal that is detected and then measured and transmitted.
By definition:

- *Oxidation* is a chemical reaction in which chemical species lose electrons:

$$H_2 \longrightarrow 2\,H^+ + 2\,e^-$$

- *Reduction* is a chemical reaction in which chemical species gain electrons:

$$F_2 + 2\,e^- \longrightarrow 2\,F^-$$

The involved chemical species are called *oxidized* and *reduced*, respectively H_2 and F_2 in the reported example.
The RedOx reaction occurs at the electrode's interface and the direction of the electron exchange depends on the polarization of the electrode (Figure 2.5): if it is negatively charged, *e.g.* cathode, it attracts the positively charged protons; while if it is positively charged, *e.g.* anode, it releases the electrons.

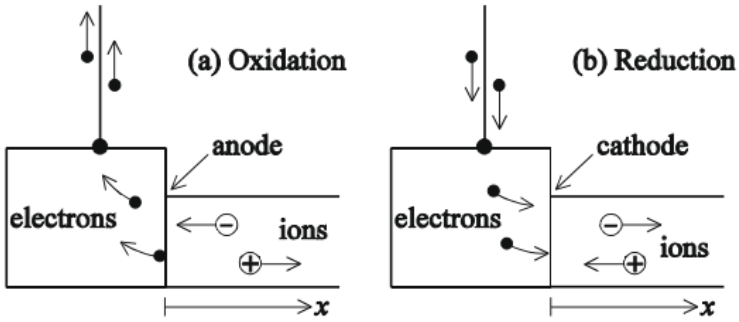

Figure 2.5: Electrode's interface where *(a) Oxidation* and *(b) Reduction* reactions occur (Reprinted by [64]).

2.1.1.1 Electrochemical Cell

To perform an electrochemical measurements it is needed to adopted an electrochemical cell, characterized by a two- or three-electrode configuration, and an electronic circuit for driving and reading out the RedOx signal. For a three-electrode configuration electrochemical cell, the different electrodes are:

- ***Working Electrode (WE)***: is the electrode where the RedOx reaction occurs. Common WE are made of inert material such as Au, Ag, Pt and glassy carbon, but its surface can be funcionalized with different molecules;

- ***Reference Electrode (RE)***: is an electrode characterized by a known stable potential, needed to correctly support the redox reactions occurring at the interface of the WE. Common used RE is Ag/AgCl. It is pivotal that the current flowing through this electrode is kept close to zero (ideally, zero). This can be ensured by using a very high input impedance from the electronic circuit (> 100 GΩ);

- ***Counter Electrode (CE)***: is the electrode completing the three-electrode configuration circuit and it gathers the RedOx current from the solution. It is usually

made of an inert material (*e.g.* Pt, Au) with a total surface area that must be larger than the WE one.

The two-electrode configuration cell has both the RE and WE, but not the CE. Figure 2.6 represents the two-electrode configuration, while Figure 2.7 shows the three-electrode setup. The former is normally adopted when any external signal has to be precisely applied to the cell, while the latter is used when a potential or a current has to be applied between the RE and the WE and, then, the current is collected through the CE.

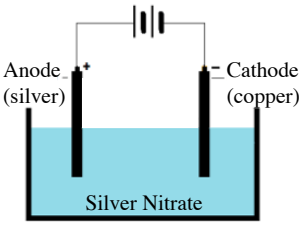

Figure 2.6: Two-electrode cell configuration (Reprinted by [37]).

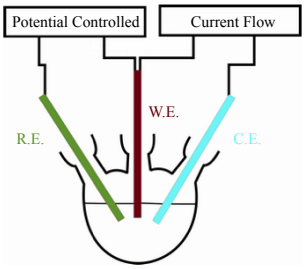

Figure 2.7: Three-electrode cell configuration (Reprinted by [37]).

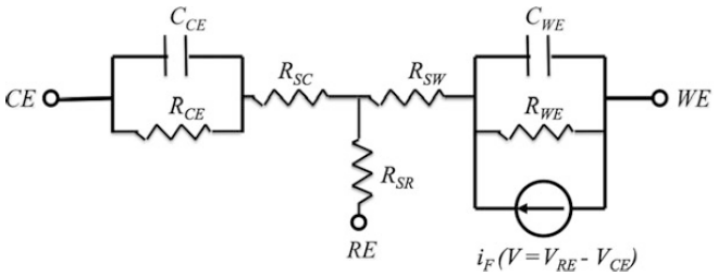

Figure 2.8: Equivalent circuit of an electrochemical cell (Reprinted by [16]).

2.1.1.1.1 Equivalent circuit of a Three-Electrodes Cell

The Figure 2.8 shows the equivalent electrical circuit for an electrochemical cell in three-electrode configuration. This equivalent circuit based on resistors, capacitors, current/voltage sources can be very useful to analyze the electrical behavior of the cell in relation with the control system. In this model R_{SC} and R_{SW} represent the solution resistance between the WE and the CE, instead the resistors R_{WE}, R_{CE}, and R_{RE} represent the charge transfer at the electrode-electrolyte interface. The presence of the capacitors C_{WE} and C_{CE} can be understood remembering the double-layer phenomenon in front of any polarized electrode immersed in the analyzed solution. This circuital representation of the electrochemical cell comes from the simpler Randles model for a polarized electrode immersed in a salt solution, shown in Figure 2.9.

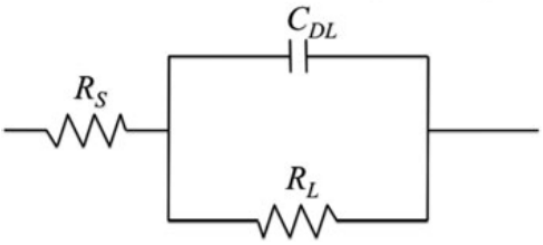

Figure 2.9: Equivalent circuit of a polarized electrode (Reprinted by [16]).

The electrical impedance of a general electrode interfaced with an electrolyte solution is calculated by the following Equation 2.1:

$$Z = \frac{R_L}{jwC_{DL}R_L + 1} \tag{2.1}$$

As we can notice by these circuital models, capacitors are also contributing in the current measured by the sensor. Hence, the measured current is composed by the faradic current contribution due to the analyte RedOx plus a capacitive current contribution due to the phenomenon at the interface, which are called *non-faradaic current*. The non-faradic current can be evaluated by the Equation 2.2:

$$I_{non-F} = \frac{V_{ref}}{Z} = \frac{jwC_{DL}R_L + 1}{R_L}V_{ref} \tag{2.2}$$

2.1.1.2 Electrochemical Detection Techniques

Different electrochemical techniques are available in electrochemistry as shown in the scheme of Figure 2.10.
It is possible to distinguish three main cases: *(a)* measuring the potential from the electrochemical cell when no current flows; *(b)* measuring the potential from the cell while controlling the current; *(c)* measuring the current from the cell while controlling the potential [37].

At the first level of the schematic, there is a first division of the techniques in static and dynamic. In the static approach, no current has to flow through the analyte solution. The only technique in this class is *Potentiometry*, in which a potential is measured in a static environment. On the other hand, the dynamic group is larger since it includes all the techniques where either the potential or the current of the cell is controlled. The *Coulometry* is the only technique where the current is controlled. On the contrary, several different techniques that imposes an external potential are available and have different behaviors and results depending if the applied voltage is fixed or variable. Typically, if the RedOx current is obtained by imposing a constant potential, this is referred as *Amperometry*, while if the current is measured at controlled

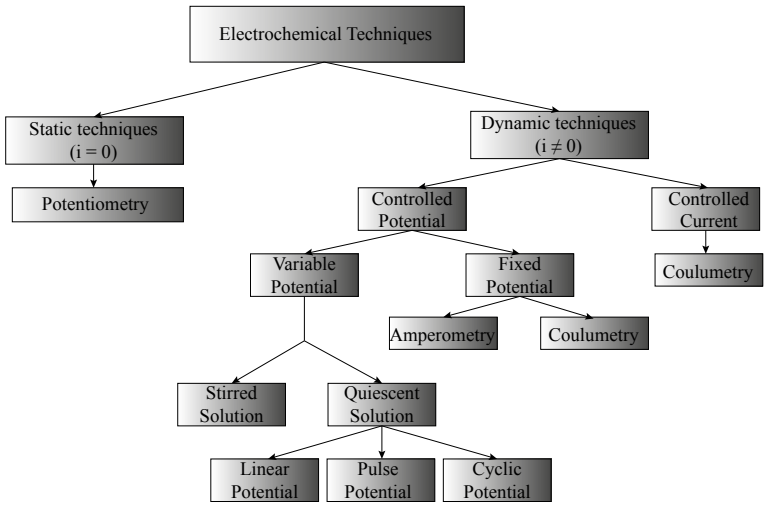

Figure 2.10: Overview on the different electrochemical techniques.

variations of the potential, this is called *Voltammetry*. By changing the excitation potential waveform different electrochemical techniques are defined. Among these techniques, *Cyclic Voltammetry (CV)*, *Differential Pulse Voltammetry (DPV)* are the most largely adopted to investigate and characterize the electrochemical behavior of a species. Once the electrochemical system is characterized, the amperometric method of *ChronoAmperometry (CA)* is adopted to quantitatively detect the analyte in a fast manner.

2.1.1.2.1 Potentiometry In potentiometry, the information about the analyte concentration in the solution is obtained from the measured potential between two electrodes (WE and RE) [24]. The stability of the RE is crucial for all the techniques, but especially for the potentiometry.
Figure 2.11 and Figure 2.12 report two examples of RE used in potentiometry.

When the RE is immersed in the analyte solution, an interface between the two ionic solutions is created, due to the difference in the ionic concentrations.
This **junction potential** represents an important contribution to be considered in the evaluation of the measured *cell potential*. Indeed, the measured *cell potential* E_{cell} is given by the three contributions expressed in Equation 2.3:

$$E_{cell} = E_{WE} - E_{RE} + E_j \tag{2.3}$$

Where E_{WE} and E_{RE} are the measured potential at the WE and RE respectively, instead the E_j is the junction potential. Mainly, potentiometric measurements detect the ion activity in the sample. The equation used to described this ideal response of the cell is the *Nernst Equation 2.4* [30]:

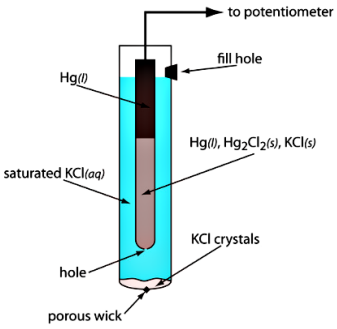

Figure 2.11: SCE with saturated solution of KCL and inner solution of Hg, Hg_2Cl_2 and KCl (Reprinted by [38]).

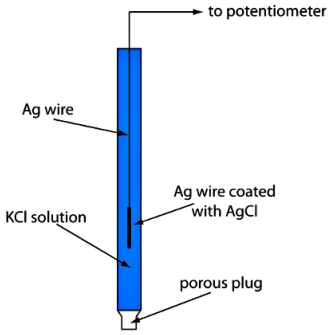

Figure 2.12: Silver/Silver Chloride Electrode with KCl solution and inner Ag wire and Ag wire coated with AgCl (Reprinted by [38]).

$$EMF = \frac{RT}{zF} \ln a_i \tag{2.4}$$

where EMF is the electromotive force (observed potential where the current is zero), a_i is the activity of the target ion I with charge z, and R, T and F are three constants (gas constant, absolute temperature and Faradaic constant, respectively).
In Figure 2.13 is plotted a typical potentiometric response where the EFM value is reported in the time.

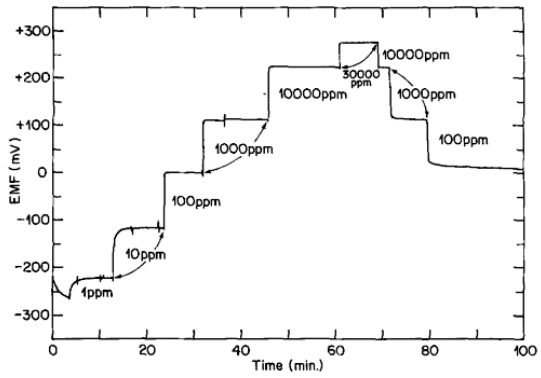

Figure 2.13: Typical response time of a potentiometric measurement (Reprinted by [18]).

2.1.1.2.2 Voltammetry

Cyclic Voltammetry (CV) *CV* is the most widely used electrochemical technique commonly employed to investigate RedOx reactions of molecular species [25]. It is performed by varying the applied potential at the working electrode as a linear sweep

potential ramp function, while the current is measured and plotted towards the applied potential.
As shown in Figure 2.14 [81], the voltage is swept between two values at a fixed rate, from a lower limit V_1 to an upper limit V_2: if the potential is stopped, we talk about *Linear Sweep Experiment*, while if the scan is reversed and the voltage is swept back to V_1, Cyclic Voltammetry happens. The rate at which this is achieved is the voltammetric *scan-rate* ($\frac{V_2-V_1}{t_1-t_0}$, V/s). A *cyclic voltammogram* (Figure 2.15) is obtained by measuring the current at the working electrode: the current (vertical axis) is plotted in function of the voltage (horizontal axis) [47].

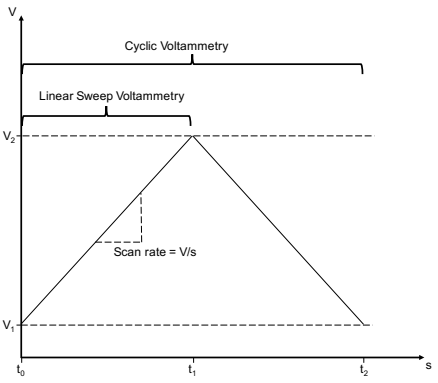

Figure 2.14: Cyclic Voltammetry waweform with V_1 and V_2, lower and upper limits.

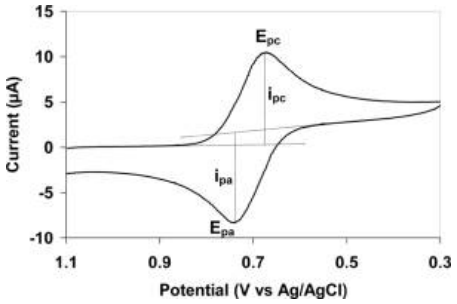

Figure 2.15: Typical Voltammogram with the potential (E_{pc} and E_{pa}) and the corrispondent current (i_{pc} and i_{pa}) respectively for the cathode and the anode.(Reprinted by [35])

In particular, the measurement in Figure 2.15 starts by increasing the voltage applied to the cell and the resulting current is measured. As soon as the applied voltage corresponds to the needed voltage for the specific RedOx to happen, a current peak is registered (i_{pc}). The shape of the peak is typical respect to the analyzed species and the height of the peak is correlated with the concentration of the analyte in the solution by the *Cottrell Equation* 2.5. Then, when the applied potential is inversed and starts to decrease, the current will inverse its flow. Also in this case a reductive peak (i_{pa}) may occur if the applied potential favorites the reaction to happen.

$$i = \frac{nFAc^0\sqrt{D}}{\sqrt{\pi}t} \tag{2.5}$$

Also for the Voltammetric Techniques, the *Nernst Equation 2.6* is very important. It is used to evaluate the potential at which the specific RedOx reaction occurs. By changing the notation for the voltammetry analysis we write here the previous Nernst Equation 2.4 in the form of:

$$E = E_0 + \frac{RT}{nF} ln \frac{C_{ox}}{C_{red}} \tag{2.6}$$

in which, E_0 is the Redox potential for the analyte involving, C_{ox} and C_{red} the concentratons of the oxidised and reduced species close the electrode's surface, n is the number of involved electrons and F is the *Faraday constant* (96,485 $\frac{C}{mol}$).
According to the Nernst Equation, when the potential is scanned during the CV, the analyte concentration in the solution near the electrode changes. In Figure 2.16 is shown an example of Cyclic Voltammetry for RedOx reaction (Reduction: $Fc+ + e^- \longrightarrow Fc$ and Oxidation: $Fc \longrightarrow Fc+ + e^-$): panels **A-G** show the concentration-distance profiles of the Fc^+ (blue) and Fc (green) species and the relatives points are indicated in the voltammograms (panel **H**).

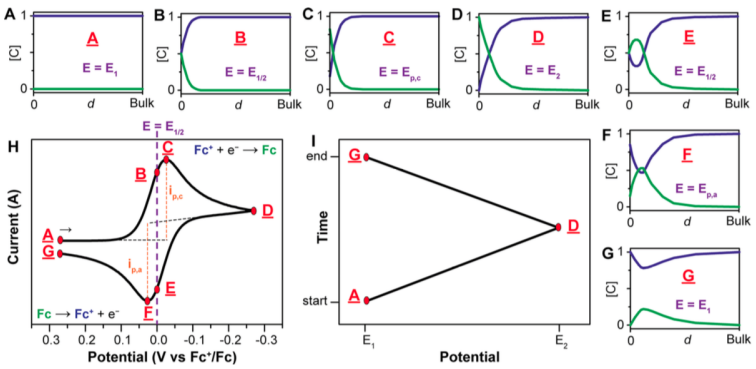

Figure 2.16: (**A-G**): concentrations profiles (mM) as a function of the distance from the electrode (d, from the electrode surface to the bulk solution); **H**: Cyclic Voltammogram; **I**: Applied potential as function of the time. (Reprinted by [25]).

From point **A** to point **D**, Fc^+ is reduced to Fc: only a small amount of Fc^+ has reacted at the electrode surface and, consequently, only a small amount of Fc has been built up. There is a diffusion layer that is still real small [14]. After that, a current peak occurrs (point **C**). From **C** to **D** the current decreases with an increasing of potential and the concentration profile shows that $[Fc^+]$ becames close to zero: while in **A** the reaction is controlled by electrode kinetics, now at this point the voltammogram is under *diffusion control*. From **D**, the scan direction is reversed and Fc is oxidized back to Fc^+ (peak occurs at point **F**): the concentration profiles show the build-up of Fc^+ and the depletion of Fc.
The voltammogram's shape is also influenced by the *scan-rate*, which controls how fast the applied voltage is scanned [25].
Increasing the scan-rate involves a decreasing of the diffusion layer, but higher currents are registered (Fig. 2.17).
The *Randles-Sevcik Equation* 2.7 shows that the current (i_p) directly proportional to

the square root of the scan rate (v):

$$i_p = 0.446nFAC^0\sqrt{\frac{nFvD_o}{RT}} \tag{2.7}$$

where n is the number of electrons involved in the redox reaction, A is the electrode surface area, D_o is the diffusion coefficient of the oxidezed analyte, and C^0 is the bulk concentration of the analyte.

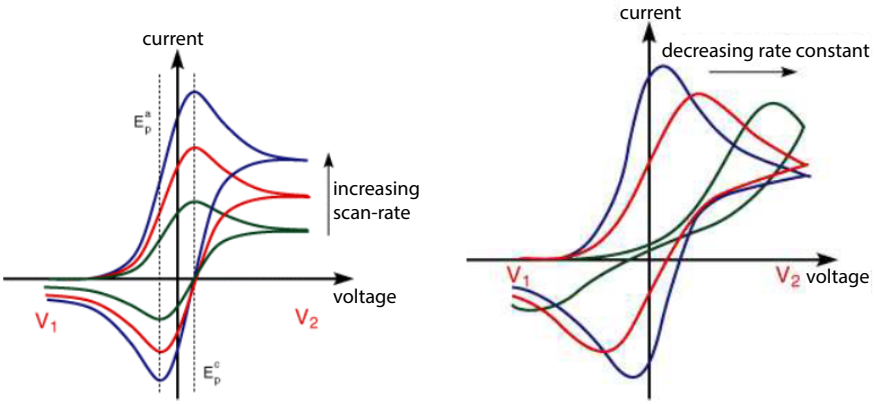

Figure 2.17: Effects of different scan rate on the Voltammogram (Reprinted by [81]).

Differential Pulse Voltammetry (DPV) Normally, CV is used for characterizing unknown electrochemical species, sweeping through a wide range of voltage. After identifying the oxidation/reduction potential, in order to improve speed and sensitivity, different potential waveforms, in the range of the previous found, can be applied. In particular the Differential Pulse Voltammetry applies a waveform which is a combination of a linear sweep potential range with a train of impulses superimposed, as shown in Figure 2.18.

In Figure 2.19 is plotted the current trend in function of the time. Here the current is sampled twice in each *Pulse Period*, before and after the pulse, and the difference between these two current values is plotted. Hence, main advantage of this technique is that the non-faradic capacitive current is excluded by the analysis and only faradic process are contributing in the output current. The sensitivity is higher respect to the other electrochemical techniques.

2.2 Electronic Read-Out

Electrochemical system is composed of two different parts: the sensor in direct contact with the target solution and the electronic circuit which controls the sensor and reads out the signal [91]. As already described in the paragraph 2.1.1.2, depending on

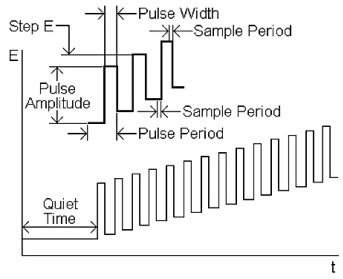

Figure 2.18: Waveform for Differential Pulse Voltammetry (Reprinted by [71]).

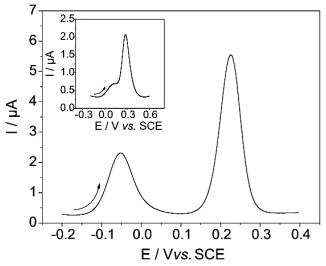

Figure 2.19: Differential Pulse Voltammograms with a potential amplitude of $50mV$ and a step potential of 5 mV. (Reprinted by [23])

the type of measurement a different output signal has to be measured. In Voltammetry (paragraph 2.1.1.2.2) it is needed to apply a voltage and to measure a current, instead in Potentiometry (paragraph 2.1.1.2.1) it is need to apply a fixed zero current and to measure a voltage. For this reason, two different read-out circuits have to be implemented to ensure a correct electrochemical detection.
The potentiostat device is adopted for voltammetric measurements [105], while the potentiometer is used in potentiometric detection.

2.2.1 Circuit Implementation

2.2.1.1 Potentiostat

A potentiostat is the electronic hardware required to control a three electrode cell and run most electroanalytical experiments. It applies the potential and reads out the RedOx current.
Figure 2.20 shows a block-diagram for the circuitry realization of a basic potentiostat.

A typical potentiostat has to guarantee two blocks: (i) a control block and a (ii) current reading block. To this aim, two different realization approaches are possible [16]:

- Grounded Counter Electrode;
- Grounded Working Electrode.

The two possible configurations are presented below.

2.2.1.1.1 Grounded Counter Electrode In this configuration (Figure (2.21)) two operational amplifiers (Appendix A) are employed and the CE is connected to the ground.
The first amplifier is adopted as Voltage Follower (Appendix A), ensuring absence

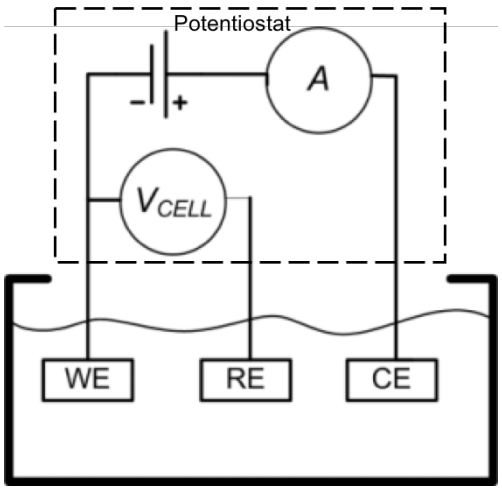

Figure 2.20: Block diagram for a potentiostat driving a three-electrode electrochemical cell (Reprinted by [63]).

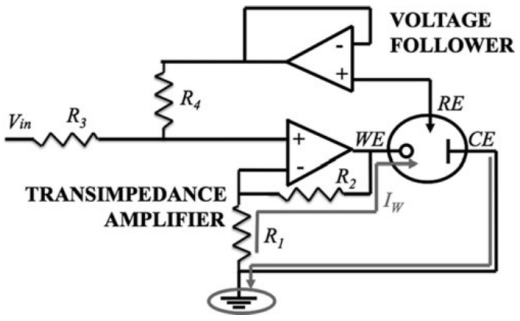

Figure 2.21: Grounded Counter Electrode Configuration (Reprinted by [16]).

of current through the RE. The second non-inverting amplifier (Appendix A) is in a Trans-Impedance Amplifier (TIA) configuration to convert the RedOx current into a voltage.
Hereafter an analysis of the circuit is provided to better characterize the relationship between the applied voltage and the measured current.

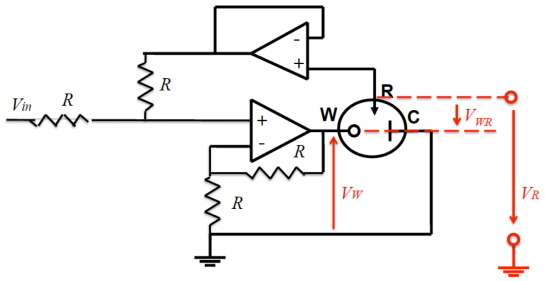

Figure 2.22: Circuit analysis of Grounded Counter Electrode Configuration (Reprinted by [16]).

Remembering that the following conditions are verified in an ideal operational amplifier:

$$V_+ = V_- \qquad\qquad I_{input} = 0 \tag{2.8}$$

and by applying *Kirchhoff's laws* for the current and the voltage, it is possible to obtain:

$$V_+ = \frac{V_{in} + V_R}{2} = V_- \tag{2.9}$$

$$V_W = 2V_- \tag{2.10}$$

Since, in agreement with the potentiostatic configuration, a voltage input (V_{in}) is applied between the WE and the RE, we have:

$$V_{in} = V_W - V_R = V_{WR} \tag{2.11}$$

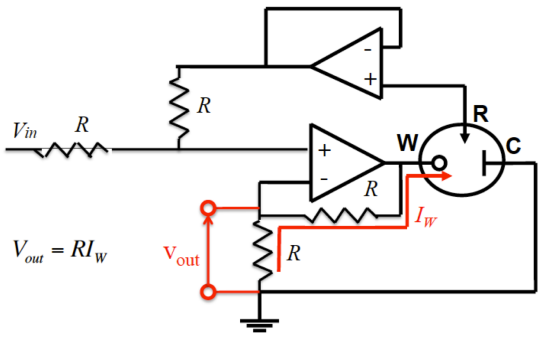

Figure 2.23: Circuit analysis of Grounded Counter Electrode Configuration (Reprinted by [16]).

The RedOx current is converted by the TIA as:

$$V_{out} = RI_W \tag{2.12}$$

The main limit of this configuration is due to the presence of a lot of components: it can be vulnerable to parameters mismatching and noise.

2.2.1.1.2 Grounded Working Electrode A possible solution for this problem, it can be represented by the *Grounded Working Configuration*, in which the working electrode is connected to the ground through a TIA (this configuration is also called *Virtually Grounded Working*). In Figure 2.24 a possible circuit implementation is reported. A *Control Amplifier*, with a very high input resistance and zero input current suitable for connecting the RE, is used to drive the electrochemical cell by imposing the potential, while a TIA is used to amplify and convert the RedOx current [16].

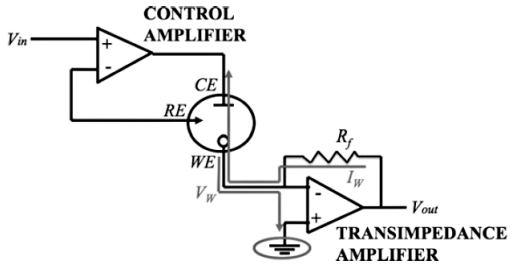

Figure 2.24: Grounded Working Electrode Configuration (Reprinted by [16]).

A circuit analysis is also for this circuit configuration. The Equations 2.8 are still valid, and we get

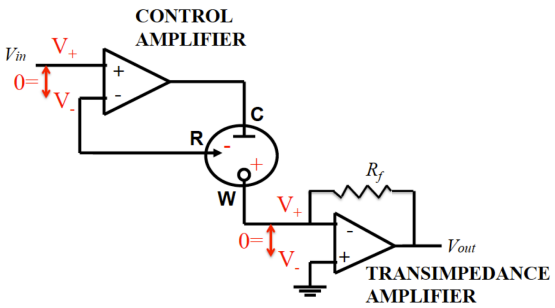

Figure 2.25: Circuit analysis of Grounded Working Electrode Configuration (Reprinted by [16]).

for the Control Amplifier:

$$V_{in} = V_+ = V_- \qquad\qquad V_- = V_R \tag{2.13}$$

For the TIA:

$$V_W = V_+ = V_- = 0 \tag{2.14}$$

The bond between the input voltage and the voltage between WE and RE is evident in Equation 2.15:

$$V_{in} = V_R = -V_{WR} \tag{2.15}$$

At the end, for the RedOx current, the TIA does the conversion in voltage, which is the measurable signal.

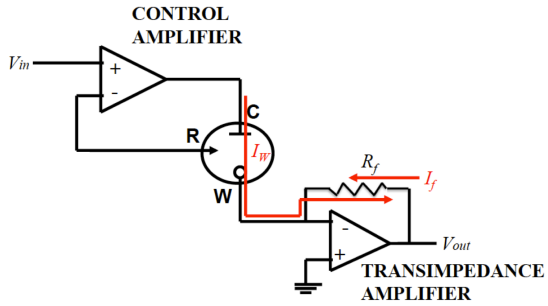

Figure 2.26: Circuit analysis of Grounded Working Electrode Configuration (Reprinted by [16]).

$$V_{out} = R_f I_f = -R_f I_W \tag{2.16}$$

Even if this configuration involved less components respect to the previous one, and hence it is less affected by noise, it is characterized by a voltage follower placed in a feedback loop which induces a risk of saturation, as shown in Figure 2.27.

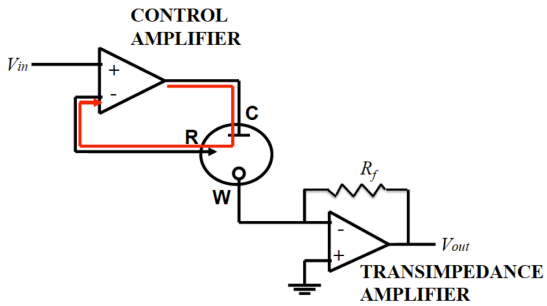

Figure 2.27: Risk of saturation of the Control Amplifier (Reprinted by [16]).

Explaining the cell with its electrical circuit and simplifying the double-layer capacitance (the only faradaic current is considered), the scheme in Figure 2.28 is obtained:

The voltage drops through the CE and the RE are derived with the Equations 2.17:

$$V_{RC} = (R_{CE} + R_{SC})I_W \qquad V_R = V_+ = V_- = V_R \tag{2.17}$$

In this way, it is possible to apply Kirchhoff's Voltage Law (KVL) around the closed circuit represented by the feedback loop:

$$V_{out|CA} = V_{in} + (R_{CE} + R_{SC})I_W \tag{2.18}$$

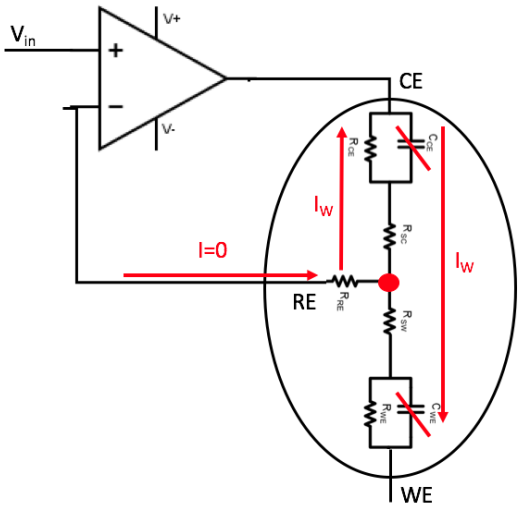

Figure 2.28: Feedback loop of the Control Amplifier (Reprinted by [16]).

The control amplifier could be saturate if the output voltage overcomes the alimentation voltage:

$$V_{in} + (R_{CE} + R_{SC})I_W > V \tag{2.19}$$

Tipically, V_{in}, R_{SC} and I_W dipend on the application, the type of redox reaction is monitored.

A third option, tried by grounding the *Reference Electrode*, shown in Figure 2.29, can not be effective.

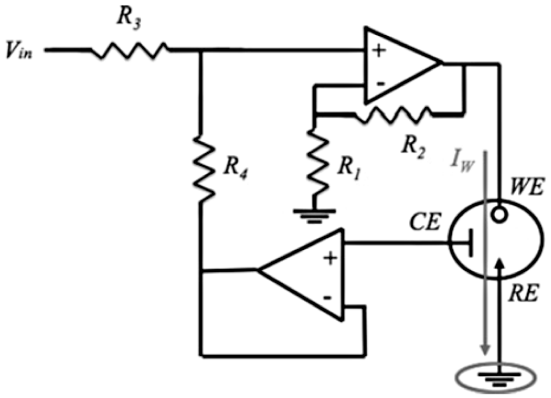

Figure 2.29: Circuit analysis of Grounded Reference Electrode Configuration (Reprinted by [16]).

Indeed, to set the RE to ground, it needs to get a null current in the CE. Hence, the current flow from the WE goes through the RE to reach ground. What you get is that now the CE works like the RE and ensures the right potential to the cell.

2.2.1.2 Potentiometer

A Potentiometer is the dedicated hardware for potentiometric experiments, in which a Open-Circuit Potential (OCP) is measured. The OCP is the potential between WE and RE when no current flows through the cell during the measurement [8]. In this type of procedure, a two-electrode configuration of the electrochemical cell is used (Figure 2.30).

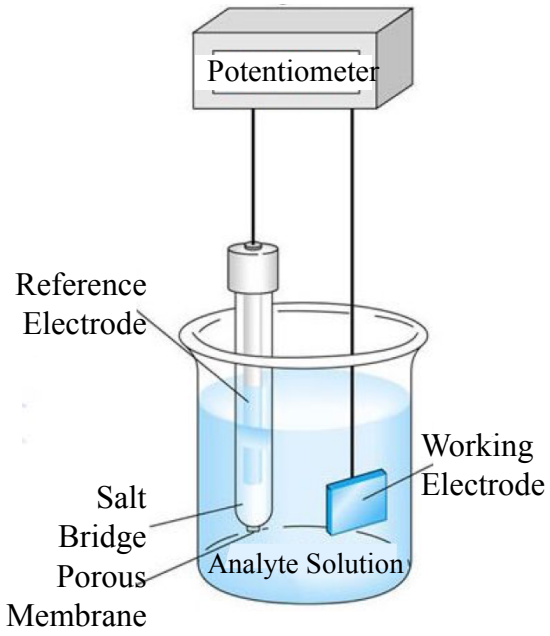

Figure 2.30: Potentiometric configuration in a two-electrodes cell (Reprinted by [37]).

First of all, it is needed to reduce the current flow in the cell to have a stable measurable potential between WE and RE. For this reason, as shown in Figure 2.31, the first stage of the potentiometer includes two voltage followers with two important purposes: (i) achieving zero current flowing at the RE thanks a very high input impedance and (ii) isolating the sensing part (electrochemical cell) from the electronic circuit.

At the end of this first stage, the potentials of RE and WE are available to be read. Then, to get the difference between these two potentials, a second block is needed (Figure 2.32):

Remembering that the following conditions are verified in an ideal operational amplifier:

$$V_+ = V_- \qquad\qquad I_{input} = 0 \tag{2.20}$$

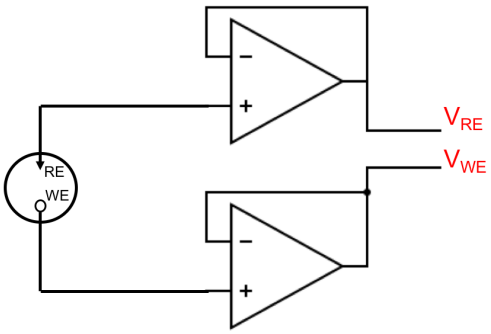

Figure 2.31: First block of a potentiometer.

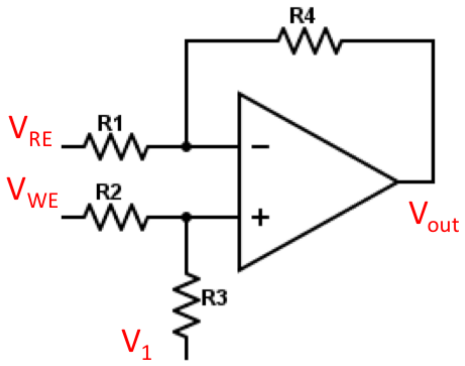

Figure 2.32: Differential block of a potentiometer.

we can solving the circuit by applying Kirchhoff's laws, obtaining the Equations 2.21:

$$V_{-} = \frac{V_{RE} + V_{out}}{2} \qquad V_{+} = \frac{V_{WE} + V_1}{2} \tag{2.21}$$

Starting from this Equations, it is possible to get the output potential as the difference between WE and RE, plus an offset voltage of 1V introduced to exploit the full dynamic of the Analog to Digital Converter (ADC).

$$V_{out} = V_{WE} - V_{RE} + V_1 \tag{2.22}$$

Chapter 3

Electronics for electrochemical multi-sensing: state-of-the-art

Over the recent years high attention has been dedicated in the realization of dedicated circuit for electrochemical analysis ([21], [54], [56]). However, the majority of these circuits are intended to perform either amperometric or potentiometric measurements. A breakthrough would be represented by the realization of a combined potentiometric and potentiostatic circuits on a single platform to be able to detect different kinds of analyte; hence offering a broader view of the patient's health status.
In this chapter, a review of the combined circuits already realized in literature is presented.

In 2011 Wang and his group realized a telemtry system for real-time amperometric and potentiometric electrochemical senisng [99]. The complete block diagram of the system is showed in Figure 3.1

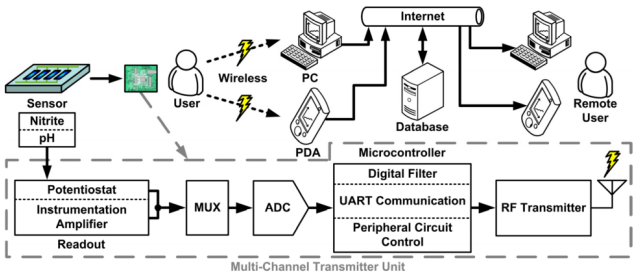

Figure 3.1: Block diagram of the real-time system proposed by Wang et al. [99].

The front-end readout circuit for the measures is realized by the use of a potentiostat and an instrumentation amplifier. After this readout block, a multiplexer is used in order to reduce the hardware and to allow the control of four-channel simultaneously. Next

step from the multiplexer (MUX) is the alalog-to-digital converter. The microcontroller (Field Programmable Gate Array (FPGA)) drives the measure and processes and transfers the data through a Radio Frequency (RF) transceiver module (by using UART serial communication). For the potentiometer circuitry, a CMOS Instrumentation Amplifier (IA) is used. Even if it provides an high input impedance to measure the *Open-Circuit Potential* (OCP), it is affected by some drawbacks: (i) the Common-Mode Rejection Ratio (CMRR) decreases due to mismatches of resistors and operational amplifiers and (ii) the presence of the three op-amps increases the complexity of the system and causes power consumption and noise. To overcame these disadvantages, a Differential Difference Amplifier (DDA) architecture has been implemented, as in Fig. 3.2. A DDA is an op-amp with four input nodes, which allows to implement more difficult circuits with a single component. Also the potentiostat has been implemented by using an op-amp as control block and a DDA for the current measurement block. The control block includes a control amplifier and a resistor R_f to which the RE and CE are connected; the WE is connected to the supply voltage of the potentiostat. The readout block comprises a negative feedback DDA, which is used to convert the voltage signal into a current ($I_f = \frac{R_f}{V_{OCP}}$).

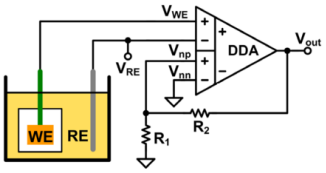

Figure 3.2: Set-up of the DDA circuit for OCP measurements (Reprinted from [99]).

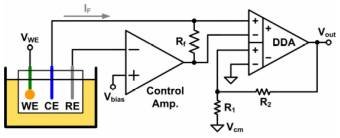

Figure 3.3: Set-up of the potentiostat circuit based on DDA and op-amp (Reprinted from [99]).

In 2013 Bembnowicz, Anastasova and their group published their work about a wearable electronic sensor able to perform simultaneously potentiometric and amperometric measurements [9]. It is a miniaturized electronic device which ensures (i) high impedance voltages and (ii) ability to detect very small values of current. Hence, this wireless and portable potentiostat enables the simultaneous detection of currents and potentials by performing both amperometric and potentiometric measurements.

Figure 3.4 sketches four different configurations of operational amplifiers for the realization of a potentiostat able to perform both amperometric and potentiometric measurements. The configuration depicted in Figure 3.4.**A** is used for potentiometry and is based on a non-inverting op-amp with a high input impedance and a gain provided by the two resistors R_1 and R_2. Figure 3.4.**B**,.**C** and .**D** show an inverting integrator, an inverting current to voltage converter and an inverting current to voltage converter with enhanced gain, respectively. These configurations represent three different possible arrangements for the amperometric measurement.

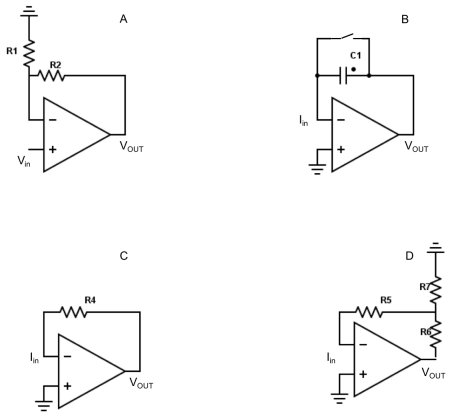

Figure 3.4: Operational Amplifier for potentiometer and potentiostatic configuration: (**A**) Non-Inverting Amplifier, (**B**) Inverting Integrator Amplifier, (**C**) Inverting current to voltage Amplifier, (**D**) Inverting current to voltage converter with increased gain (Reprinted by [9]).

The combined circuit is completed by a MSP430 microcontroller, which allows the analog to digital conversion of the electrochemical signal and the radio transmission of the data.

In 2016 Gao and his company represented an important step towards the realization of wearable sensor technologies for personalized medicine. They realized a fully integrated wearable sensor arrays for analysis of different compounds in sweat [27].

As illustrated in Fig. 3.5, the combined circuit drives a Flexible Integrated Sensing Array (FISA), which allows simultaneous measurement of a panel of metabolites and electrolytes. The FPCB technology is used to ensure flexibility and portability of the device. Standard blocks for reading, processing and wireless transmission of the signals are used in the circuit: (i) (**1-4**) amperometric blocks with trans-impedance amplifiers (**1** and **3**) and low-pass filters (**2** and **4**); (ii) (**5-9**) potentiometric blocks with a voltage buffers (**5** and **8**), a differential amplifier (**6**) and a low-pass filters (**7** and **9**). A microcontroller (**10**) module is also integrated to drive all the units and to transmit the data to a smart-phone via the bluetooth transceiver (**11**), as in Fig. 3.6.

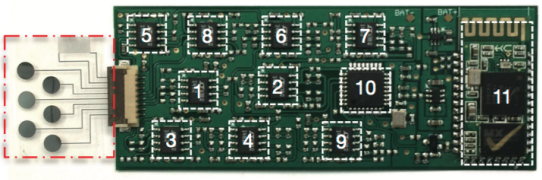

Figure 3.5: Flexible integrated combined circuit interfaced with the sensor array (Reprinted by [27])

After a study of the state-of-art of combined circuits present in literature and the related choices in terms of circuits for potentiometric and potentiostatic measurements,

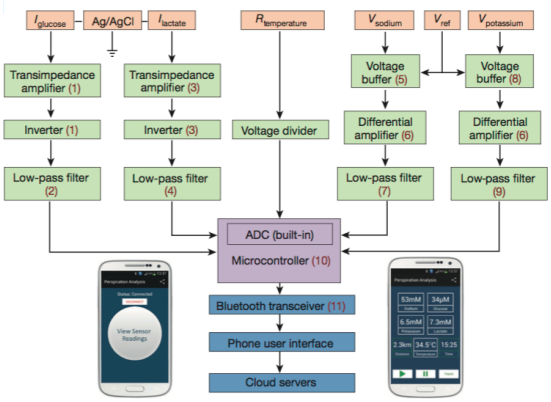

Figure 3.6: System-level block-diagram with both the amperometric and potentiometric readouts (orange), conditioning (green), processing (purple) and wireless transmission (blue) blocks (Reprinted by [27]).

this thesis wants to perform an electronic combined circuit to drive electochemical cells. Compared to [9], this circuit wants to implement an indipendent potentiostat and potentiometer to allows the different measurments at the same time, while compared to the device realized by [99], this work is focused on a flexible and wearable implementetion. At the end, we have taken inspiration from the last device analyzed [27], and have introduced some changes in terms of electronics component and in compounds detected. With the purpose to realize a sport monitoring application for patients suffering of mental disorder during physical exercise (Chapter 1), the system proposed in this work wants to implement a combined detection of two related compounds: Lactate and Lithium, the latter ion substitutes Potassium and Sodium detected in [27].
Besides, in order to implement a system for athletic or sportive men/women, the choice of dimensions is not random: indeed, the use of an armband is quite common during physical excercise. The idea to use a single case which could include both circuit and eventually smartphone for user interface, can be more comfortable and can reduce considerably the cost of the complete system.
Mainly important for a wearable application is to ensure a low power consumption of the components: the board implemented has been electrically characterized showing a power consumption of 200 mW, with 3.6 V power supply.
In the following Chapters the innovations and the changes introduced with the present work are described. Chapter 4 and Chapters 5 and 6 show in detail the features of the complete system in terms of hardware and software implementation of the ciruit and, the last two chapters, describe the functionalized sensors for Lactate and Lithium detection.

Chapter 4

System Implementation

Flexible bio-electronic systems represent a revolutionary approach for medical instrumentations ensuring portability, wearability, small dimensions and fast performance. Indeed, smart and flexible sensing electronic devices are essential in the realization of wearable health monitoring systems [100]. This thesis aimed to implement and realize a wearable sensing system for potentiostatic and potentiometric measurements. Fig. 4.1 shows the developed electronic board printed on a flexible substrate.

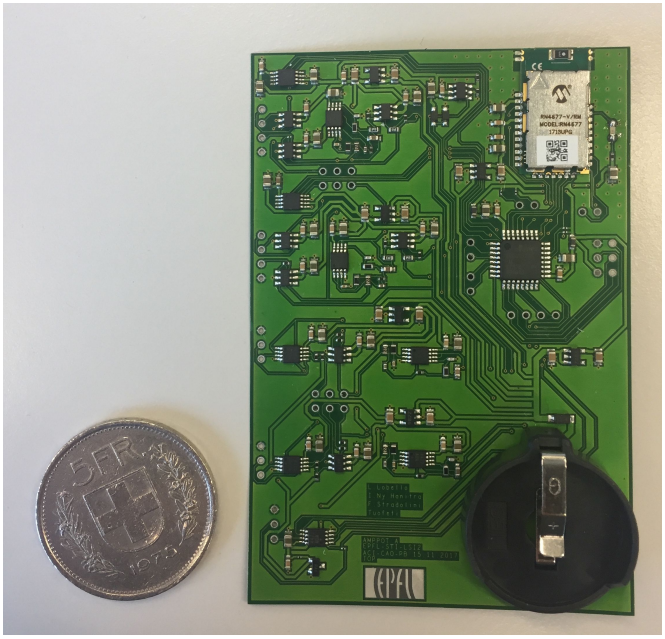

Figure 4.1: Flexible electronic platform realized in small dimensions for fit in arm-band case (Height: 97mm, Width: 66mm).

A FPCB can be used as alternative to the traditional rigid *Printed Circuit Board* (PCB): its flexibility, twistability, and light weight ensures a more comfortable realization

for wearable smart applications [51].
To sum up, a flexible sensing system for wearable health application needs of: (i) a flexible substrate (Fig. 4.2), (ii) some sensing electrodes and (iii) a portable case to wear the device (Fig. 4.3). In this case, a very common and cheap arm-band has been used as case. The board is encapsulate in the arm-band case is connected to the sensing electrodes through small wires. The arm-band is waterproof and it protects the electronic board from the environment and from the collected sweat analyzed by the sensors.

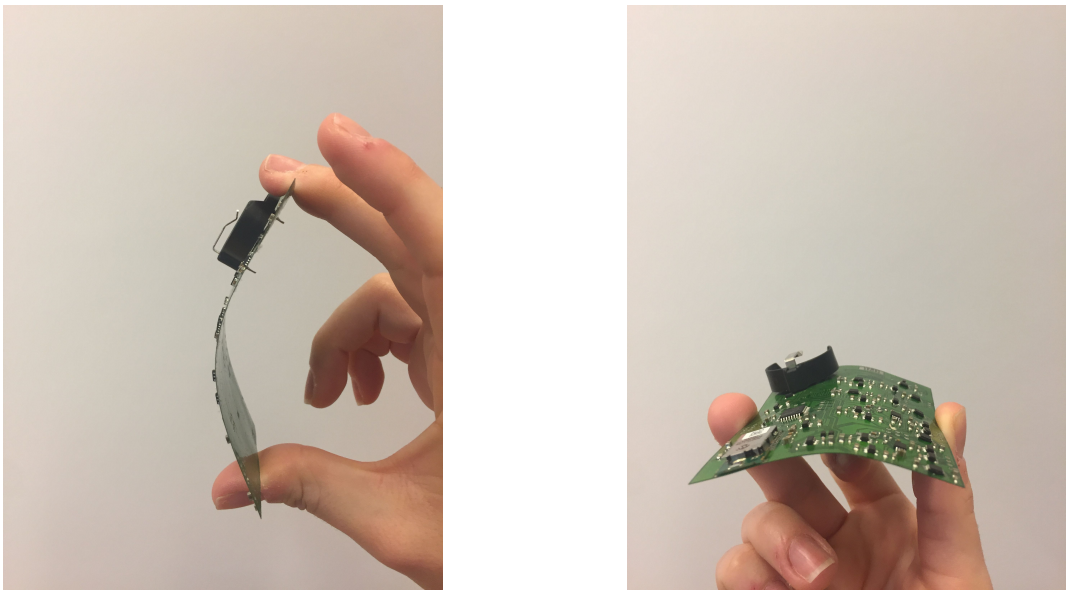

Figure 4.2: Electronic circuit printed on a flexible substrate.

Figure 4.3: Wearable health monitoring device consisting of a flexible electronic PBC encapsulated in a arm-band case and connected to electrochemical sensors in direct contact with the subject's skin.

As illustrated in Figure 4.4, the FPCB technology is exploited to incorporate the analog front-end, the processing blocks and the wireless transmission of the data. All these modules are realized with integrated circuit *Commercial-Off-the-Shelf* (COTS)

components. Seven main blocks can be identified: (1) four independent electrochemical cells can be driven by this board (two in the three-electrodes configuration for potentiometry, and four in two-electrodes configuration for potentiostatic measurements, as described in section 4.31), (2) amperometric read-out circuit which includes *Amplification*, *Filtering* and *Offset* stages, (3) potentiometric read-out circuit with *Filtering* block, (4) button cell battery which provides a low power supply of 3.3 V, (5) the microcontroller (*ATxmega32E5* by Atmel AVR XMEGA ([6])) which is the logic unit of the circuit, (6) the *Bluetooth Low Energy* (BLE) module for the wireless transmission of the data to a PC or smart-phone and (7) the UART output module for RS232 communication.

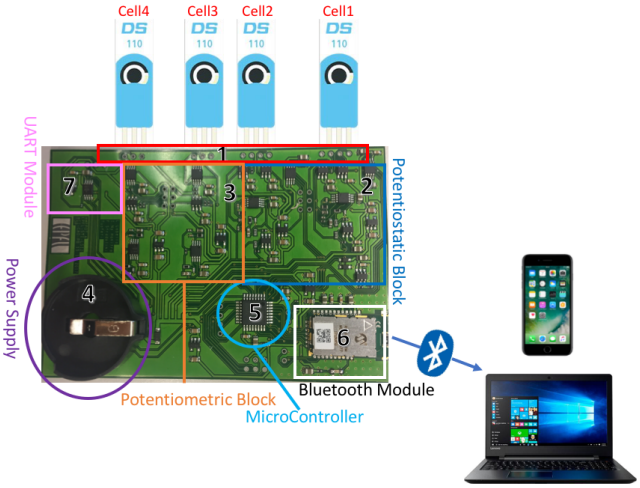

Figure 4.4: FPCB for amperometric and potentiometric measurements with Bluetooth data transmission.

In Figure 4.5 two block diagrams depict the schematics of both the circuits:

For the implementation of the schematic *Altium Designer Enviroment* was used. This software supports all aspects for electronic products development. The programming and the debugging of the microcontroller has been done in *Atmel Studio 7*.

4.1 FPCB Components

4.1.1 Control unit: Microcontroller

The microcontroller is programmed to start the measurements, to process the data and to send the data by enabling the BLE module. We have chosen to adopt the ATxmega32E5 microcontroller since it belongs to a family of low-power, high-performance and because it is based on Reduced Instruction Set Computer (RISC) architecture. This type of chip allows to perform a great number of instructions in a serial manner and in short time.

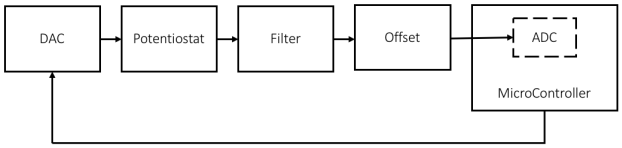

(a)

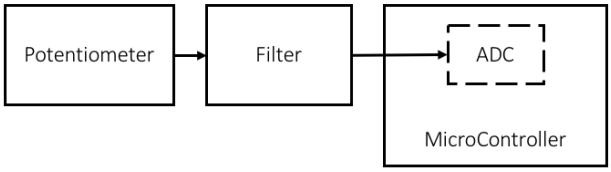

(b)

Figure 4.5: General block diagram for: **(a)** amperometric and **(b)** potentiometric measurements.

Main components of a microcontroller are visible in Fug. 4.6 and can be listed as: the Central Processing Unit (CPU), which executes the code and performs all calculations, a lot memories, which can be divided in *program memory* and *data memory*, the system clock and the programmable input/output peripherals.

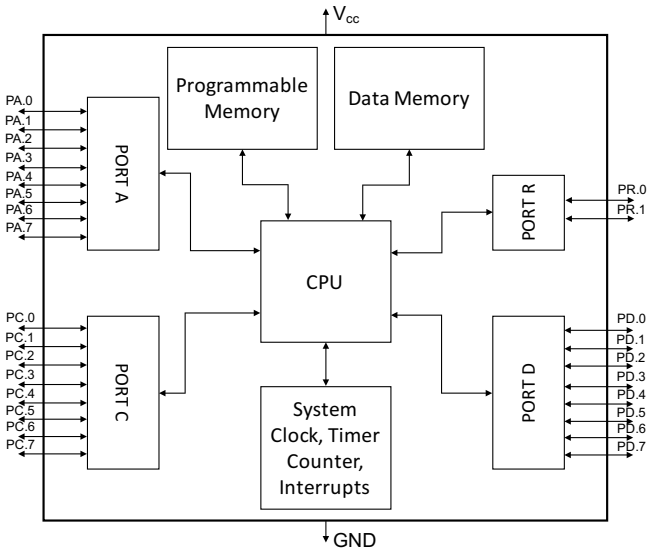

Figure 4.6: Block diagram with main components of a microcontroller.

Mainly, a microcontroller is used to connect and interface with any peripheral device to drive and activate their tasks or to time their activity. It is essential to know the different protocol which allow the microcontroller to communicate with these connected devices in order to establish a bidirectional exchange of data. It is important to define the

difference between a **serial communication**, where the bits representing the data are transferred one by one on the communication line, and the **parallel communication**, where more bits are transmitted at the same time.

4.1.1.1 Communication Protocols

4.1.1.1.1 Serial Peripheral Interface (SPI) Serial Peripheral Interface (SPI) is a serial communication protocol for fast synchronous data transfer between the microcontroller and the peripheral devices, which can be also another microcontroller. The two devices involved in this type of communication must act as master or slave: the master is the device which establishes and controls the communication, while the other device is the slave.

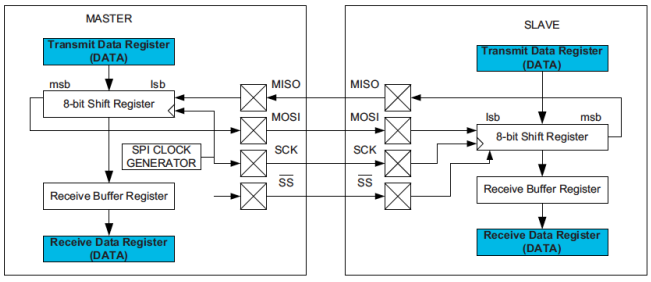

Figure 4.7: Master and Slave interconnection with SPI (Reprinted by [6]).

In Figure 4.7 is shown a typical peripheral interface between a master and a slave. Four pins are needed to enable the bidirectional communication: Serial Clock - SCK, Master In Slave Out (MISO), Maste Out Slave In (MOSI) and Slave Select - SS. The communication starts when the master pulls the slave select $(\overline{SS})$ signal low; at this moment the data to send are ready either in master or in slave shift registers, depending on the direction of the communication. Then, a clock signal must be generated by the master on the *SCK* line; at the end, the data are shifted through *MOSI* line when communication is from master to slave or through *MISO* line if vice-versa.

There are four different SPI configurations, as summarized in Figure 4.8. They differ from the combination of the SCK phase and polarity with respect to the serial data. For the *Mode 0* data is sampled at the leading rising edge clock, instead in *Mode 1* data is sampled at the leading falling edge of the clock. At the same way, *Mode 2* and *Mode 3* are dual for the training edge (falling and rising respectively). Each SPI configuration is **full-duplex**: data is sent from the master to the slave and from the slave to the master at the same time. As concerning the data package, SPI does not define any structure for the data stream, this means that the package composition is completely decided by the designer.

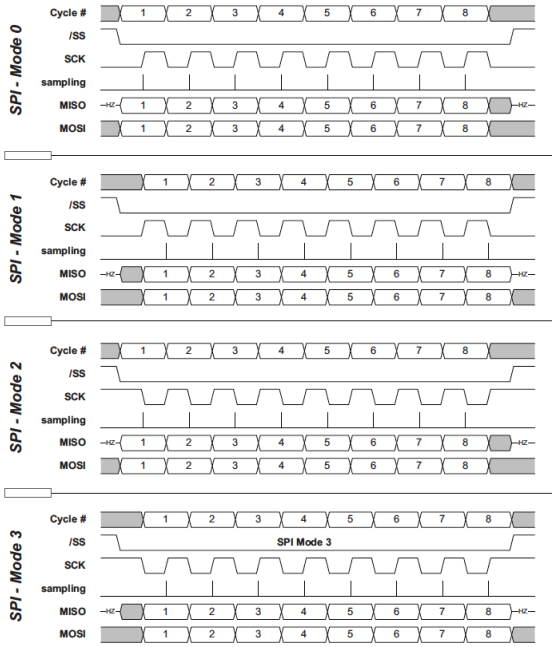

Figure 4.8: SPI Data Transfer Modes (Reprinted by [6]).

4.1.1.1.2 Inter Integrated Circuit (I2C) Inter Integrated Circuit (I2C) is a serial protocol which allows multiple slave chips to communicate with one or more master chips. It requires only two lines and is intended for short-distance communications.
Two-Wire Interface (TWI) is a bi-directional, I2C compatible interface. Two connected devices can act as master or slave, indistinctly. The only external required component in this configuration is the pull-up resistor for each line R_p in Fig. 4.9. The R_p provides a high level on the line whenever no device is connected.
This type of communication consists of two lines: Serial Clock Line (SCL) which is the line that scans the clock of communication and Serial Data Line (SDA) which is the line where data can be transfered (Fig. 4.9).

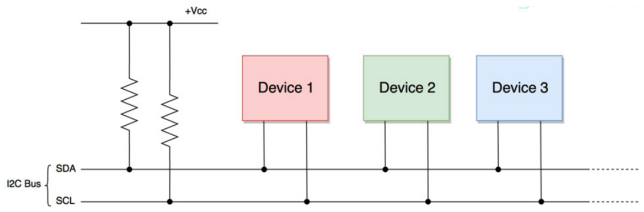

Figure 4.9: Physical I2C Bus (Reprinted by *"Basics of I2C Communication:Hardware, Data Transfer, Configuration"*).

One single master can drive several slaves. The master can direct the communication to the target slave device by using its unique ID address.

- **START** and **STOP**: there are only two conditions to indicate the beginning of

the transmission (START) and its end (STOP). A START condition is indicated by a low-level of the SDA line, while, on the contrary, the STOP conditions is identified by a transition to the high-level of the same SDA line. During both the transitions, the SCL line is kept to the high-level.

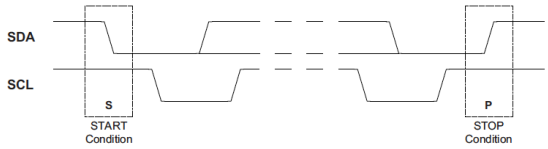

- **ADDRESS**: the Address frame is needed to indicate the slave with which the master wants to start the communication. It is a 7-bit address; hence 2^7 devices can be connected to the bus. The 8^{th} bit informs the slave if master is writing to it (W, bit is 0) or is reading from it (R, bit is 1).

- **DATA**: at the end, a data packet is sent with the information of the communication, it is a 9-bits packet where there is a byte with information and the last bit is the acknowledge bit, which indicates that the receiver must acknowledge (A) or not-acknowledge ($\overline{A}$) each byte received.

In Figure 4.10 a typical data packet for the I2C communication protocol is represented.

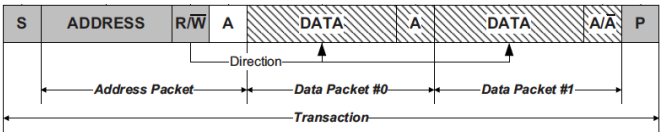

Figure 4.10: Communication packet for I2C protocol (Reprinted by [6]).

4.1.1.1.3 Universal Asynchronous Receiver-Transmitter (UART) The Universal Asynchronous Receiver-Transmitter (UART) is an hardware device for asyncronous serial communication. It can be an individual Integrated Circuit (IC), but commonly it is integrated in the microcontroller. *Shift registers* are essential in the UART communication because they performs the conversion between parallel and serial transmission. The **transmitter** (e.g. Device 1 in Fig. 4.11) takes the data bytes and, after the conversion of the shift register, it transmits all the bits in a sequential manner through the **TX** line; on the contrary, the **receiver** (e.g. Device 2 in Fig. 4.11) reassembles in data bytes the received bits from the **RX** line.

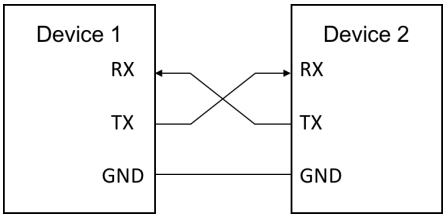

Figure 4.11: UART communication between two devices.

Different UART configurations are possible:

- **Simplex**: transmission is allowed only in one direction:

- **Half-duplex**: devices can be set as transmitter or receiver:

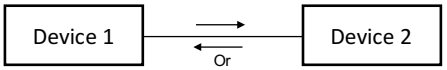

- **Full-duplex**: devices can send and receive at the same time:

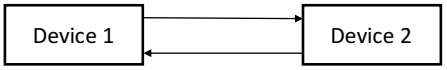

In this type of communication it is important to consider the mechanism which regulates fast data transmission. For asynchronous communication there is not an external clock signal associated with the transmitted data, but receiver and transmitter have to share the same **baud-rate**. The baud-rate (f_{baud}) is the frequency (bps, bits per second) corresponding to the time (s) employed to transmit one bit. A common value used for the baud-rate is 9600, but it is possible to choose any other value (keeping in mind that too high values can cause errors in the transmission).

Frame Formats The data-frame starts with the start bit, followed by the data bits (8 or 9 bit, LSB first and MSB last), eventually a *parity bit* and one or two stop bits. A **parity bit** is an error-detection bit added at the end of the byte, it can be:

- *odd parity*: parity bit is set to one if the data contains an even number of logical-high bits;
- *even parity*: parity bit is set to one if the data contains an odd number of logical-high bits.

IDLE state indicates no transfer on the communication line and it is set to high by default.

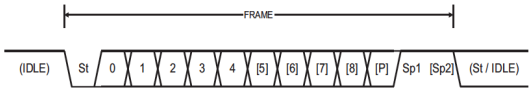

Figure 4.12: Possible combinations of frame formats in UART communication (Reprinted by [6]).

4.1.1.2 ADC

The Analog-to-Digital-Converter (ADC) converts analog signals to digital values. Analog quantities are characteristic of phenomena in the "real world", e.g. the signals deriving from electrochemical cell, while digital language is common in "computing world", in transmission and control system [45].

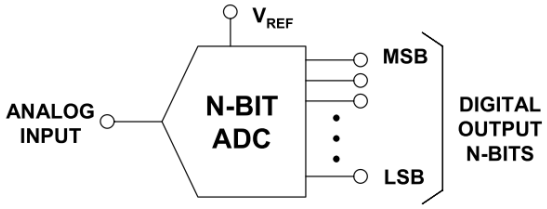

Figure 4.13: Analog-to-Digital conversion (Reprinted by [45]).

Three different input sources can be selected as measured voltage input and converted by the ADC:

- *Differential Input*: positive and negative input have to be selected, it is also possible to choose 1/2x, 1x, 2x, 4x, 8x, 16x, 32x, and 64x gain.;
- *Single-ended Input*: all input pins can be used as inputs, while the negative input depended on the signed and unsigned mode. Connected to the ground for the first one and to half of the voltage reference minus a fixed offset for the second ($\frac{V_{REF}}{2} - \Delta V$, with $\Delta V = V_{REF}0.05$). Normally the gain is imposed to be 1x;
- *Internal Input*: using the ADC is possible to measure some internal signals.
  - Temperature Sensor
  - Band-gap voltage
  - AV_{cc} scaled
  - DAC output
  - Pad ground and Internal ground

  As in the previous case, also here the negative input depends on the signed and unsigned mode.

For the Voltage Reference (V_{REF}), different options can be adopted: in the present case, an internal $AV_{cc}/1.6$ voltage has been chosen.
The ADC resolution of our module (ATxmega32E5) is of 12-bits, this means that it can encode an analog input to one of 4096 different levels, since $2^{12} = 4096$. In particular, for unsigned mode, the values can represent in the range from 0 to 4095, while in the signed mode from -2048 to +2047.
The ADC transfer function is:

$$RES = \frac{V_{INP} - V_{INN}}{V_{REF}} \cdot GAIN \cdot (TOP - 1) \tag{4.1}$$

where RES is the digital value, V_{INP} and V_{INN} are positive and negative analog input, respectively, GAIN depends from the input source and TOP is the maximum of the range and it depends from the selected mode.

The ADC setup for this implementation is shown in the following code:

Listing 4.1: Setup of ADC

```
/* Configure the ADC module:
* - signed, 12-bit results
* - Vcc/1.6 voltage reference
* - f_ADC = 500 kHz
* - manual conversion triggering
*/
adc_set_conversion_parameters(&adc_conf,ADC_SIGN_ON,
ADC_RES_12,ADC_REF_VCC);
adc_set_clock_rate(&adc_conf,500000UL);
adc_set_conversion_trigger(&adc_conf,ADC_TRIG_MANUAL,1,0);
adc_write_configuration(&ADCA,&adc_conf);

/* Set Analog inputs for ADC channels PA.0 -- PA.3*/
adcch_set_input(&adcch_conf,ADCCH_POS_PIN0,ADCCH_NEG_NONE,1);
adcch_set_input(&adcch_conf,ADCCH_POS_PIN1,ADCCH_NEG_NONE,1);
adcch_set_input(&adcch_conf,ADCCH_POS_PIN2,ADCCH_NEG_NONE,1);
adcch_set_input(&adcch_conf,ADCCH_POS_PIN3,ADCCH_NEG_NONE,1);
```

where ADC_SIGN_ON, ADC_RES_12 and ADC_REF_VCC define the signed mode, 12-bit ADC resolution and $AV_{cc}/1.6$ as voltage reference, respectively. At the same time, for the four different ADC inputs the single-ended mode is chosen (ADC_NEG_NONE).
The ADC transfer in our case becames:

$$RES = \frac{V_{INP}}{V_{REF}} \cdot 2047 \tag{4.2}$$

Two important corrections have to be introduced to adjust the *offset* and the *gain* errors. The offset error is defined as the difference between the current and the ideal

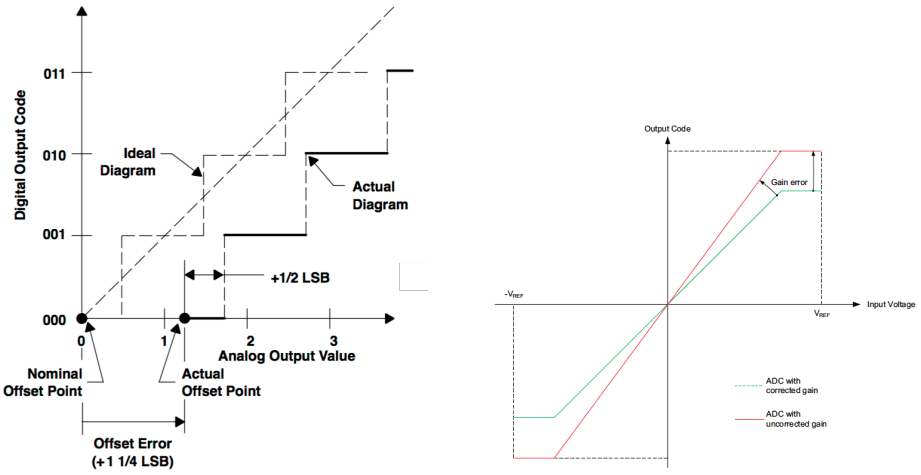

(a) (b)

Figure 4.14: **(a)** ADC Offset correction (Reprinted by [45]) and **(b)** ADC Gain correction (Reprinted by [6]).

offset point, which is the mid-step when the digital output value is zero [45]. This error affects all the output by the same amount and, therefore, it is subtracted from the converted data before writing the result. Instead, the gain error is a deviation of the last output step mid-point from the ideal line [6]; usually this error is corrected multiplicand a GAINCORR value before to write the converted result.

$$RES = (V_{IN} - OFFSETCORR) \cdot GAINCORR \tag{4.3}$$

In Figure 4.14 the two ADC corrections are reported.

4.1.2 Potentiostatic Circuit

4.1.2.1 Potentiostat

As already described in the Chapter 2 (paragraph 2.2.1.1) there are three different configurations for the potentiostatic circuit. In this thesis the *Grounded Working Electrode Configuration* has been implemented (as senne previously, the WE is grounded through a TIA and for this reason is called *Virtually Grounded Working*).

As visible in Figure 4.15, differently from the original working configuration, the circuit is virtually grounded at half value of the power supply ($V_{off} = \frac{V_{cc}}{2}$). This is introduced to allow positive and negative voltages.

The *Transimpedence Amplifier* (TIA) converts the measured current in voltage and it introduces a first stage of amplification enabling the possibility to sense few μA current signals. The resistor R_F has to be dimensioned depending on the input current to avoid saturation (we have chosen $10k\Omega$ and $30k\Omega$ for the two channels),

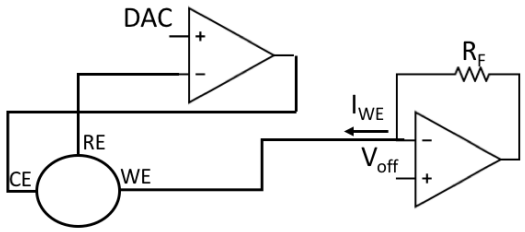

Figure 4.15: Grounded Working Electrode Configuration.

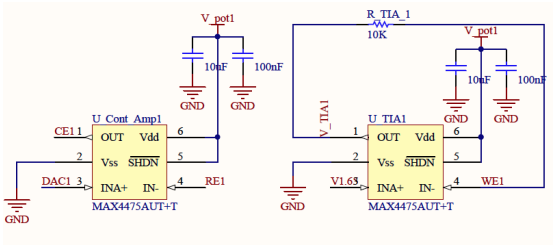

Figure 4.16: Grounded Working Electrode Configuration for the first channel in Altium.

In Figure 4.16 the Altium schematic for Grounded Working Electrode Configuration is shown. Two MAX4475 operational amplifiers have been adopted to exploit their wide-band, low noise and low-distortion properties.

4.1.2.2 Filtering and Offset Blocks

A signal conditioning block is implemented before transmitting the data to the user (Fig. 4.17). In this case two successive steps are implemented: (i) the filtering and (ii) the offset.

In order to eliminate the high frequency noise a 4_{th} order low-pass filter (LPF) is implemented in this circuit. Precisely, a cascade of two 2^{th} order Sallen-Key low-pass filter (Appendix A), with an overall -3 dB cut-off at 200 Hz are used. Figure 4.18 shows the bode diagram of the LPF, with the parametric simulation (using *Wolfram Mathematica 11.3*) of the filter characteristics, providing the sizing of the filter elements.

The offset block introduced at the end of the filtering block applies an offset voltage to the signal, in this way it ensures to exploit all the dynamic of the ADC (see paragraph 4.1.1.2). By considering the circuit (**b**) in Figure 4.17, it is easy to deduce the offset voltage applied to the filtered signal:

$$V_+ = V_{SK}\frac{R_6}{R_6 + R_5} = V_- \tag{4.4}$$

considering $R_6 = R_8 = 100k\Omega$ and $R_5 = R_7 = 39k\Omega$ and applying *Kirchhoff's current law* at the inverter input:

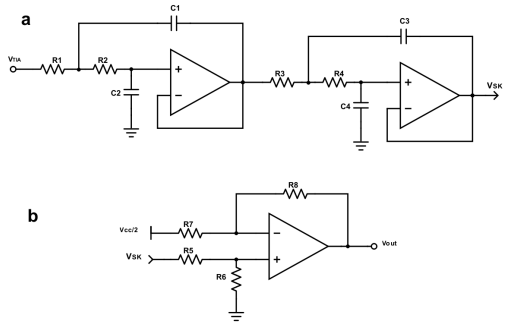

Figure 4.17: Signal conditioning block: **a)** 4_{th} order *Sallen-Key Filter*, **b)** Offset Amplifier.

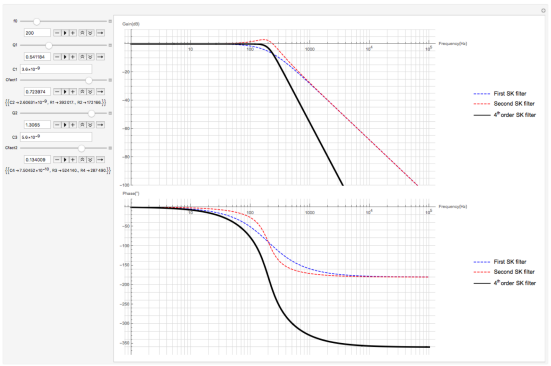

Figure 4.18: Simulation on *Wolfram Mathematica 11.3*: Bode diagram of Sallen-Key filter with sizing of the components.

$$\frac{V_{cc/2} - V_-}{R_7} = \frac{V_- - V_{out}}{R_8} \longrightarrow V_{out} = -\frac{R_8}{R_7} V_{cc/2} + V_{SK} \tag{4.5}$$

Also in this case, the integrated chips we have used are from the Maxime family operational amplifiers: MAX4477 includes two Op-Amps to perform the Sallen-key cascade filter and MAX4475 for the offset block (Fig. 4.19).

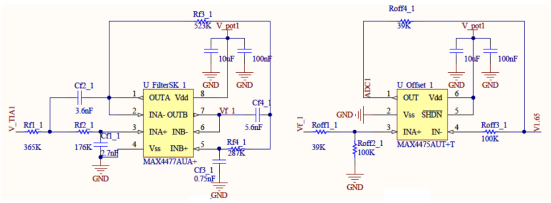

Figure 4.19: Signal conditioning block in Altium.

4.1.2.3 DAC

The potentiostat applies programmable voltage waveforms to the sensor. This is possible thanks to a Digital-to-Analog-Converter (DAC) before the control amplifier module. The DAC is driven by the micro-controller and it converts the received digital input into an analog voltage and applies it to the non-inverter input of the op-amp. The MCP4911 (Fig. 4.20) was used as a single channel voltage output 10-bit DAC device [73]. This microchip operates with a single supply voltage from 2.7 V to 5.5 V (in the present case, the supply voltage is $V_{cc} = 3.3V$) and with a SPI compatible interface which allows the communication with microcontroller. It is common and recommended to use a bypass capacitor of about $0.1\mu F$ (ceramic) to ground and also an additional $10\mu F$ capacitor (tantalum) in parallel to further attenuate high-frequency noise which might be introduced in the application boards.

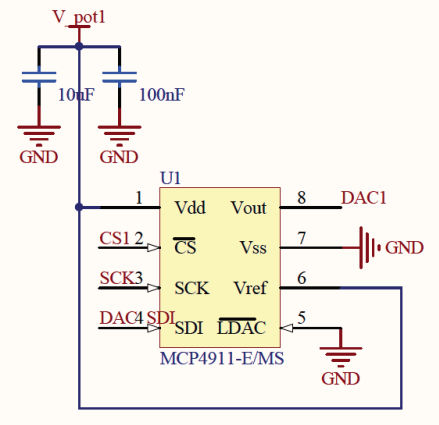

Figure 4.20: The MCP4911 10-bit DAC device in Altium.

The analog output from the DAC is obtained through the Equation 4.6

$$V_{out} = \frac{V_{REF} D_n}{2^n} G \tag{4.6}$$

where V_{REF} is the external voltage reference, D_n is the DAC input code (signal which arrives from the microcontroller), G is the Gain Selection (1 for $<\overline{GA}>$ bit =1 or 2 for $<\overline{GA}>$ bit =0) and n indicates the DAC resolution. For the current use, we have imposed $V_{REF} = V_{cc} = 3.3V$, $<\overline{GA}>$=1 and so G = 1 and n is equal to 10, this means that the ideal output range is from 0V to 1023/1024*V_{REF}. The Gain selection and the V_{REF} defines also the Least Significant Bit (LSB), the ideal voltage difference between two successive codes: $V_{REF}/1024$.

4.1.2.4 Timer/Counters and Waveforms Generation

The ATmega32E5 microcontroller has a set of flexible, 16-bit Timer/Counters (TC). Through them it is possible to generate waveforms with a fixed frequency and set an accurate program execution timing. **PORTC** has two timer/counter **TCC4** and **TCC5**, while **PORTD** has only one timer/counter **TCD5**.
TCC4 and TCC5 lead cells 1 and 2, respectively and allow to generate triangular waveform and a ramp up pulse, for CV and DPV measurements; while TCD5 is employed for the potentiometric cells and defines the start and stop measurement.
The CPU frequency is of $2MHz$ but with 64 divisions of frequency, the peripheral clock used has a frequency of $2MHz/64 = 31,25KHz$.
For the DPV Measurements a ramp up pulse waveform has to be applied: for a single pulse a first and a second period are defined, the former is at the downstep, while the latter is at the upstep. Each of these periods are divided in "*measurement step*" during which the measurement occurs and an "*hold step*" in which the measurement is kept. An example of DPV parameters to obtain a ramp up pulse waveform is listed in Table 4.1.

Table 4.1: Set of parameters for DPV Measurments.

DPV Measurements		
Start_V (mV)	**End_V** (mV)	**Step_V** (mV)
-100	1100	3.22
Pulse_Width (ms)	**Pulse_Ampl** (mV)	**Pulse_Period** (ms)
50	60	68

Instead, for the triangular waveform required by the CV Measurements a "*sampling period*" has to be imposed, this is the duration of the voltage plateau for each step, and

also the "*voltage step*" is needed which defines how much each step increases. Also here an example of CV parameters is shown in Table 4.2.

Table 4.2: Set of parameters for CV Measurments.

CV Measurements		
Start_V (mV)	**End_V** (mV)	**Step_V** (mV)
-100	1100	3.22
Samp_Period (ms)	**Scan_Rate** (V/s)	
32	0.1	

The stop measurement signal is set providing a value of 512 to the DAC: indeed, remembering that the TIA has a non-inverting input of $\frac{V_{cc}}{2}$ and that the measurment has to finish when the voltage at the WE is equal to the applied voltage, to have 0 V as difference between RE and WE voltage, the applied voltage must match $\frac{V_{cc}}{2}$. In digital values, this means that half of the whole dynamic of the DAC has to be imposed, exactly 512.

For the potentiometric measurements only the "*measurement step*" and "*hold step*" are defined to start the measurement and keep it.

4.1.3 Potentiometric Circuit

4.1.3.1 Potentiometer

The circuit for the potentiometer consists of two parts shown in Figures 4.21 **(a)** and 4.22 **(a)** and presented in the Chapter 2 (paragraph 2.2.1.2): (i) a voltage buffer with high input impedance is connected at each terminal of the cell (MAX44242 buffers with up to $0.5\mu A$ bias current are used as in Fig. 4.21 **(b)**) and (ii) a differential amplifier with a gain of 2, along with an offset shift of 1V (MAX4475 chip is used as differential amplifier, visible in Fig. 4.22 **(b)**).
At the end of these two blocks, the signal is amplified to exploit the whole dynamic range of the successive stage, the ADC.

Before the analog conversion of the digital signal, a filtering block has been introduced also for the potentiometric measurements. The same 4^{th} order low-pass Sallen-Key filter is used (block **a** in Fig. 4.17 with the same features as previously described).

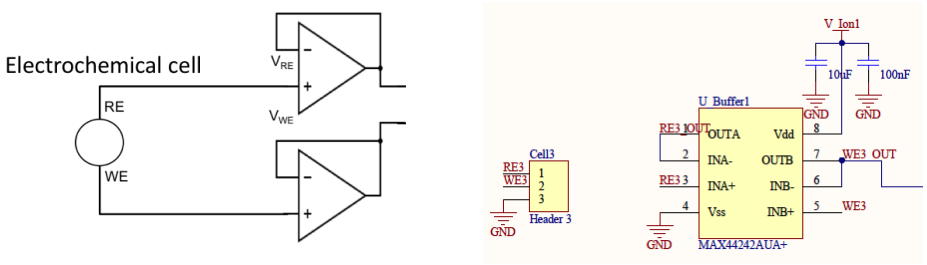

(a) (b)

Figure 4.21: Voltage buffers for potentiometric cells **(a)** and corrispondent MAX44242 component in Altium **(b)**

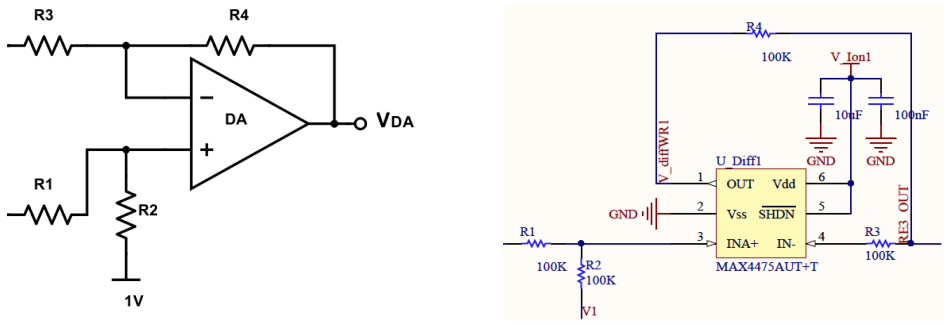

(a) (b)

Figure 4.22: Differential amplifier with 1V offset voltage **(a)** and MAX4475 operational amplifier for differential block in Altium scheme **(b)**.

Figure 4.23: LIR2477 button cell battery.

4.1.4 Power Supply

All the system is powered by a button cell rechargeable battery, the LIR2477 (Fig. 4.23), which is a popular, high quality, long life $3.6V$ variety of lithium coin cell from Conrad energy supplier. In Table 4.3 the main features of this battery are described.

A diode has been added in the circuitry after the battery to protect from power inversion. The power supply block includes also a great number of voltage regulator MCP1801 devices, one for each independent block (μC, potentiostat of cell 1, potentiostat of cell 2, potentiometer of cell 3, potentiometer of cell 4 and bluetooth module); they belong to the family of Complementary Metal-Oxide Semiconductor (CMOS) *Low Drop Regulator (LDO)* regulators. This device is used for applications that need low current consumption, but have to ensure an output voltage regulation. The operating voltage range is from $2.0V$ to $10.0V$; in this case the output voltage is fixed to $3.3V$. The LDO output is stable with a minimum of $1\mu F$ of output capacitance.

Table 4.3: Technical Data of a Lithium Conrad energy LIR2477 Button Cell.

Category	Button cell (rechargeable)
Size	LIR2477
Voltage	$3.6V$
Capacity	$180mAh$
Technology	Lithium
Height	$7.7mm$
Diameter	$24mm$
Content	1 pc(s)
Rechargeable	Yes

A typical LDO configuration is shown in Figure 4.24. A general recommendation is usually to split the PCB plane into an Analog plane and a Digital plane, in order to not overlap each other and to minimize capacitive coupling (Fig. 4.25). For this reason a power supply decoupling circuit is recommended: the MCP1801 creates this safe interface between digital and analog signals. To optimize this interface some main rules have to be respect (Fig. 4.26) [1]:

- A large electrolytic capacitor (10 μF - 100nF) should be placed close to the chip: it is a reservoir of charge to answer to an instantaneous request of supply;
- A smaller capacitor (1 μF) should be placed close to the power pins: it cuts the high frequency noise;
- A small ferrite bead in series with the supply pin can be placed: it allows to localize the noise in the system and to keep external high frequency noise from the circuit.

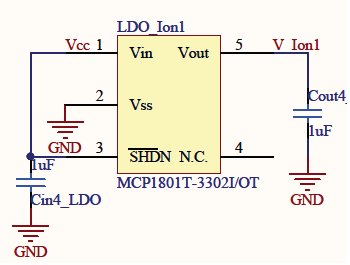

Figure 4.24: An example of LDO configuration for power supply in Altium.

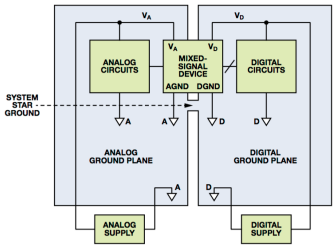

Figure 4.25: Mixed-Signal ICs: single PCB with analog and digital signals (Reprinted by [106]).

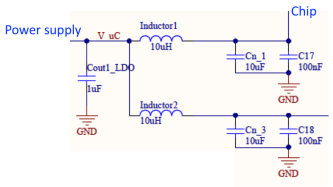

Figure 4.26: Decoupling techniques needed to reduce noise at analog/digital interface (from Altium scheme).

4.1.5 Bluetooth Module and Wireless transmission

The wearability and the portability of the monitoring system is fueled by the possibility to transfer wirelessy the data and to interface with the user. Hence, the

BLE module is a very important component of the circuit. The RN4677 device has been selected for this aim since it is a complete, fully-certified Bluetooth 4.0 (Basic Rate (BR)/Enhanced Data Rate (EDR)/Low Energy (LE)) module. LE is an important characteristic of this chip since it can maintain a low-power wireless connection, in this way it can ensure a longer lifetime of the battery, which represents an pivotal characteristic for wearable devices. A serial communication between the μC and the RN4677 is used by UART interface.

To start measurement, acquire data and stop the process, the user has to give the input

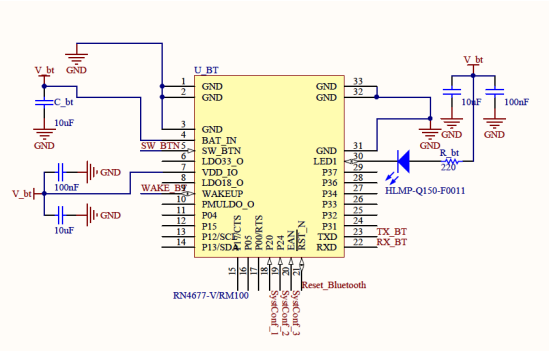

Figure 4.27: RN4677 Bluetooth module configuration in Altium schem.

to bluetooth module which communicate by UART with the μC. For that purpose, a Graphical User Interface (GUI) has been developed in Matlab. The communication between GUI and FPCB is done through the serial port of the host computer and of the Microcontroller Unit. For the initial board validation, an USB to RS232 levels serial UART converter cable is connected from the computer to the UART module. The latter is a level shifter and inverter that converts RS232 levels into [0;3.3] V, that are the voltage levels of the MCU. It limits also the current output by the host computer. RN4677 can operate in two modes: Data mode (default) and Command mode. Here the defaulf configuration is used. When a bluetooth module is connected to another device acts as a data pipe, and so anything received from UART (from μC in this case) is transferred to the connected device through Serial Port Profile (SPP) if is a Bluetooth Classic device, or via Generic Attribute Profile (GATT) service if is a BLE device. This BLE connectivity provided by the dual mode RN4677 bluetooth module is named "*Transparent UART*" and is used to establish a wireless communication between the FPCB and the GUI. When RN4677 is connected to a computer and a serial port, some port settings are imposed:

- baud rate of 115200 bps;
- 8 bits;
- No Parity bit;

- 1 stop bit;
- Hardware flow control disabled.

The communication starts when a request is made by the user: he can ask either to start a measurement, or send the data, or acquire the signal, or stop the transmission of data or stop a measurement. At first a setting byte has to be sent in which the selected electrode and electrochemical technique are chosen.
Figure 4.28 shows the main screen of the interactive interface with the multiple possible choices for the user:

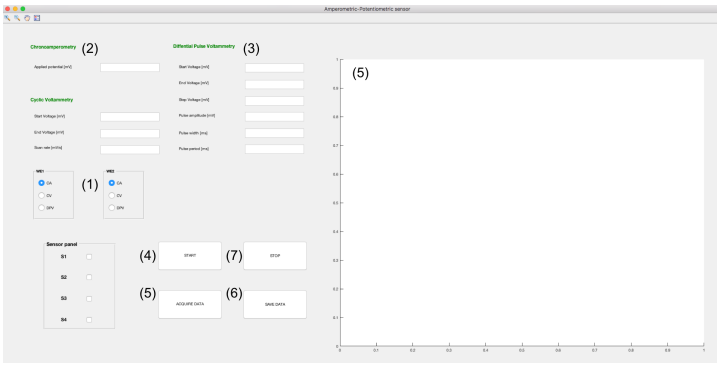

Figure 4.28: GUI developed in Matlab for setting and colletting data for electrochemical measurements: **(1)** select the interested sensor, **(2)** set the CV parameters (*start voltage*, *end voltage* and *scan rate*), **(3)** set the DPV parameters (*start voltage*, *end voltage*,*step voltage*, *pulse amplitude*, *pulse width* and *pulse period*), **(4)** start measurement, **(5)** request for acquiring data and plotting them in the panel in real-time, **(6)** save the data in an Excel sheet for processing, **(7)** stop measurement.

When the user choice is defined at the GUI and wireless transmitted to the Bluetooth module, an UART interface ensure the transfer of the info to the microcontroller for the effective command execution.

4.2 Analysis of Noise and main challenges in mixed signal design

An important aspect, which is needed to consider, is that the circuit realized interfaces an electrochemical cell and so is continuously in contact with an electrolyte solution. This means that, for the analysis of noise, not only the **elctronic noise** has to be evaluate, but also the noise caused by interfering molecula which can react at the electrode surface and produce **chemical noise** [90]. The bio-sensign system can be equaled to a typical mixed circuit system (Fig. 4.29), indeed at electrode interface a chemical signal is converted in electrical one, and a current or voltage has to be read

from the electrode (Sensing). At the same time, a parallel circuit has to be implemented to apply the specific voltage waveform to make sure that the RedOx reaction occurs (Actuating). For this reason, it is needed to talk about the main challenges and problems of interferences and noise due to the development of a mixed-signal circuit.

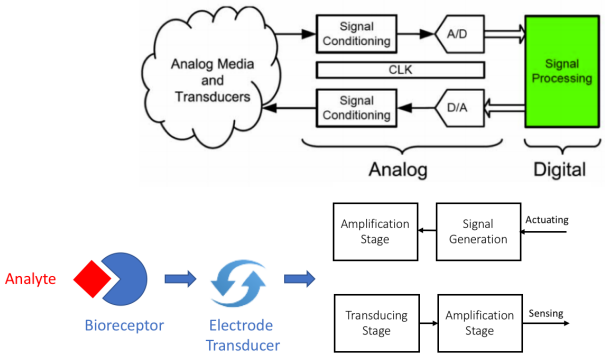

Figure 4.29: A parallelism between a typical mixed signal system and a bio-sensor interface (Reprinted by [59]).

At first, the constrains due to the analog components have to be considered. The main analog circuit trade-off are: *Speed* and *Accuracy*. While for the speed a linear relation with power dissipation exists (power grows linearly with the speed), the relation with the precision is more complex. In Figure 4.30 these trade-off are sketched: power dissipation has a fundamental relation with the speed and the noise, instead is non-fundamentally related to the matching and linearity constrains. The noise, component matching and linearity are the three categories in which the accuracy can be divided. It is common semplifying the system and considering only the noise as a fundamental drawback for the accuracy relation with the power dissipation.

In a bio-application, usually the output signal is due to the sum of three components:

$$I_{out} = I_f + I_c + I_n \tag{4.7}$$

- I_F is the only Faradaic contribution and so the only signal that has real information about the analyte concentration;

$$I_F = \frac{nFA\sqrt{D}}{\sqrt{\pi t}} \cdot C \tag{4.8}$$

- I_C is the non-Faradaic capacitive current due to the characteristic of electrode interface, there are some specific electrochemical techniques which can remove

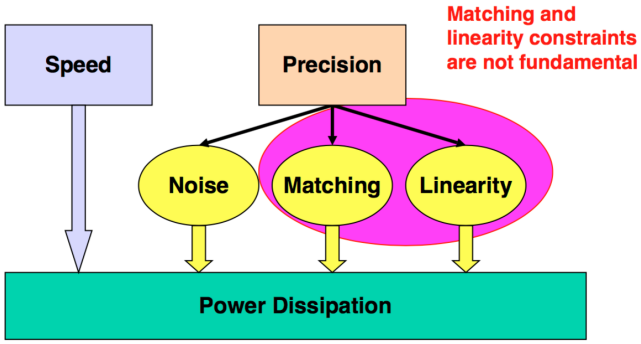

Figure 4.30: Analog circuit trade-off: power disspipation is directly related to the speed and the noise, while there is a non-fundamental relation with component matching and linearity (Reprinted by [58]).

this contribute (e.g. *Differential Pulse Voltammetry*);

$$I_C = \frac{1 + jwC_{DL}R_L}{R_L} \cdot V_{ref} \tag{4.9}$$

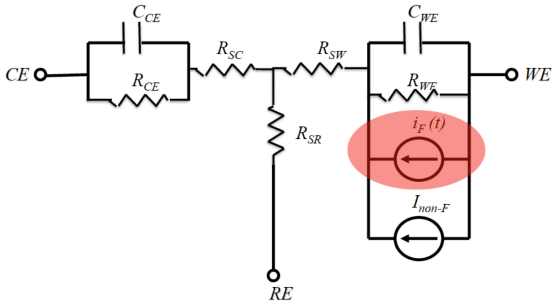

Figure 4.31: Faradaic and non-Faradaic contribution at eletrode interface (Reprinted by [16]).

- I_n is another non-Faradaic current that corresponds to the total noise in the output signal and is determined by three different noise sources:

$$I_n = I_{thermal} + I_{shot} + I_{flicker} \tag{4.10}$$

  - $I_{thermal}$, defined as *thermal noise* (*Johnson-Nyquist noise*), is the electronic noise due to the thermal agitation of electrons, within electrical conductors, generated when a voltage is applied [42].
    The mean squared value of this noise is:

$$< V^2 >= 4RkT\Delta f \tag{4.11}$$

    where R is the resistance of the conductor, k is *Boltzmann's constant*, T is the absolute temperature, and Δf is the bandwidth of the measurement instrument.

– I_{shot}, named *shot noise*, is due to the fluctuations in current and originates from the discrete nature of electric charges [42].
The corrispondent to the previous one mean squared value for the shot noise is:

$$< {i_{sh}}^2 >= 2ei_{dc}\Delta f \tag{4.12}$$

where e is the charge of the electron, i_{dc} is the average current and Δf is the bandwidth of the measurement instrument.

– $I_{flicker}$, known as *flicker noise*, is the main noise source which has a dominant effect in term of signal destruction at low frequencies. Indeed there is a $1/f$ dependence from the frequency, and this means that lower is f higher is the noise:

$$I_{flicker} = \frac{A}{f} \tag{4.13}$$

This is extremely important if we consider an electrochemical measurement in which the current signals is the order of pA in the kHz bandwith.

After this noise analysis, to obtain a good mixed-signal circuit some important warnings have to be kept in mind: (i) reducing the noise generation, (ii) isolating sensitive circuits and (iii) making analog components more noise-tolerant (high CMRR, Power Supply Rejection Ratio (PSRR) and minimum BandWidth).

In conclusion, it is very difficult to ensure good results for a electronic circuit because there are many aspects which have to be kept in mind: it is important to examine the constrains, noise sources and signal amplitudes. More attention is required when the electronic circuit has to guide an electrochemical cell and so we have a Bio-CMOS interface: indeed if the circuit is not completely co-designed and correctly integrate with the transducer, also high performance of the circuit could not guarantee good results.

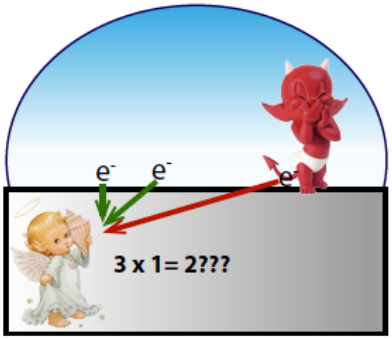

Figure 4.32: Cartoon animation which rapresents a bad Bio-CMOS interface when undesirable agents corrupt the output correct signal.

Chapter 5

Amperometric Measurements: L-Lactate Detection

Metabolites detection has relevant importance since it is possible to extract important information about physical conditions, organism metabolism and possible presence of illness. To the aim of this thesis, lactate has been already introduced in the Chapter 1 as important metabolite in the context of sport medicine ([43], [84]), shock trauma [98] and food industry [69]. For this reason, its detection is of great interest, and different sensing methods have been already inaugurated and improved. Traditional analytical methods, such as High Performance Liquid Chromatography (HPLC) [104], Fluorometry [39], Colometric Test [65] and Chemiluminescense [102] suffer from several drawbacks in terms of machinery costs, no portability and long duration of the exam. Therefore, novel approaches have been required by the market. Electrochemical biosensors represent an innovative solution to overcome these limitations and to ensure reliability, portability, high-specificity and low costs of production and treatment. In particular, amperometric biosensor, which measures the current produced by the oxidation or reduction of the target analyte as consequence of the excitation potential waveform (fixed or variable voltage) applied to the electrochemical cell, has been shown to be suitable for lactate detection [78].

5.1 Electrochemical Detection of L-Lactate Concentration

Lactic Acid (right side in Fig. 5.1) is an organic compound $C_3H_6O_3$ which is ionized in proton lactate (left side in Fig. 5.1) in the human body.

As seen in the Chapter 2, the detection of many compounds require more selective electrochemical biosensors which can be realized by performing a functionalization

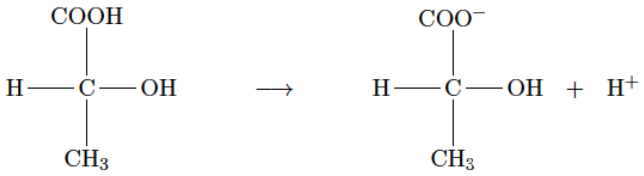

Figure 5.1: Deprotonation of Lactic Acid (right side) in Lactate (left side).

process with a specific recognition element, for example the enzyme. Indeed, for the electrochemical detection of lactate, the WE has to be covered by a bio-layer of enzyme in order to let the redox reaction to occur.
Enzymes are proteins which catalyze biochemical reactions by increasing the speed while decreasing the energy, as shown in Fig. 5.2 [77].

The molecules with which the enzyme acts are called *substrates*: the first step is

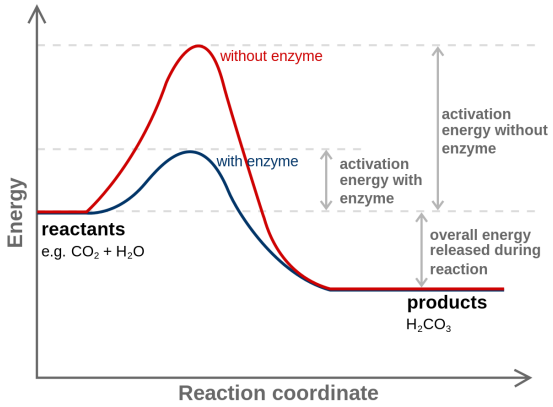

Figure 5.2: Example of readox reaction: variation of the activation energy level with and without the enzyme (Reprinted by [20]).

characterized by the recognition between the substrate (S) and the enzyme (E), at this point S and E creates the ES group; afterwards the S is converted in product (P), which initially remains combined with the enzyme as EP group; the last step requires the split of the EP group with the formation of the final P and the E returns at its original form.

$$E + S \leftrightarrow ES \leftrightarrow EP \longrightarrow E + P \tag{5.1}$$

Enzymes involved in the lactate detection can be divided in two types: *L-Lactate Dehydrogenase (LDH)* and *L-Lactate Oxidase (LOD)*.

L-Lactate Dehydrogenase (LDH) LDH is a quaternary protein which is present in all living cells of animals, plants, and prokaryotes. It is an important enzyme that plays a fundamental function in the clinical diagnosis of pathologic processes [60].
In this thesis, LDH has been considered for the significant role that it performs in the

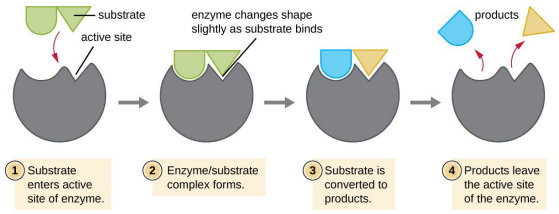

Figure 5.3: The active site of the enzyme and the changing in the binding of ES and EP complexes with successive formation of the final product. (Reprinted by *OpenStax College, Biology, CC BY 3.0.*)

Lactate detection. This enzyme catalyzes the conversion of Lactate to Pyruvic Acid and viceversa; furthermore, it also converts NAD^+ to NADH and viceversa.

$$Lactate + NAD^+ \xrightarrow{LDH} Pyruvate + NADH + H^+ \tag{5.2}$$

As shown in the Reaction 5.2, this enzyme works in presence of a co-enzyme found in all living cells: *Nicotinamide adenine dinucleotide*, simply indicated as **NAD**. This co-enzyme can exist either in the oxidized form NAD^+ or in the reduced form NADH. Its main function is to facilitate the electrons transfer: during the metabolism, in presence of LDH, this co-enzyme is involved in the redox reaction and it generates a flow of electrons proportional to the L-Lactate concentration in the solution. Indeed, the occurring RedOx reaction that has to be evaluated during an electrochemical measurement is described in 5.3:

$$NADH \longrightarrow NAD^+ + H^+ + 2\,e^- \tag{5.3}$$

Lactate Oxidase (LOD) LOD is a globular flavoprotein deriving from a great variety of bacteria, as Pediococcus, Mycrobacterium smegmatis and Aerococcus viridans [55]. The main catalytic function of this enzyme is the oxidation of L-Lactate to Pyruvate in the presence of dissolved oxygen (O_2) with successive production of Hydrogen Peroxide (H_2O_2), as shown in the Reaction 5.4.

$$Lactate + O_2 \xrightarrow{LOD} Pyruvate + H_2O_2 \tag{5.4}$$

This enzyme is immobilized on the electrode surface where the electrochemical reaction occurs and the measured current is proportional to the L-Lactate concentration. In this case the information is given by the second product of the first reaction, *e.g.* the H_2O_2, which is electrochemically activate. It can be either reduced or oxidized, and the current derived from its RedOx provides the desired information on the lactate concentration.

$$H_2O_2 \longrightarrow O_2 + 2\,H^+ + 2\,e^- \tag{5.5}$$

Both of LDH and LOD enzymes can be involved in the realization of biosensors for lactate detection. However, both of them present some drawbacks due to, for example, the needed of the presence of the coenzyme in case of LDH, or the fluctuations in the oxygen concentration that affect the measure in case of LOD. Furthermore, the reaction which occurs presence of LOD enzyme might be affected by interfering problems due to other species in the solution. This is due to the fact that the H_2O_2 requires a high oxidation potential suitable also for other electrochemical species.

The possibility to choose the immobilization of two different enzymes and the wide variety of immobilization techniques, we allow to sweep among a great number of lactate biosensors, finding for each ones positive and negative aspects.
Below a comprehensive overview on the biosensors based on the electrochemical lactate detection is shown. This will include a description of different techniques for enzyme immobilization and a state-of-art of the already presented lactate biosensors.

5.2 Biosensor for L-Lactate: state-of-art

Enzymatic biosensors have been highly improved in terms of enzyme immobilization, stability and selectivity. Three deferent biosensor generations can be identified and recognized within the recent years (Fig. 5.4) [74]:

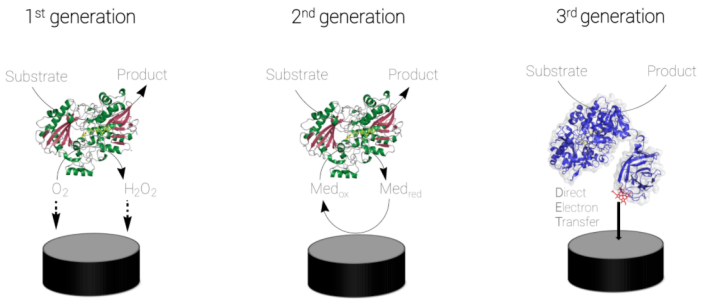

Figure 5.4: Summarizing sketch of the first, the second and the third generation of enzymatic biosensors (Reprinted by *directsens Biosensors*).

- 1^{st} ***Generation Biosensors***: in the first generation the enzyme is placed close to the electrode's surface. The substrate is not in direct contact with the electrode; hence, after the recognition, the enzyme produces an additive species that is involved in the redox reaction and that produces current proportional to the

analyte concentration (biosensor based on the LOD immobilization belongs to this class of sensors);

- 2^{nd} ***Generation Biosensors***: the second generation is born to overcome issues of the first one, as for example the high potential required by the H_2O_2 in the LOD biosensor. A synthetic mediator is immobilized on the electrode surface and it replaces the second chemical species needed for the catalytic reaction (e.g. O_2). These mediators oxidize at lower potentials and, in this way, the interferences due to the other species decrease. The mediator may be dissolved in the solution or immobilized on the electrode's surface;

$$Substrate + Mediator_{oxidized} \xrightarrow{enzyme} Product + Mediator_{reduced} \tag{5.6}$$

$$Mediator_{reduced} \longrightarrow Mediator_{oxidized} + \mathrm{ne}^- \tag{5.7}$$

- 3^{rd} ***Generation Biosensors***: in the last biosensors generation, the enzyme is immobilized directly onto the electrode surface or into an adjacent matrix, such as a conductive polymeric matrix. Some different immobilization techniques can be used [78]:
  - *adsorption*;
  - *membrane confinement*;
  - *covalent binding*;
  - *cross link formation*;
  - *electrical polymerization*;
  - *monolayer formation by self-assembly*;

Starting from the different immobilization techniques and analyzing the wide variety of supports which can be employed, a Lactate biosensors classification can be useful. Figure 5.5 shows the main electrode supports for the immobilization of LDH or LOD for lactate detection.

1. ***Screen Printed Electrode (SPE) Based***
   This type of sensors are realized by using a Screen Printed Electrode; a chemically inert substrate that hosts on its surface the three-electrodes printed using screen printing strategies. Usually the reference and counter electrodes are used in their original form, while the working electrode can be funtionalized, as in the case of lactate detection. Several immobilization techniques of SPE have been already studied and improved during the years, to improve the stability and the signal from the detection. Some examples are listed below.
   As an example, in [69] Multi-Walled Carbon NanoTubes (MWCNTs), Nafion,

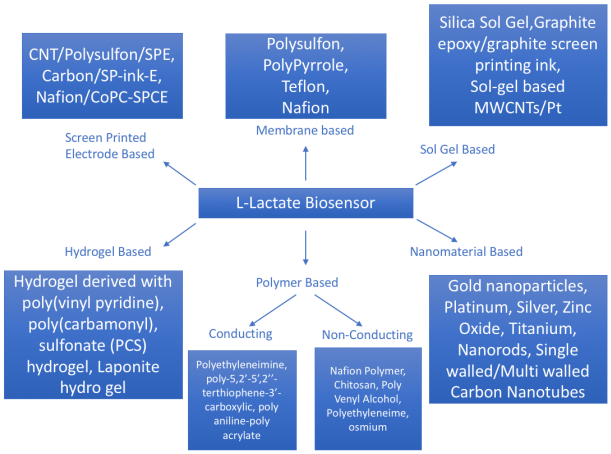

Figure 5.5: Different electrode supports available for the enzyme immobilization on the WE for lactate detection (Reprinted by [78]).

PolySulfone (PS) and FerroCene (FC) membranes were further deposited onto a Carbon SPE to facilitate and augment the incorporation of LOD and Horseradish Peroxidase (HPR) enzymes, as shown in Fig. 5.6.**a**; in [68] a Nafion membrane has been deposited on a Platinum SPE with a LOD enzyme immobilization layer realized by a prepolymer and Polyethylenimine (PEI), as in Fig. 5.6.**b**; in [28] a Carbon SPE has been modified with both HPR and LOD enzymes, shown in Fig. 5.6.**c** and in [88] a Carbon SPE has been functionalized with Cobalt Phthalocyanine (CoPC-SPCE) and coated with a Nafion layer, the LOD enzyme was immobilized using a polymer matrix of denatured polyvinyl alcohol, in Fig. 5.6.**d**.

2. ***Membrane Based***
   Electrode surface can be functionalized with membranes characterized by different porosities that facilitate the attachment of the enzymes. This type of immobilization may increase the stability, extend the lifetime of the biosensor and also prevent from the loss of the enzyme. For example, a Nafion membrane with Mucin/Albumin hydrogel was placed on a platinum electrode, where a LOD matrix has been previously immobilized [82] (Fig. 5.7.**a**) or a hydrophilic porous membrane was used to cover a mesoporous silica (FSM8.0) formed on a screen-printed Prussian Blue (PB) modified electrode and the LOD enzyme was immobilized on it [89] (Fig. 5.7 (**b**)).

3. ***Sol-gel Based***
   The enzyme is trapped and immobilized in a porous and transparent gel matrix. It allows the immobilization by the presence of an organic or an inorganic orthosilicate: a network of sol-gel is created around the enzyme and ensures the stability.

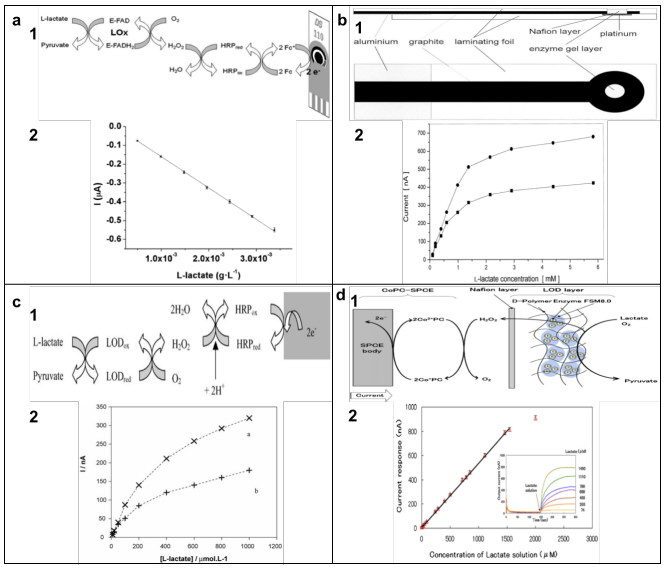

Figure 5.6: **a 1)** Functionalized SPEs and specific reactions involved for the lactate detection, **2)** L-Lactate calibration curve (Reprinted by [69]). **b 1)** Schematic diagram of functionalized platinum SPE with top view and longitudinal section, **2)** L-Lactate calibration curve with different Nafion concentrations (Reprinted by [68]). **c 1)** Functionalization of SPE and LOD enzyme reaction, **2)** L-Lactate calibration curve with (a) and without (b) LOD enzyme (Reprinted by [28]). **d 1)** Enzyme preparation of electrode surface, **2)** L-Lactate calibration curve and current-time curve in the inset (Reprinted by [88]).

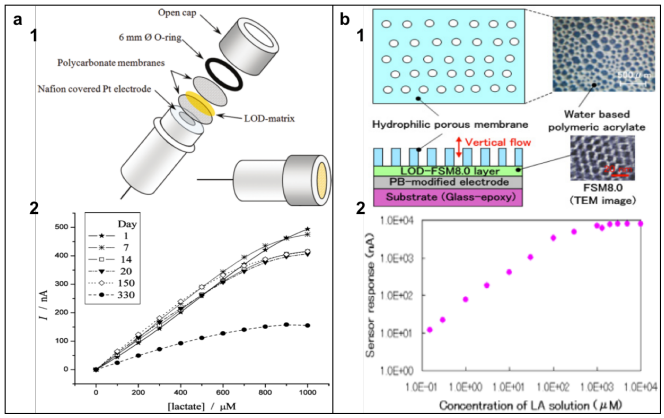

Figure 5.7: **a 1)** Scheme of construction of a lactate biosensor with immobilization of LOD enzyme between polycarbonate membranes, **2)** Calibration curve of lactate biosensor exposed to different lactate concentrations (Reprinted by [82]). **b 1)** Scheme of the HPM/LOD-FSM8.0/PB-SPCE biosensor, **2)** Calibration curve of the sensor (Reprinted by [89])

.

Previous works about this type of biosensor are: (i) a LOD enzyme immobilized in a sol-gel matrix formed by alkoxysilanes on a Prussian Blue modified electrode [103]; (ii) a sol-gel membrane ((3-aminopropyl)trimethoxysilane (3-APTMS), 2-(3,4-epoxycyclohexyl)ethyl-trimethoxysilane (EE- TMS), polyethylene glycol 6000 (PEG 6000) and deionised water) was placed on a platinum working electrode containing Teflon [70].

4. ***Nanoparticles (NPs) Based***
   A great improvement for the lactate biosensors development has been introduced by nanomaterials-based electrodes [44]. Indeed, several different NPs has been investigates, as Zinc Oxide nanostructures (ZnO) in Fig. 5.8) by [61] or Au and Pt NPs by [92]. NPs enhance the electrical binding of LDH or LOD enzymes providing great advantages in terms of stability, sensitivity and increase of the electro-active surface area.

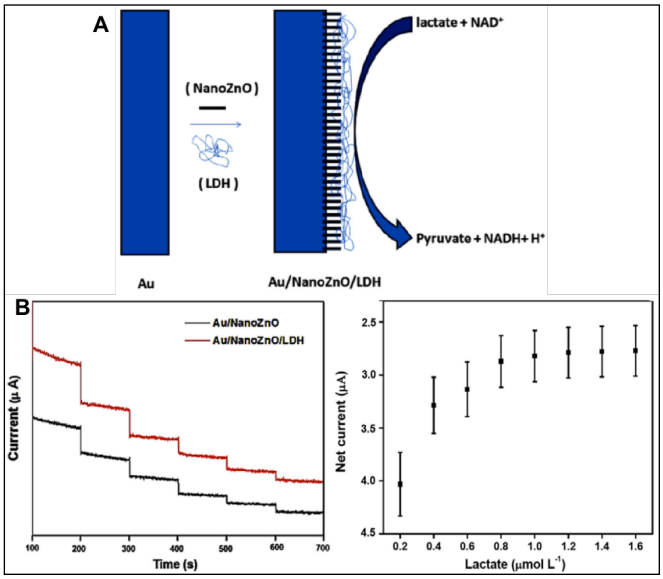

Figure 5.8: **A** LDH immobilization on NanoZnO modified gold electrode **B** Amperogram with and without LDH on the electrode and calibration curve for different lactate concentrations (Reprinted by [61])

.

5. ***Polymeric Matrices Based***
   Polymers can represent an important group of materials, since they can create a selective coating on the WE and reduce the risk of interferences from other species. They are flexible, biocompatible and cheap.

   - *Non-conducting polymer matrices based*: (i) a chitosan/PVI-Os(polyvinylimidazole-Os)/CNT(carbon nanotube)/LOD (lactate oxidase) network nanocomposite

was placed on a Au electrode [22]; (ii) a glass substrate covered by MWCNTs and LOD enzyme is immobilized in a Chitosan sandwich (Fig. 5.9) [57].

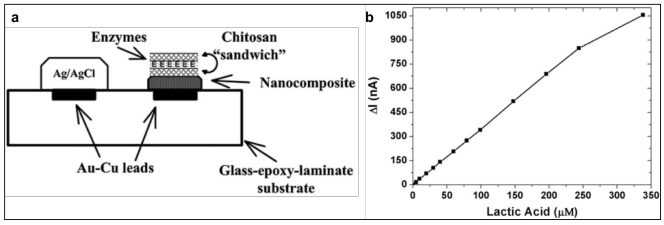

Figure 5.9: **a** Sketch of functionalization of electrode with chitosan sandwich structure and **b** L-Lactate calibration curve increasing the concentration at each injection (Reprinted by [57]).

- *Conducting polymer matrices based*: (i) biosensor based on pTTCA/MWCNT with LDH and NAD^+ immobilized on Au electrode [76] (Fig. 5.10.**a**) and (ii) a Glassy Carbon (GC) electrode with a poly-aniline/poly-acrylate (PANI–PAA) film and LDH enzyme (Fig. 5.10 **b**) [36].

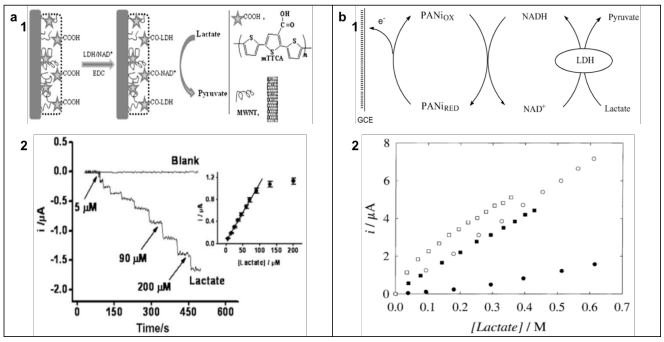

Figure 5.10: **a 1** Schematic representation of the fabrication of pTTCA/MWNT/LDH/NAD^+ Au electrode and **2** Current-time curve with calibration curve in the inset (Reprinted by [76]); **b 1** Functionalization of a GC electrode with PANI-PAA film and LDH enzyme and **2** Lactate calibration curve (Reprinted by [36]).

6. ***Hydrogel Based***

   Also in this case a polymeric matrix is used, but, this time, it creates a three dimensional network where the enzyme is bounded into the polymer chains. These structures are hydrophilic and highly adsorbent and it is possible to distinguish between natural or synthetic hydrogel. An hydrogel-based sensor was realized for lactate detection with the immobilization of three enzyme (salicylate hydroxylase (SHL), l-lactate dehydrogenase (LDH) and pyruvate oxidase (PyOD)) entrapped in poly(carbamoyl) sulfonate (PCS) hydrogel on a Teflon membrane [49].

5.3 Lactate concentration: Blood vs Sweat

Most of the biosensors previously analyzed, were realized and tested for the Lactate detection in blood. However, the determination of lactate in blood implicates some challenges as low accuracy, high costs and need of highly qualified medical staff for the execution of the exams [101]. Nowadays, the request for a non-invasive, inexpensive and easy-to-use solution for the lactate detection is increasing. The research in the last years has been dedicated to study biologic fluids, different from blood, that can be adequate for the lactate detection. It was discovered that, at the end of the metabolism, not only blood has information about lactate, but also the saliva, the urine and the skin excretion (sweat) have [84]. Therefore, they may provide an easier method for evaluating the lactate concentration.
More attention was dedicated for *sweat*. Indeed, sweat is not only simple water solution, but, with different concentration levels, it contains a lot of dissolved salts and compounds, as also the lactate (it is function of the eccrine gland metabolism). Normally, during physical efforts the production of lactate not only increases in the bloodstream, but also in the sweat. The correlation between lactate concentration in sweat and in the whole blood has been investigated before and after a physical test, to understand what is the specific range of detection for each solution [2]. The concentration of blood lactate is usually of 1-2 $mmolL^{-1}$ (1 $mmolL^{-1} = 1\ mM$), but it increases during physical exercise and can reaches values of 20 $mmolL^{-1}$ [66]. On the contrary, sweat lactate concentration can be, on average, 10 times higher then the one in blood. During daily activities, in a healthy human the sweat lactate concentration is in the range of 4-25 mM, but during physical subject it may increase up to 50-80 mM [72].
In 2010 Sakharov's group tested 14 trained athletes in cycling sports before and after their training, defining the lactate concentration ($mmolL^{-1}$) in venous blood, sweat and capillary blood. Venous and capillary blood was collected at the same time. In the venous blood the lactate concentration was measured through spectrophotometry, while the capillary blood was tested through electrochemical methods. The lactate concentration in sweat was measured using screen-printed planar electrode. From this

Table 5.1: Lactate concentration in blood and in sweat [84]

Specimen	Lactate concentration, $mmolL^{-1}$	
	Before Exercise	After Exercise
Venous Blood	3.0 ± 5.0	7.2 ± 0.7
Sweat	20.4 ± 6.7	62.2 ± 16.3
Capullary Blood	1.6 ± 0.5	9.7 ± 1.2

experiment, they discovered that lactate concentration in the whole body does not describe or reflect the intensity of the exercise; for this reason it is more useful to

evaluate the increment of the concentration directly in proximity of the working muscle. Experimental data showed a correlation between the increment of lactate concentration in sweat and in capillary blood (Fig. 5.11).

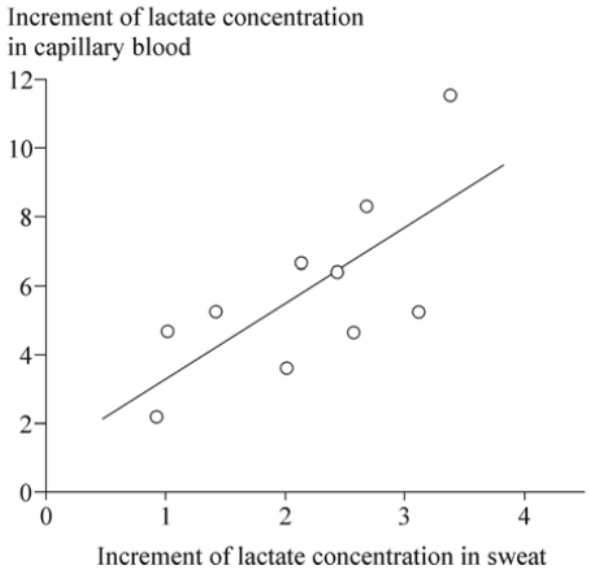

Figure 5.11: Correlation between increment of lactate concentration after exercise in capillary blood and in sweat (Reprinted by [84]).

5.4 Laboratory Experiments: Realization and Validation of Lactate Sensing Platform

In this thesis a complete wearable device able to provide simultaneously information on ions, e.g. lithium, and metabolites, e.g. lactate, concentrations in sweat samples has been realized. To that aim, different lactate electrodes were investigated to provide an optimized solution. In the following Chapter, all the steps and the validation tests performed in laboratory experience will be analyzed in detail.

5.4.1 Materials and Methods

5.4.1.1 Electrode's Preparation

- **Screen Printed Electrode (SPE)** Screen printing technology is used to transfer ink onto a substrate in a precise manner, following an imposted design. It is characterized by great deposition precision and flexibility in the materials; therefore, it is used in several industrial and research applications. One of the possible application is the electrochemical environment. Electrodes manufactured through this technique have great interest because of their easy fabrication process,

which offers an easy-to-use device to be employed in research and in industrial tests [53].
Screen-printed electrodes can be based on carbon, gold, platinum, silver or carbon nanotubes inks. Usually silver ink is used as conductive tracks: an example of fabrication process is shown if Fig. 5.12.**a** where a plastic substrate is covered by silver ink for the tracks, carbon ink is used for both tracks and pads and Ag/AgCl is used for the reference.

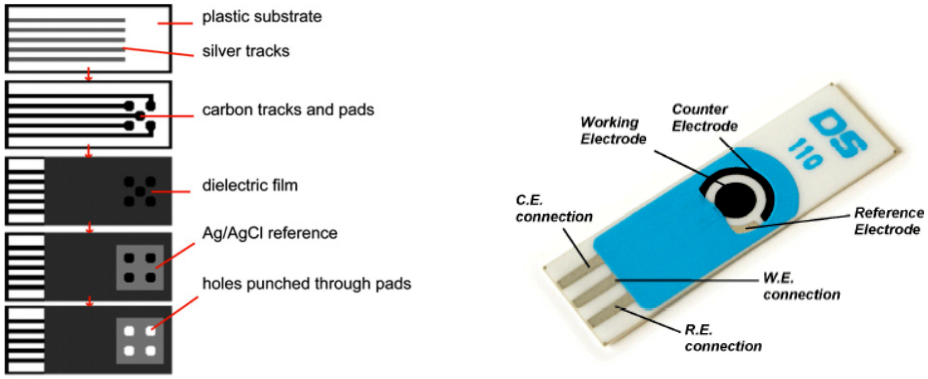

(a) (b)

Figure 5.12: **(a)** Schematic with manufacturing process for a SPE (Reprinted from [53]) and **(b)** Example of a SPE with WE, RE and CE and their related connection (from *DropSens*).

Common SPE configuration is shown in Figure 5.12.**b**,it provides a full electrochemical cell by hosting on its surface the RE, the CE and the RE.
Its working features make the device a low-cost, easy-to-use and ready-to-use solution to be adopted for micro-volumes of sample and for different analysis purposes.

In this work, three different SPEs have been considered and tested (Ceramic substrate: L33 x W10 x H0.5 mm and Electric contacts: silver):

- ***Screen-printed Carbon Electrode***:
  - *Working Electrode*: Carbon (4*mm*)
  - *Counter Electrode*: Carbon
  - *Reference Electrode*: Silver (Ag/AgCl)
- ***Screen-printed Gold Electrode***:
  - *Working Electrode*: Au (4*mm*)
  - *Counter Electrode*: Au
  - *Reference Electrode*: Silver (Ag/AgCl)

– ***Screen-printed Platinum Electrode***:
  * *Working Electrode*: Pt ($4mm$), high or low temperature curing ink
  * *Counter Electrode*: Pt, high or low temperature curing ink
  * *Reference Electrode*: Silver (Ag/AgCl)

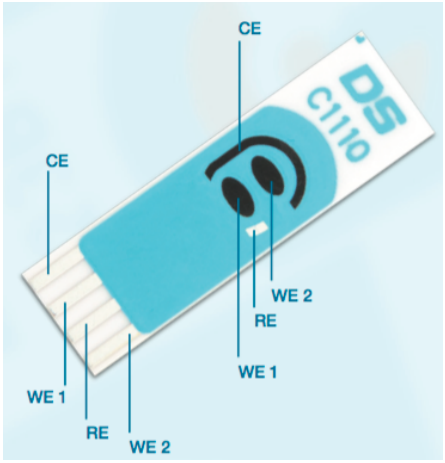

Figure 5.13: C1110 DropSens Electrode (from *DropSens*).

The SPE WE area can be functionalized to make it suitable for a specific detection purpose. The Carbon SPE chosen in this work are in the dual WE configuration, in Fig. 5.13, with two working electrodes on the surface. Therefore, the area of the two WEs is reduced respect to the single configuration, but parallel measurements can be performed, facilitating the comparison.

- **Carbon Nanotube (CNT) Electrode** Carbon NanoTube (CNT) Electrodes are high-quality inkjet-printed sensors where CNTs cover the working and counter electrodes' areas, while the reference electrode is composed by Ag/AgCl. Thanks to their small size and good electrochemical properties CNTs have become very attractive for bio-sensing applications [32]. CNTs are composed by graphene sheets with carbon atoms linked to each other in allotropic (sp^2) form.
  The CNTs can be divided in three categories, according to the number of tubes in their structural form: (i) *Single-Walled CNTs (SWCNTs)* made of only one wrapped graphene sheet (Fig. 5.14.**a**), (ii) *Double-Walled CNTs* composed of two concentric tubes (Fig. 5.14.**b**) and (iii) *Multi-Walled CNTs (MWCNTs)* made of multiple concentric grahene sheets (Fig. 5.14.**c**).

  These CNTs electrodes are printed on transparent plastic (PET) material which ensure great flexibility and re-usability. They are characterized by high conductivity (700 Ω/sq), transparency, homogeneous coating, large surface area, fast

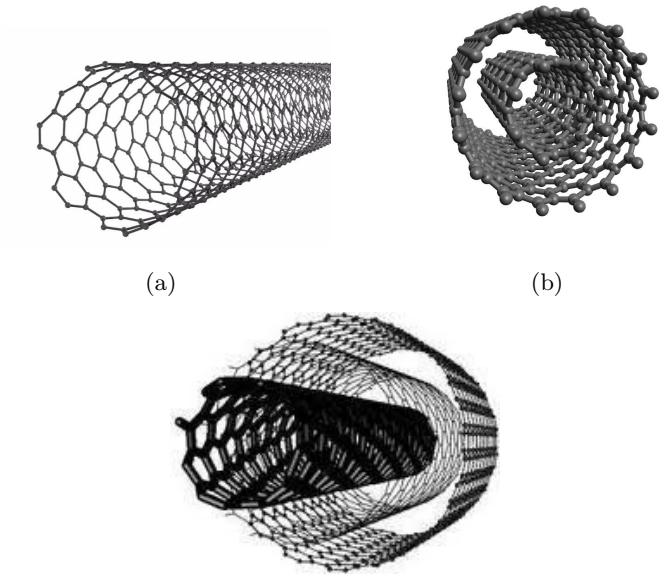

(a) (b)

(c)

Figure 5.14: Example of CNTs: **(a)** Single-Walled CNT, **(b)** Double-Walled CNT and **(c)** Multi-Walled CNT (Reprinted from [41])

electrons transfer (very important for electrochemical measurements) and excellent adhesion and stability. In Figure 5.15 a sample of CNTs electrode is shown; it has with an enhancement of the active area due to the CNTs.

Figure 5.15: Carbon Nanotube Electrodes with indication of WE, CE and RE (from *SENSàSION*).

- **Bamboo Electrode** and ***Pencil Graphite Electrode*** **(PGE)** Bamboo electrode and PGE are two carbon-based electrodes with different properties and features. The first one, in Fig. 5.16, meets the needs of green, renewable and low-cost innovative biosensor [62]. It is characterized by high conductivity and porosity, which improves the surface functionalization of the surface making it more selective for the detection of specific analytes. The second one, in Fig. 5.17, is composed by a super polymer fine leads, extremely break-resistant with HB degree of hardness (from *Faber-Castell* description).

  These electrodes are used as WE; hence it is needed to provide external reference

Figure 5.16: Pyrolyzes bamboo electrode (provided by Politecnico of Turin).

Figure 5.17: Pencil Graphite Electrode (PGE) (from *Faber-Castell*)

and counter electrodes to realize an electrochemical cell.

5.4.1.2 Enzyme immobilization

As described in the paragraph 5.1, there are two different enzymes involved in the lactate detection: *L-Lactate Dehydrogenase (LDH)* and *Lactate Oxidase (LOD)*. For a complete analysis, we have functionalized the biosensors with both enzymes.

- **LDH immobilization** Carbon SPEs (dual WEs) were functionalized with LDH enzyme through polymeric Nafion and Chitosan membranes. Enzyme deposition was performed in three steps:

  1. **Electrode Preparation**: MWCNTs and Nafion solution $(0,5\mu l)$ was deposited by drop casting on the WE, until its complete coverage. Then, WE was covered for 10 minutes by a drop of *Phosphate Buffered Saline (PBS)* (10 mM, pH:7.4) to make the surface hydrophilic. At the end, residue of PBS was removed with a pipette and the electrode was dried by compress air.

2. **Enzyme solution preparation**: $5.5\mu g$ of Lactate Dehydrogenase (purchased from *CalBioChem*) was added to $1ml$ of distilled water and $20\mu l$ of glutaraldehyde (2%).
3. **Enzyme deposition**: drop casting of $40\mu l$ of enzyme solution was performed on the previously modified Carbon SPE. The sensor was kept at $4°C$ in humid atmosphere overnight.

The same procedure was followed for the realization of functionalized electrode with Chitosan instead of Nafion.
Because of different shapes, Bamboo electrodes and PGEs were not functionalized by drop casting. They were dipped in $0.5ml$ of enzyme solution and kept in humid atmosphere overnight.

- **LOD immobilization** Carbon, Pt and Au SPEs were functionalized with LOD enzyme through polymeric Nafion membrane. Enzyme functionalization was performed in three steps:

1. **Electrode Preparation**: a Nafion membrane was realized on the WE by three successive depositions of $1ml$ of Nafion solution (*Nafion perfluorinated resin solution* $5wt.\%$ from Sigma-Aldrich (Switzerland)). Between each deposition, it was waited 20-25 min.
2. **Enzyme solution preparation**: $2.21mg$ of Lactate Oxidase (purchased by ROCHE (Switzerland)) were dissolved in $10.7ml$ of ultrapure water.
3. **Enzyme deposition**: $2ml$ of enzyme solution was dropped on the screen printed Nafion modified working electrode. The sensor was kept at $4°C$ in humid atmosphere overnight.

CNTs, Bamboo and Pencil Graphite electrodes were functionalized by dipping them in the functionalizing solution instead of by drop casting.

5.4.1.3 Lactate Stock solutions prepration

The experiments were carried out by adding multiple injections of $100\mu l$ of lactate stock solution, in PBS and in artificial sweat, in $10ml$ of PBS blank solution. *Phosphate Buffered Saline* (PBS, 10 mM pH 7.4) was prepared using $200mL$ of ultrapure water adding a tablet of PBS, while *Artifical Sweat* (AS) was prepared according to the composition in [46], with compounds listed in Table 5.2 and purchased by Sigma-Aldrich (Switzerland).

Lithium Lactate 95% from Sigma-Aldrich (Switzerland)) was used. Knowing that the Mass Weight (MW) of lactate is of $96.01g/mol$ and that $1mol/l = 1M$, to have

Table 5.2: Composition of Artificial Sweat

Compound	Concentration
NaCL	10 g/L
NH_4Cl	17.5 g/L
Acetic acid	5 g/L
DL-Lactic acid	15 g/L
Ascorbic acid	10 μM
Glucose	0.17 mM
Uric acid	59 μM
Pyruvic acid	0.18 mM
Glutamic acid	0.37 mM
Urea	10 mM

$100\mu l$ of lactate stock solution at $20mM$, $1.9202g$ of Lithium Lactate was added to $10ml$ PBS or AS solution.

5.4.2 Electrochemical Measurements: Amperometric Setup

Chronoamperometry (CA) procedure was performed to test the biosensors for lactate detection. To ensure comparability among all the tested electrodes, RE and CE were set as external, even in the case of SPEs and CNTs electrodes where the three-electrodes configuration is already available. This choice was also advantageous if we consider that the deposition on the WEs was performed manually; therefore, it can not be excluded the risk of errata deposition outside the WE area. Also for this reason, external RE and CE were preferred. During the CA test, a fixed voltage is applied between RE and WE, while a RedOx current is measured. The measured current is plotted over time. The applied voltage for Lactate detection has been set at 650 mV.
The duration of the experiments is not fixed, but depends on the electrode stability: indeed, before starting an electrochemical calibration, the biosensor has to be stabilized and the required time for this stabilization can be also very long. The electrode is stabilized in a blank solution containing only $10ml$ of PBS. Subsequently, an injection of lactate stock solution is added in the PBS volume to evaluate the response of each bio-electrode. For each injection, $100\mu l$ of lactate solution at $20mM$ is added.

To perform these experiments AUTOLAB potentiostat/galvanostat (PGSTAT) is

used, with electrochemistry software *Nova 1.11*.

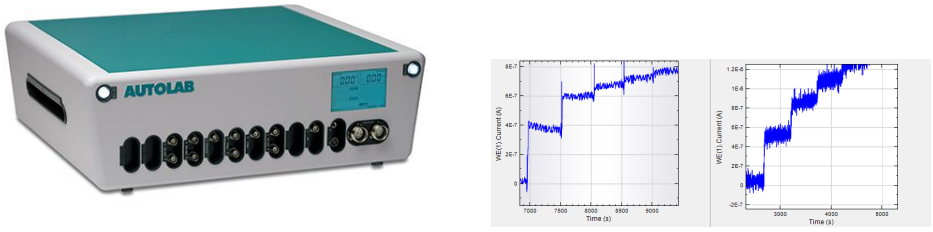

(a) (b)

Figure 5.18: **(a)** Photo of Autolab potentiostat used during the experiments (from *Metrohm*) and **(b)** two screens of the Nova interface during the measurements.

AUTOLAB potentiostat/galvanostat is an electrochemical instrument able to perform both potentiometric and potentiostatic measurements depending on the physical setup of the electrochemical cell and on a specific procedure set on Nova. The electrochemical cell setup for a potentiostatic measurement, where a current is measured while applying a voltage, is shown in Fig. 5.19. The physical cell is connected to the Autolab through five cell cables: (i) Counter Electrode cable, (ii) Reference Electrode cable and (iii) Working Electrode cable which, as indicated by the name, connect the corrispondent electrodes, while (iv) Grounded electrode is a connector which allows to have the same ground between the cell and the potentiostat and a (v) Sense Electrode always connceted to the Working Electrode. Usually, if it interfaces with SPEs an apposite cable is used to connect the electrode to the Autolab's cables.

Nova 1.11 is the software designed to control AUTOLAB instruments with USB

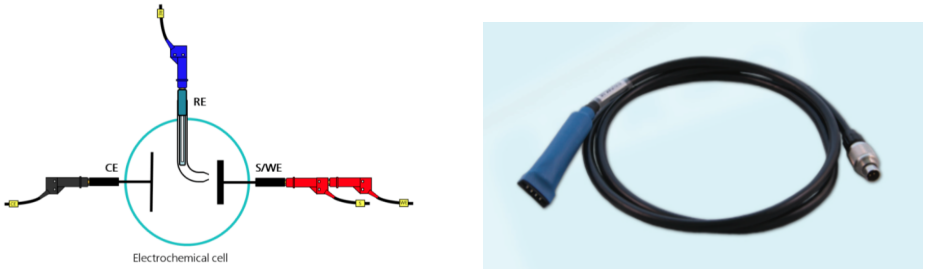

(a) (b)

Figure 5.19: **(a)** Three-Electrodes cell setup for amperometric measurement through AUTOLAB (from *Metrohm* documentation) and **(b)** Cable connector for SPEs (from *Dropsens*).

interface. Setting a specific procedure on this software, in terms of current, potential

and deposition time, it is possible to performe a wide number of experiments, with an intuitive graphical interface to plot data, and with an easy commands to save and processing them.

In Figure 5.20 two different experimental setups are shown. The configuration is based on bio-functionalized WE and external RE and CE all immersed in the analyzed solution.

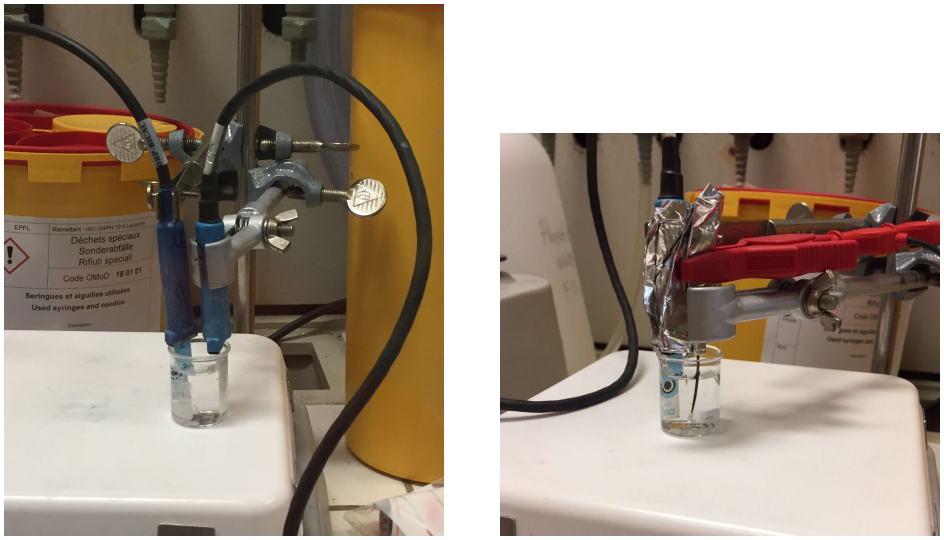

(a) (b)

Figure 5.20: Photo of electrochemical cell for lactate detection with a Carbon SPE used for RE and CE and a functionalized SPE WE **(a)** or Bamboo Electrode **(b)**.

Table 5.3 summarizes all the realized electrodes and their pros and cons on the basis of the obtained results for lactate detection.
In particular, all electrodes functionalized with LDH enzyme were not able to sense lactate concentration changes. We have tried to improve the performance of these electrodes by changing the mambrane support for the electrode; hence a polymeric Chitosan membrane was used. All of these electrodes were tested, after reaching the stability in blank solution, by adding lactate stock solution with the aim of calibrate their response. Nevertheless, the current, which was expected to increase proportionally to the lactate concentration, was not behave as expected. Some possible explanations for this behavior could be: (i) a non-efficient immobilization of the enzyme on the electrode surface, (ii) a low affinity of LDH for Nafion or Chitosan membranes, (iii) a non-activation of LDH since NAD^+ co-enzyme was not present, (iv) a non suitable substrate provided by Carbon for this kind of detection.
We obtained better results with the other enzyme, the LOD. Carbon, Gold and Platinum

SPE were functionalized at first with Nafion and then LOD was immobilized. Carbon electrode continued to not respond to lactate concentration variations, and also Au resulted to be non suitable substrate for this detection. On the contrary, Pt SPE gave satisfactory result in lactate detection. Subsequently, this Nafio/LDO functionalization

Table 5.3: List of tested electrodes for lactate detection

Electrode	Functionalization	Enzyme	Lactate test
Carbon SPE	MWCNT/Nafion	LDH	not working
Bamboo Electrode	None	LDH	not working
PGE	None	LDH	not working
Carbon SPE	MWCNT/Chitosan	LDH	not working
Carbon SPE	Nafion	LOD	not working
Au SPE	Nafion	LOD	not working
Pt SPE	Nafion	LOD	working
CNTs Electrode	Nafion	LOD	not working
PGE	Nafion	LOD	not working
Bamboo Electrode	Nafion	LOD	working

was tested on PGE, CNTs and Bamboo electrodes. Because of their shape and their reduced working electrode area, the PGEs are not able to give a positive response in terms of lactate detection. Instead, the failure due to CNTs Electrodes can be related to their innovative configuration which makes these electrode insuitable for functionalization. Indeed, even if the CNTs technology has the advantage to improve and increase the area of the elctrode, as visible in Figure 5.21, the configuration of these sensitive electrodes gives better performance when it is used in direct contact with the analyte solution. In application described in the picture, a microfluidic channel allows a rapid flow of the solution and so a better contact with the electrode. It is possible to adfirm that a manually functionalization of these electrodes is not a good working method and that this electrode can be an innovative substrate for application which does not require the immobilization of a recognition element on the substrate but uses directly the proprierties of the CNTs, e.g the nicotine detection in sweat.

5.4.3 Pt/Nafion/LOD Electrode

CA lactate calibration procedure was successfully performed with Pt/Nafion/LOD electrode; the measured data have been analyzed and processed with *Matlab R2017a* software. The measures, acquired by an Autolab potentiostat driven by *Nova 1.11* electrochemical software, were imported in *Excel* and subsequently in *Matlab*.
The data analysis has been performed by implementing a *Matlab* script performing same

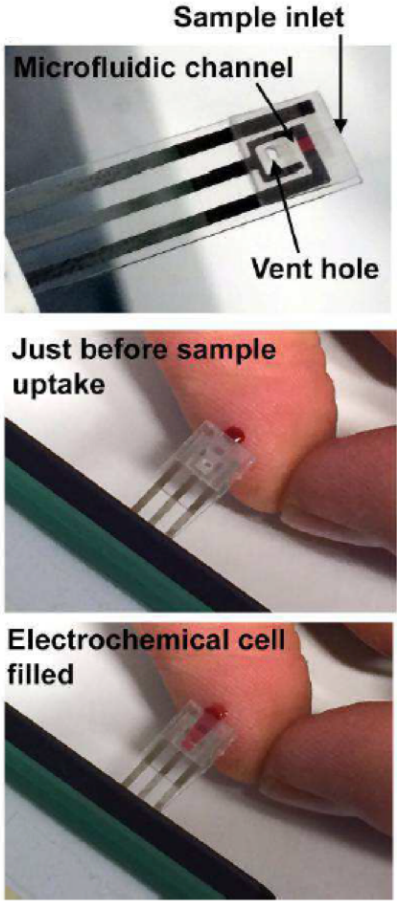

Figure 5.21: Inkjet printed sensor with three-electrode configuration integrated in a microfluidic channel for rapid measurements. Indeed a direct contact of the electrodes with the interest solution is guaranteed (Reprinted from [95]).

steps for all the measurements, either in PBS or in Artificial Sweat. In this way, it was possible to calibrate the electrode response respect to increasing lactate concentrations in different background solutions. Sweat was our target background solution, since we were aiming to realize a wearable system for athletes monitoring. It is a more complex fluid respect than PBS, hence PBS was used to preliminary characterize the bio-sensors. The *Matlab* script implements a first step of filtering (Savitzky–Golay filter) to reduce noise due to the instrumentation, the electrode functionalization and the environment.

```
order = 3;
framelen = 111;
filt = sgolayfilt(current,order,framelen);
```

The implemented Savitzky-Golay smoothing filter is a digital low pass filter applied to a set of digital values able to, without distorting the signal, smooth the data and increase the Signal to Noise Ratio (SNR). Through a process of convolution, this type of filter creates successive local polynomials of specific order defined by the user ($order = 3$), using a subset of adjacent data points (number defined by *framelen*).
In Figure 5.22.**(b)** and .**(d)** the two CAs are shown. For a more significant representation, in case of PBS stock solution the first 5500 s are cut from the plot. Doing a comparison of these two trends, it is visible that the first current stabilizes in the blank solution after a longer period of time: this can be caused by a higher instability of the first electrode or a worst immobilization process of the enzyme. The experiment was ending when the analyzed electrode was reaching the saturation, therefore, not able to detect further increase of the lactate concentration. It was evident that, in both cases, the current was increasing up to a stable value when the analyzed solution of 20 mM of L-Lactate was measured. Further, the current steps were decreasing with larger lactate concentrations.
The main difference of the two CAs is that the detection of lactate in sweat stock solution allows to reach higher concentration and the electrode saturates later respect to the PBS case. From Figure 5.22.**(d)**, is also evident that in the experiments with stock solution in sweat the current has a higher baseline with respect of the PBS case and for this reason also the current levels are normally higher the other one.

To obtain a correlation between the current increase and the lactate concentration, calibration lines were analyzed in *Matlab*. After the stabilization of the electrode in blank solution, a new injection of lactate was performed every 500 s (8 min). Considering that the sample frequency was of two samples per second, each step have about 1000 samples. To evaluate the average of the current step, the center of each step was identified and the mean of 41 samples (from center minus 20 samples, from center plus 20 samples, included the center) was evaluated. For each average, the standard deviation was also calculated to have information about the amount of variations among the considered data. Figure 5.23 both **(a)** and **(b)** show the calibration lines with the error bars

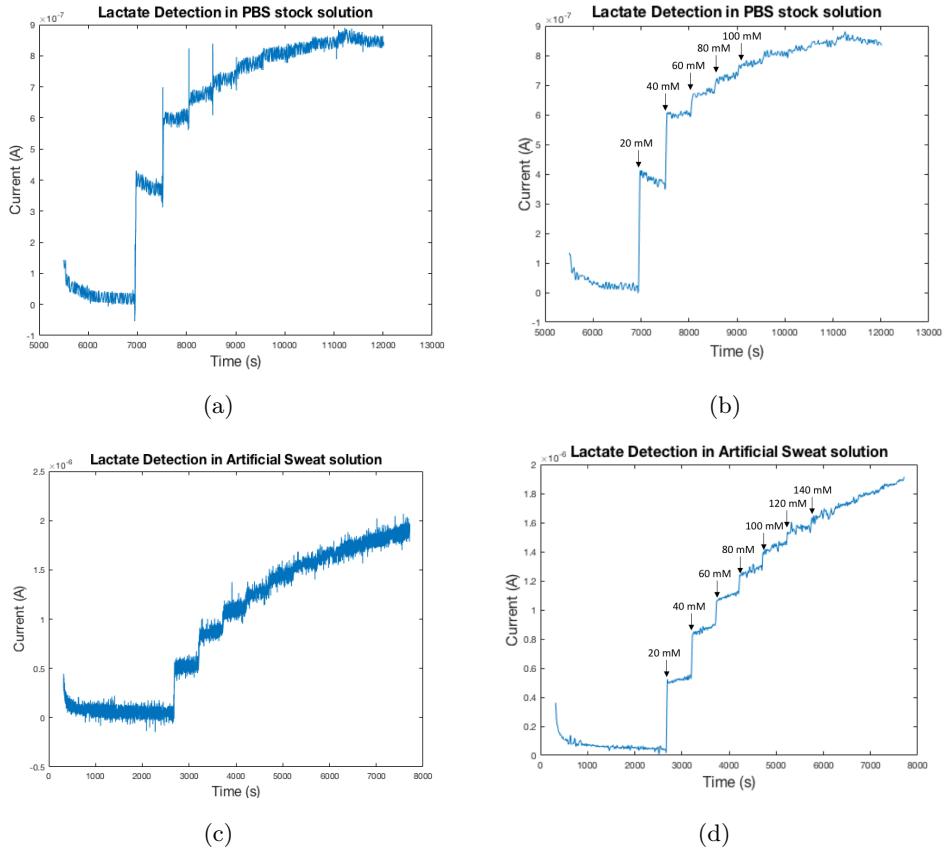

Figure 5.22: Amperogram of Pt/Nafion/LOD electrode for different concentrations of Lactate before ((**a**) and (**c**)) and after ((**b**) and (**d**)). (**a**) and (**b**) show trends for lactate solution in PBS, while (**c**) and (**d**) for lactate solution in Artificial Sweat (*Savitzky–Golay filter* realized in *Matlab R2017a*)

provided by the standard deviation. All of the current steps were measured respect to the average of the stabilization step in blank solution.

The most common way to fit a the measured data points is by using a linear or

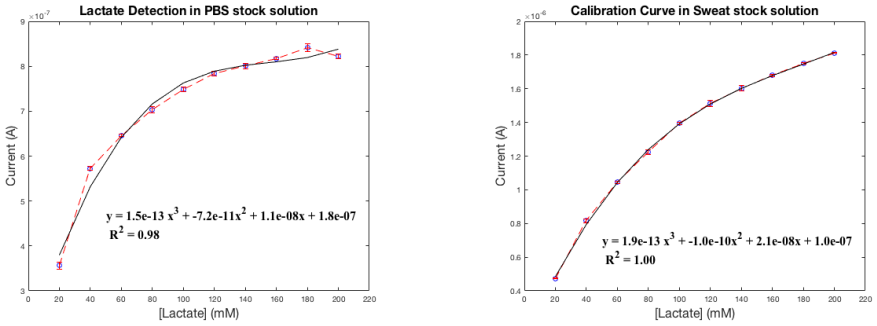

(a) (b)

Figure 5.23: Calibration curves of Pt/Nafion/LDO electrode: electrode current vs L-Lactate concentration (**(a)** in PBS stock solution and **(b)** in Sweat stock solution) (realized on *Matlab R2017a*).

non-linear regression finding polynomial terms. Through *Matlab* function *polyfit* the coefficients for a polynomial of 3^th order were found (the order choice is due to visible experience after having tested 1^st and 2^nd orders).

```
p = polyfit(conc,dati,3);
yfit = polyval(p,conc);
```

The *Root-Mean-Square Value* (R^2) is calculated by considering the difference between the predicted value and the actual one, to estimate the precision of the regression curve for approximating the real data.

Indicating the actual values with y (y_1,...,y_n) and the predicted values with f (f_1,...,f_n), and measuring (i) the sum of squares of residuals SS_{resid} (Eq. 5.8) and (ii) the total sum of squares SS_{tot} (Eq. 5.9), it is possible to define the R^2 coefficient (Eq. 5.10) as:

$$SS_{resid} = \sum_i (y_i - f_i)^2 \tag{5.8}$$

$$SS_{tot} = \sum_i (y_i - \overline{y})^2 \tag{5.9}$$

$$R^2 = 1 - \frac{SS_{resid}}{SS_{tot}} \tag{5.10}$$

The more this value is close to one, the better the regression approximates the data set, because it means that $\frac{SS_{resid}}{SS_{tot}}$ is very low and so the difference between y_i and f_i is also low. In this case, as visible in the plots, this value is equal to 0.98 and 1, means that the second approximation is very good.

Finally, also the Limit of Detection (LOD) was evaluated for each curve. The LOD is the smallest concentration of analyte that can be detected by the sensor, in other terms it is the minimum amount of target analyte that is clearly distinguishable from the measurement of the blank solution [3]. It is evaluated as the analyte concentration required to provide an output signal equal to the blank solution plus three times the standard deviation of the blank solution (Eq. 5.11):

$$LOD = \frac{3 \cdot \sigma_B}{S} \tag{5.11}$$

where S is the sensitivity (Chapter 2) evaluated from the calibration curve. In our case, since the regression was not linear, S was evaluated as the slope of the tangent line in a determined point (x value equal to 100 mM) of the calibration curve. The LOD for PBS stock solution was evaluated to be equal to $12.77mM$, while a lower value was obtained for the sweat solution as $2,46mM$.

5.4.4 Bamboo/Nafion/LOD Electrode

Following the same procedure, a data analysis has been performed also for the Bamboo/Nafion/LO Electrodes. In Figure 5.24 it is visible the CA for two different bamboo electrodes with the same functionalization. What is evident, also from a comparison with the previous experiment, is that the electrodes reach the saturation level at lower concentration of lactate (80 and $60mM$). After three lactate injections (each of $100\mu l$) the current does not increase anymore. Furthermore, the registered current levels are higher respect to the platinum electrode: this phenomena can be justified from the fact that, in blank solution, a higher background current level is measured.

A linear regression curve is suitable for this trend, both for PBS and AS analysis.

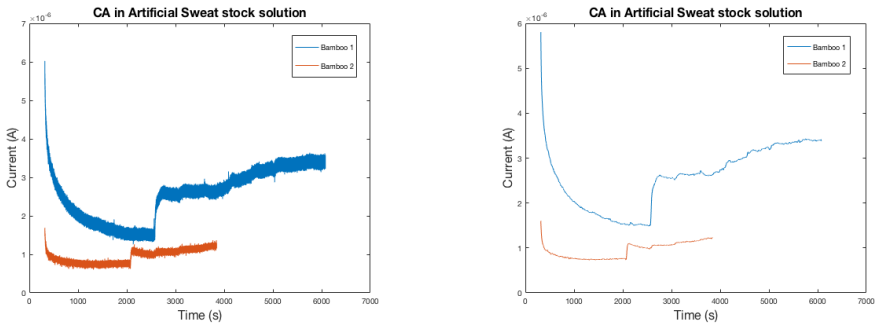

(a) (b)

Figure 5.24: Amperogram of two Bamboo/Nafion/LOD electrodes for different concentrations of Lactate in AS solution before (**(a)**) and after (**(b)**) filtering with *Savitzky–Golay filter* (realized on *Matlab R2017a*)

The polynomial degree is 1 and the sensitivity is evaluated directly as the slope of the

regression line. By calculating the *Root-Mean-Square Value* we could notice that more stable results are obtained for "Bamboo 2", but "Bamboo 1" registered a lower LOD requiring a lower amount of analyte to start the detection (2.86 mM vs 3.49 mM of the second one). Furthermore, "Bamboo 1" electrode allows to detect also higher lactate concentrations before reaching the saturation.

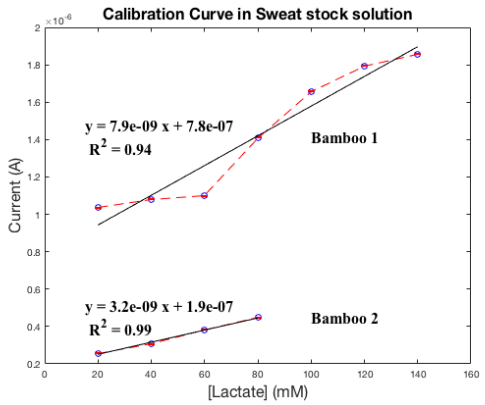

(a)

Figure 5.25: Calibration curves of Bamboo/Nafion/LDO electrodes: current vs L-Lactate concentration in AS stock solution (realized on *Matlab R2017a*).

To sum up, it was evident that Pt SPE offers the most suitable substrate for Nafion/LOD functionalization for lactate detection. The higher levels of lactate concentration that can be detected by this sensor before reaching saturation enable the possibility to detect successfully the lactate in sweat, considered as complex biologic fluid of high interest especially for sportive applications.

Chapter 6

Potentiometric Measurements: Lithium Detection

6.1 Ion sensign

Ion sensors are very important electrochemical devices used as detection systems, which can be suitable in many different applications. Usually, potentiometric measurements, used to detect the concentration of target ions in different biologic or chemical fluids, require the use of *Ion-Selective Electrodes (ISEs)* and very accurate reference electrodes [40]. The ISEs, which convert the ion activity into an electrical potential, have undergone significants developments. These electrodes offer high selectively, long lifetime and small potential drift. Indeed, they consist of an *Ion-Selective Membrane*, an internal contacting solution and a reference internal electrode (Fig. 6.1 **(b)**) [94]. What happens at the interfaces are redox reactions where chemical species exchange electrons. A cation target in sample solution (M^+) is recognized and trapped from the selective membrane which contains a neutral ionophore (L) and an anionic site (R^-) (redox reaction which occurs: $M^+ \Longleftrightarrow MLn + R^-$). Now, a second RedOx reaction occurs at the second interface, so the sample solution coentration is compared with the inner solution and if this difference of concentrations is non-zero a differencial potential is generated accross the membrane (membrane potential E_M) accordign to *Nerst equation* 6.1 [94]:

$$E_M = \frac{RT}{z_i F} \cdot \ln \frac{a_i^{'}}{a_i^{''}} = E_i^0 + s \lg a_i^{'} \tag{6.1}$$

where $a_i^{'}$ is related to the external sample solution, while $a_i^{''}$ to the internal solution, z_i is the valence of the target and R,T and F are repsectively the general gas constant,the absolute Temperature and the Faradaic constant. In this case, we may expect a linear dependence between the internal potential and the logarithm of the target concentration, with slope (s) which is the sensitivity of the sensor. At the end of a conventional

ISE, there is a AgCl/Ag wire which works as inner reference electrode: a third RedOx reaction occurs at this interface with the Cl^- contained in the inner solution; this reaction ensures the ion-to-elctron transduction: $AgCl(s) + e \iff Ag(s) + Cl^-(aq)$.

The internal filling solution can present some different drawbacks as, for example,

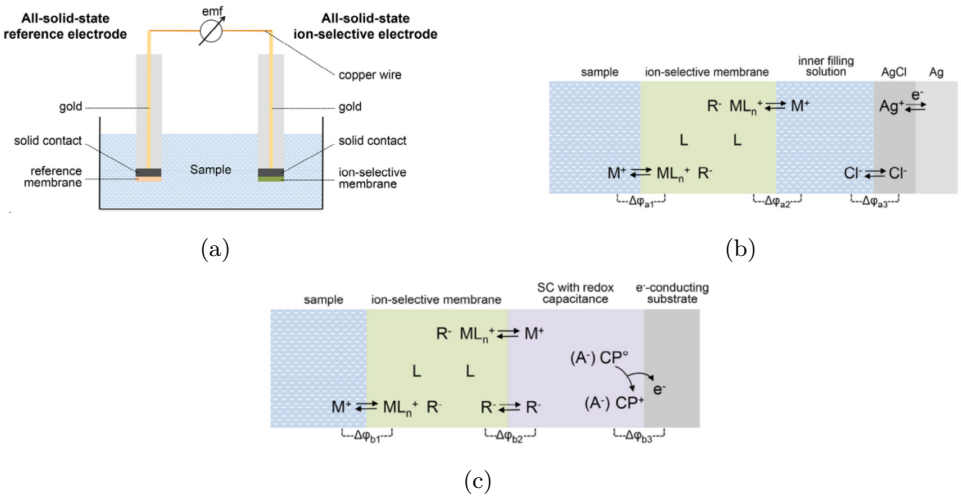

Figure 6.1: **(a)** Example of a potentiometric cell with ISE; **(b)** and **(c)** interface working principle for ISM with filling solution and solid contact, respectively (Reprinted from [40])

evaporation and an high sensibility to the temperature and pressure changes. For this reason, in the last years, several *all-solid-state* ions senors have been developed (Fig. 6.1 **(c)**) ([11], [17], [12], [13]). They are based on a solid contact between the membrane and the metallic surface of the elctrode. Usually, **Conducting Polymers (CPs)** are used as solid-contacts and these are able to convert the ions into electrons through the oxidation/reduction reactions described following:

$$CP^+A^-_{solidcontact} + M^+_{membrane} + e^- \iff CP^\circ A{-}M^+_{solidcontact} \tag{6.2}$$

Another materials that can be employed in the solid-contacts for ISEs, and that have been used in this thesis, are the **Nanostructured materials** (Fig. 6.2) ([92], [40], [50], [52]). They represent a valid alternative to the CPs and also have a great number of advantages with respect to them. The main difference between this type of contact and the CPs is that in this case the interfacial potential is not related to redox reactions, but it is related to the amount of charge accomulated in the double layer. Indeed the ions accumulation on one side of the interface, thanks to the precense of the ISM, induces an electrons accumulation on the other side of the interface creating an asymmetric capacitor which is evaluated by the potentiometric measurments.

In the following discussion, an example of application of these nanostructured materials employed in a potentiometric detection of Lithium concentration is described.

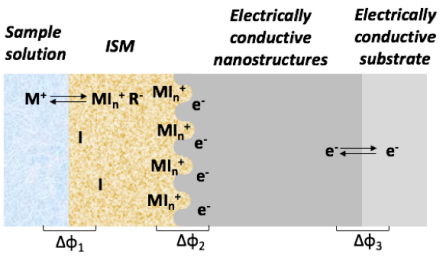

Figure 6.2: Structure and working principle of ISEs based on nanostructures solid-contacts (Reprinted from [40])

6.2 Lithium Detection: Electrodes Realization and Validation

As seen in Chapter 1, the detection of Lithium is essential for drug monitoring of patients which suffer of mental disorder. In this Thesis, highly stable Li^+ ISEs [5] based on nanostructured materials are proposed, with a vitro validation and an accurate data analysis.

6.2.1 Electrode Functionalization

Platinum Screen Printed Electrodes (SPEs) (description in Chapter 5, paragraph 5.4.1.1) are used as substrate and submitted to a successive functionalization. Nobles metals (Pt and Au) nanostructures were electrodeposited onto the Pt SPEs through an *Autolab Potentiostat* controlled by *Nova 1.11* software. Usign a three-electrodes setup Au (*AuNanocorals*) and Pt (*PtNanoflowers*) nanostructures were deposited on the electrode surface applying -3 V and -1 V, respectively. Nanostructures solution were prepared following [5]: $HAuCl_4$ ($5mM$) and NH_4Cl ($1.25M$) for Au nanoparticles, H_2SO_4 ($50mM$) and H_2PtCl_6 ($25mM$) for Pt nanostructures. The Ion Selective Membrane was obtained mixing, in a volume of $10\mu l$, the following compounds: $28.00wt\%$ Poly(vinyl chloride) high molecular weight, $1wt\%$ Li Ionophore VI, $0.7wt\%$ Potassium tetrakis(4-chloropheny)borate and $70.3wt\%$ 2-Nitrophenyl octyl ether. By drop-casting, 100 mg of mixture dissolved in 1 mL of Tethraydrofuran (THF) were deposited on SPEs. The membrane was kept in a dark enviroment for 24 hours for the solvent evaporation, and then conditioned for 24 hours at 0.01 M LiCl.
Four different types of Li^+ electrodes were realized, combining these materials:

- Pt/PtNanoflowers-AuNanocorals/ISM
- Pt/AuNanocorals-PtNanoflowers/ISM
- Pt/PtNanoflowers-AuNanocorals

- Pt/AuNanocorals-PtNanoflowers

By means of a *Scanning Electrode Microscopy (SEM)*, it was possible to see the morfology of Pt SPE before and after the nanostructures deposition: bare Pt electrode visible in Fig. 6.3a, while the PtNanoflowers-AuNanocorals and AuNanocorals-PtNanoflowers deposition visible in Fig. 6.3b and 6.3c respectively. From the pictures, it is evident

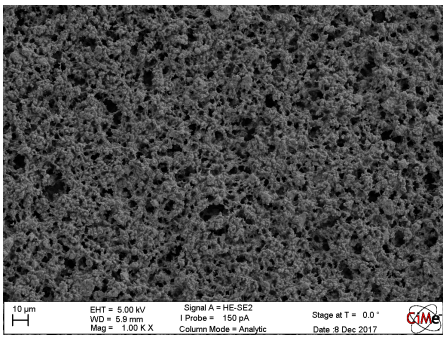

(a)

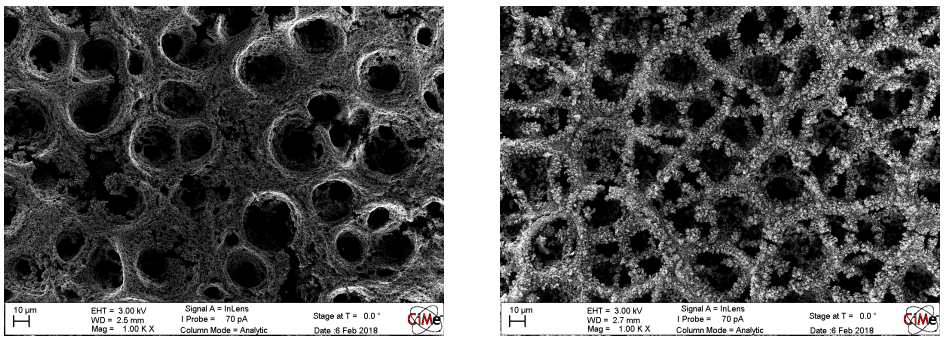

(b) (c)

Figure 6.3: SEM imaging from Merlin microscope in SE mode placed at EPFL: **(a)** Pt bare electrode, **(b)** Pt/PtNanoflowers-AuNanocorals and **(c)** Pt/AuNanocorals-PtNanoflowers

that, in both cases, conformal and homogenous depositions are obtained. In addition, thanks to the nanostructures deposition, the surface roughness shifts from micro- to nanoscale.

6.2.2 Electrochemical Measurements: Potentiometric Setup

A two-electrodes cell configuration is used to perform the potentiometric measurements with the ISEs, realized from Pt SPE, as Working Electrodes and a double junction Sension+ Reference Electrode, purchased from Hach, United States (example of potentiometric setup visible in Figure 6.4).

The electrode perfomance has been characterized with Current Reversal Chronopotentiometry (CRC) and CV.

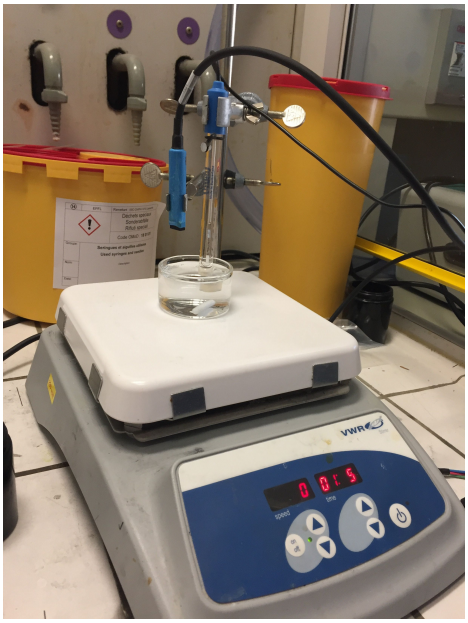

Figure 6.4: Photo of potentiometric setup of experiments in vitro for Lithium detection.

In particular, CRC is a very useful and common method used to investigate potential stability of the elctrodes; indeed a fixed current of a few nA is applied to the WE, while the potential is measured between WE and RE and it is plotted as function of time [75]. In Figure 6.5 are shown the two CRCs of the functionalized Pt electrodes: the jump visble from the plots occurs when the current changes in direction. *Origin* is used for data analysis and plotting.

In Figure 6.6 are reported the comparinson of different CRCs related to the electrodes

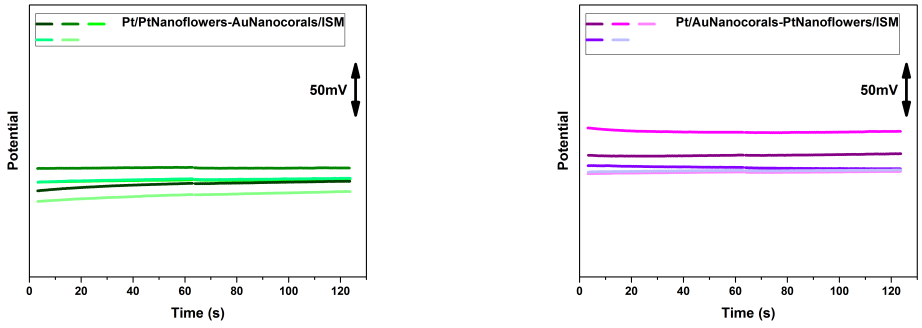

(a) (b)

Figure 6.5: CRC of Pt/PtNanoflowers-AuNanocorals/ISM **(a)** and of Pt/AuNanocorals-PtNanoflowers/ISM **(b)** (obtained with *Origin*).

tested: from **(a)** is evident the comparison with the ISM directly deposited on the platinum SPE and the great improvement in terms of potential stability introduced

by the nanostructures. In **(b)**, instead, is evaluated the effect of the double layer of nanostructures with respect to a single layer: less evident than the previous plot, but also in this case the present electrodes offer a slightly more stable response. From the

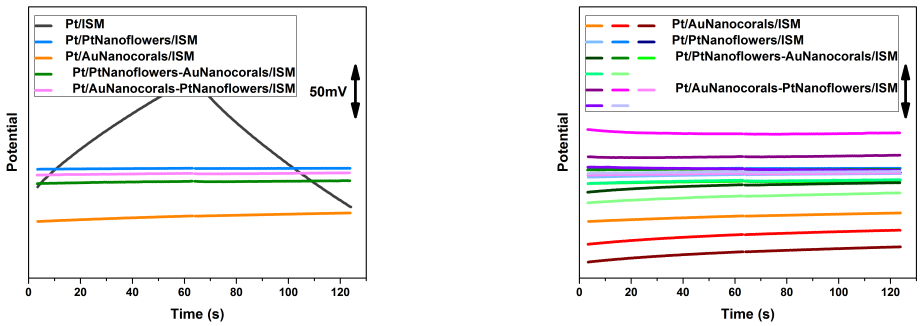

(a) (b)

Figure 6.6: Comparisons of CRCs: **(a)** with Pt/ISM and **(b)** with a single layer of nanostructures (obtained with *Origin*).

CRC results, it is possible to obtain a quantitative comparison of the SC-ISEs in terms of resistance, potential drift and capacitance values. In particular, the resistance is calculated using Ohm law ($V = Ri$), where i is the fixed current applied and V is the potential measured; the potential drift is defined as the slope of the curve of potential as function of logarithmic concentration of lithium and the capacitance value is deducted from the equation: $C = \frac{i}{dE/dt}$.

From an analysis of data shown in Table 6.1, it is evident that the resistance value

Table 6.1: Resistance, potential drift and capacitance of different Li^+ ISEs evaluated from CRC measurements. Five samples tested for each typology.

Electrode	R[kΩ]	dE/dt [mV/s]	C [μF]
Pt/ISM	146 ± 76	1.8 ± 0.29	2.5 ± 0.1
Pt/PtNanoflowers/ISM	28 ± 3.5	0.03 ± 0.02	195.3 ± 96.8
Pt/AuNanocorals/ISM	41 ± 19	0.12 ± 0.06	50.5 ± 24.0
Pt/PtNanoflowers-AuNanocorals/ISM	46 ± 19.9	0.02 ± 0.007	242 ± 70
Pt/AuNanocorals-PtNanoflowers/ISM	79 ± 29	0.03 ± 0.02	361 ± 454

decreases using nanostructures, even if the double layers caused higher values with respect of the single layers. In both cases, the lowest values in terms of resistance are achieved with Platinum Nanoflowers, this means that there is an increase of conductivity. Concerning potential drift, the nanostructures decrease the CRC slope by one or two

order of magnitudes. In addition, it is possible to observe that the highest performance is achieved when the PtNanoflowers layer is the only or the first one on the Pt SPE. At the end, also the comparison of capacitances confirms that the nanostructures introduce significant improvements: Pt/AuNanocorals-PtNanoflowers/ISM produce the highest value in terms of capacitance, and this result is evident also from the CRC graphs.
The increase in the electrode capacitance is evident also by CVs (Fig. 6.7): as found in CRC, Pt/AuNanocorals-PtNanoflowers/ISM electrode produces the highest capacitive current of the system.

From both CV and CRC mesurements, it is widely evident that nanostructures offer

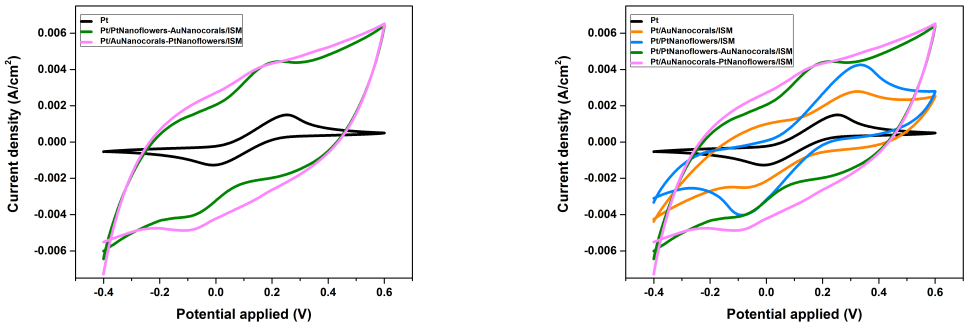

(a) (b)

Figure 6.7: Comparisons of CVs: **(a)** Pt, Pt/PtNanoflowers-AuNanocorals/ISM and Pt/AuNanocorals-PtNanoflowers/ISM and **(b)** Pt, Pt/PtNanoflowers/ISM, Pt/AuNanocorals/ISM, Pt/PtNanoflowers-AuNanocorals/ISM and Pt/AuNanocorals-PtNanoflowers/ISM (obtained with *Origin*).

improvements in terms of potential stability and reproducibility for the ISEs. Furthermore, the double layer of nanostructured electrode represents an innovated and highly performing solid contact.

An example of a typical Li^+ calibration time trace is given in Fig. 6.8 for a Pt/PtNanoflowers-AuNanocorals/ISM ISE. It was performed adding injections of Lithium at different concentrations (in Table 6.2 are listed the volumes added with each injection, the concentration and after how much seconds was added the successive quantities).

To obtain a correlation between the potential increase at the lithium concentration, calibration lines were analyzed in *Matlab*. Starting the Calibratiion, a new injection of lactate was performed every 50 s. To evaluate the average of the potential step, the center of each step was identified and the mean of 21 samples (from center minus 10 samples, from center plus 10 samples, included the center) was evaluated. Figure 6.9 shows the calibration curve: it is evident that a Nernstian behavior is achieved (slope of

Table 6.2: Calibration of Li^+ Pt/PtNanoflowers-AuNanocorals/ISM

Injection n°	Concentration (M)	Volume (μl)	Time (s)
1	$1.000 \cdot 10^{-9}$	6	50
2	$1.000 \cdot 10^{-8}$	54	100
3	$1.000 \cdot 10^{-7}$	546	150
4	$1.000 \cdot 10^{-6}$	55	200
5	$3.16228 \cdot 10^{-6}$	132	250
6	$1.000 \cdot 10^{-5}$	420	300
7	$3.16228 \cdot 10^{-5}$	13.2	350
8	$1.000 \cdot 10^{-4}$	42	400
9	$3.16228 \cdot 10^{-4}$	133	450
10	$1.000 \cdot 10^{-3}$	424	500
11	$3.16228 \cdot 10^{-3}$	17	550
12	$1.000 \cdot 10^{-2}$	53	600
11	$3.16228 \cdot 10^{-2}$	168	650
13	$1.000 \cdot 10^{-1}$	537	700
14	$1.000 \cdot 10^{-1}$	537	750

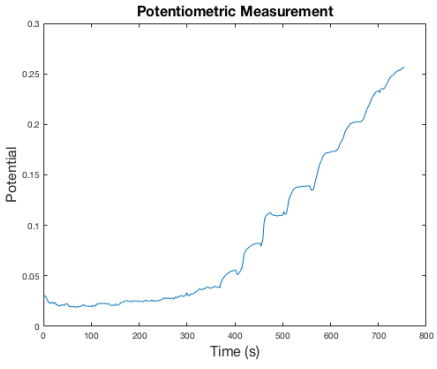

Figure 6.8: Potentiometric trend obtained during the calibration of Li^+ Pt/PtNanoflowers-AuNanocorals/ISM ISE (with *Matlab 2017a*).

53.7mV). The limit of detection was computed according to IUPAC definition as the intersetion of the linear portions of curve. The value is around $1.28 \cdot 10^{-5} M$.

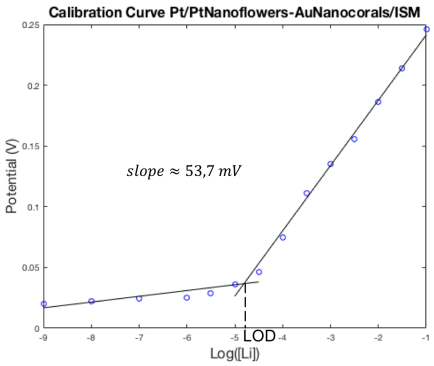

Figure 6.9: Calibration curve of Li^+ Pt/PtNanoflowers-AuNanocorals/ISM ISE (with *Matlab 2017a*).

Chapter 7

Conclusion

The design and the implementation of all the parts of a wearable electrochemical system for athletes monitoring has been presented in this thesis. In particular, the system is composed by an electronic board which is interfaced with electrochemical senors for ions and metabolites sensing.

Lithium and Lactate have been chosen as model for ion and metabolite detection, respectively. Indeed, lactate is the basis conjugate of lactic acid, that is produced whenever there is lack of energy in the human metabolism, while lithium is a difficult-to-dose mood stabilizer administered to subjects suffering from mental disorders, which are common in athletes undergoing extreme physical trainings. Therefore, the detection of these two compounds in athletes is of high relevance.

The realized mixed-signal readout circuit supports four multiplexed channels: two for potentiometry and two for amperometry. The former performs an OCP which allows the reading of the difference of potential between RE and WE. The latter involves a control amplifier to drive the electrochemical cell and a transimpedance amplifier to read out the faradaic current and convert it in a potential value. Both potentiometric and potentiostatic circuitries implement a fourth order Sallen-Key filter for signal conditioning and noise rejection.
The system is enriched by a wireless communication performed through a Bluetooth Low Energy (BLE) module. The measured data and the circuit parameters to be set are accessible by the user thanks to an user-friendly GUI, which was realized in *Matlab*. The flexibility and the wearability of the electronic platform are ensured by a flexible substrate (FPCB) and by the small dimensions ($97 \cdot 66$ mm) suitable to fit in a commercially-available armband case.

This hardware system is designed to interface with electrochemical sensors for lactate and lithium detection in sweat.
The lactate detection has been achieved after having investigated different electrode functionalization processes. The optimum performances have been reached with platinum (Pt) SPE functionalized with a Nafion membrane and Lactate Oxydase (LOD)

enzyme.
For lithium sensing Pt SPEs have been modified with nanostrucutres, e.g. Au Nanocorals and Pt Nanoflowers, to enhance the substrate performances and an Ions Selective Membrane (ISM) for lithium ions has been deposited on the electrodes' surface.
The performance of the electrochemical sensors have been characterized by performing multiple calibration processes to ensure reproducibility and stability of the measures.

Next steps and future work will include the integration of the custom-built FPCB electronics with the electrochemical sensors in order to realize a complete system for sport monitoring applications. Further, an additional improvement would be to reduce the system dimensions to integrate it with an hair-band or in a wrist-band, where it can be less visible and where more sweat sample can be collect.

Bibliography

[1] Analog Devices. Decoupling Techniques. *Application Note, Analog Devices*, pages 1–14, 2009.

[2] S. Anastasova, B. Crewther, P. Bembnowicz, V. Curto, H. M. Ip, B. Rosa, and G. Z. Yang. Corrigendum to "A wearable multisensing patch for continuous sweat monitoring" (Biosensors and Bioelectronics (2016) 93 (139–145) (S0956566316309198) (10.1016/j.bios.2016.09.038)). *Biosensors and Bioelectronics*, 94(September 2016):730, 2017.

[3] D A ARMBRUSTER, M D TILLMAN, and L M HUBBS. Limit of Detection (Lod) Limit of Quantitation (Loq) - Comparison of the Empirical and the Statistical, Methods Exemplified With Gc-Ms Assays of Abused Drugs. *Clinical Chemistry*, 40(7):1233–1238, 1994.

[4] Anthony Turner Biosensors: then and now Trends in biotechnology, Elsevier, Vol. 31, number 3, pages 119–120, 2013.

[5] Francesca Criscuolo, Irene Taurino, Francesca Stradolini, Sandro Carrara and Giovanni De Micheli Highly-stable Li+ ion-selective electrodes based on noble metal nanostructured layers as solid-contacts submitted to Analytica Chimica Acta, 2018

[6] Atmel Avr and Xmega Microcontrollers. Xmega e manual. 2014.

[7] Amay J. Bandodkar and Joseph Wang. Non-invasive wearable electrochemical sensors: A review. *Trends in Biotechnology*, 32(7):363–371, 2014.

[8] Allen J Bard, Larry R Faulkner, New York, Chichester @bullet, Weinheim Brisbane, and Singapore E Toronto. *ELECTROCHEMICAL METHODS Fundamentals and Applications*. 1944.

[9] Paweł Bembnowicz, Guang Zhong Yang, Salzitsa Anastasova, Anna Maria Spehar-Délèze, and Pankaj Vadgama. Wearable electronic sensor for potentiometric and amperometric measurements. *2013 IEEE International Conference on Body Sensor Networks, BSN 2013*, (1):2–6, 2013.

[10] Tanu Bhardwaj. A review on immobilization techniques of biosensors. *International Journal of Engineering Research & Technology (IJERT)*, 3(5):294–298, 2014.

[11] T R Bhat and J Shankar. 1Oa et 8.20. (Iii):2–6, 1970.

[12] Johan Bobacka. Potential stability of all-solid-state ion-selective electrodes using conducting polymers as ion-to-electron transducers. *Analytical Chemistry*, 71(21):4932–4937, 1999.

[13] Johan Bobacka, Mary Mccarrick, and Ari Ivaskat. octylthiophene) Solid Internal Contact *. 119(September):1985–1991, 1994.

[14] Dale A.C. Brownson and Craig E. Banks. *The Handbook of Graphene Electrochemistry*. 2014.

[15] Joseph J. Carr and John M. Brown. Sensor Terminology. *Introduction to Biomedical Equipment Technology*, pages 1–11, 2013.

[16] Sandro Carrara. *Bio/CMOS Interfaces and Co-Design*. Lausanne, doi 10.100 edition.

[17] R. W. Cattrall, Henry Freiser, and R. W. Cattrall. Coated Wire Ion Selective Electrodes. *Analytical Chemistry*, 43(13):1905–1906, 1971.

[18] A Chamberland. Solid-State Detectors for the Potentiometric Determination of Gaseous Oxides.

[19] James P Chambers, Bernard P Arulanandam, Leann L Matta, Alex Weis, and James J Valdes. Biosensor Recognition Elements. pages 1–12, 2002.

[20] Vittorio Ciocca. Un biosensore per la rilevazione dell ' acido lattico. *Tesi di Laurea, Università degli studi di Padova*, Corso di L, 2017.

[21] Andres Felipe Diaz Cruz, Nicolas Norena, Ajeet Kaushik, and Shekhar Bhansali. A low-cost miniaturized potentiostat for point-of-care diagnosis. *Biosensors and Bioelectronics*, 62:249–254, 2014.

[22] Xiaoqiang Cui, Chang Ming Li, Jianfeng Zang, and Shucong Yu. Highly sensitive lactate biosensor by engineering chitosan/PVI-Os/CNT/LOD network nanocomposite. *Biosensors and Bioelectronics*, 22(12):3288–3292, 2007.

[23] Alaécio P dos Reis, Cézar Tarley, and Lauro T. Kubota. Micelle-Mediated Method for Simultaneous Determination of Ascorbic Acid and Uric Acid by Differential Pulse Voltammetry. *J. Braz. Chem. Soc*, 19(8):1567–1573, 2008.

[24] Analytical Electrochemistry and Third Edition. Potentiometry 5.1. 1970.

[25] Noémie Elgrishi, Kelley J. Rountree, Brian D. McCarthy, Eric S. Rountree, Thomas T. Eisenhart, and Jillian L. Dempsey. A Practical Beginner's Guide to Cyclic Voltammetry. *Journal of Chemical Education*, page acs.jchemed.7b00361, 2017.

[26] Kevin J Fraser, Vincenzo F Curto, Shirley Coyle, Ben Schazmann, Robert Byrne, Róisín M Owens, George G Malliaras, Dermot Diamond, Kevin St, Centre Microélectronique De Provence, Ecole Nationale, Mines De Saint, and De Mimet. Wearable electrochemical sensors for monitoring performance athletes. *SPIE 8118 Organic Semiconductors in Sensors and Bioelectronics IV*, pages 1–12, 2011.

[27] Wei Gao, Sam Emaminejad, Hnin Yin, Yin Nyein, Samyuktha Challa, Kevin Chen, Austin Peck, Hossain M Fahad, Hiroki Ota, Hiroshi Shiraki, Daisuke Kiriya, Der-hsien Lien, and George A Brooks. multiplexed in situ perspiration analysis. *Nature*, 529(7587):509–514, 2016.

[28] Fouad Ghamouss, Sophie Ledru, Nadine Ruillé, Françoise Lantier, and Mohammed Boujtita. Bulk-modified modified screen-printing carbon electrodes with both lactate oxidase (LOD) and horseradish peroxide (HRP) for the determination of l-lactate in flow injection analysis mode. *Analytica Chimica Acta*, 570(2):158–164, 2006.

[29] Andrew Gill, Geoffrey Lillie, Giosi Farace, and Pankaj Vadgama. Biocompatible interfaces for biosensors. *International Journal of Environmental Analytical Chemistry*, 85(9-11):699–725, 2005.

[30] J H Gilmore. NIH Public Access. *North*, 29(10):1883–1889, 2008.

[31] E Gongadze, S Petersen, U Beck, and U Van Rienen. Classical Models of the Interface between an Electrode and an Electrolyte. *Proceedings of the COMSOL Conference Milan*, pages 18–24, 2009.

[32] J. Justin Gooding. Nanostructuring electrodes with carbon nanotubes: A review on electrochemistry and applications for sensing. *Electrochimica Acta*, 50(15):3049–3060, 2005.

[33] Dorothee Grieshaber, Robert MacKenzie, Janos Vörös, and Erik Reimhult. Electrochemical Biosensors - Sensor Principles and Architectures. *Sensors*, 8(3):1400–1458, 2008.

[34] Damien Gruson, Abdelkrim Lallali, Valérie Furlan, Anne Marie Taburet, Alain Legrand, and Marc Conti. Evaluation of a new lithium colorimetric assay performed on the Dade Behring Dimension® X-pand™ system. *Clinical Chemistry and Laboratory Medicine*, 42(9):1066–1068, 2004.

[35] Jordi De Haes. Electrochemical investigation of apomorphine with glutathione , determined by using voltammetric techniques.

[36] Catherine M Halliwell, Evelyne Simon, Chee-seng Toh, Philip N Bartlett, and Anthony E G Cass. Immobilisation of lactate dehydrogenase on poly (aniline)– poly (acrylate) and poly (aniline)– poly- (vinyl sulphonate) films for use in a lactate biosensor. 453:191–200, 2002.

[37] David Harvey. Electrochemical Methods. *Analytical Chemistry 2.0*, pages 667–781, 1996.

[38] David Harvey. Electrochemical Methods. *Analytical Chemistry 2.0*, Chapter 11, 2016.

[39] Ai-ling Hu, Yin-huan Liu, Hao-hua Deng, Guo-lin Hong, and Ai-lin Liu. Biosensors and Bioelectronics Fluorescent hydrogen peroxide sensor based on cupric oxide nanoparticles and its application for glucose and L -lactate detection. *Biosensors and Bioelectronic*, 61:374–378, 2014.

[40] Jinbo Hu, Andreas Stein, and Philippe Bühlmann. Rational design of all-solid-state ion-selective electrodes and reference electrodes. *TrAC - Trends in Analytical Chemistry*, 76:102–114, 2016.

[41] Khalid Saeed Ibrahim. Carbon nanotubes-properties and applications: a review. *Carbon letters*, 14(3):131–144, 2013.

[42] Introduction Intrinsic. Shot and thermal noise. pages 1–14, 1928.

[43] Wenzhao Jia, Amay J. Bandodkar, Gabriela Valdés-Ramírez, Joshua R. Windmiller, Zhanjun Yang, Julian Ramírez, Garrett Chan, and Joseph Wang. Electrochemical tattoo biosensors for real-time noninvasive lactate monitoring in human perspiration. *Analytical Chemistry*, 85(14):6553–6560, 2013.

[44] Kagan Kerman, Masato Saito, Eiichi Tamiya, Shohei Yamamura, and Yuzuru Takamura. Nanomaterial-based electrochemical biosensors for medical applications. *TrAC - Trends in Analytical Chemistry*, 27(7):585–592, 2008.

[45] Walt Kester, Dan Sheingold, and James Bryandt. Fundamentals Of Sampled Data Systems. *Fundamentals Of Sampled Data Systems*, 21(5):411–5, 1973.

[46] Tugba Kilic, Valerie Brunner, Laurent Audoly, and Sandro Carrara. Smart e-Patch for drugs monitoring in schizophrenia. *2016 IEEE International Conference on Electronics, Circuits and Systems, ICECS 2016*, pages 57–60, 2017.

[47] Peter T. Kissinger and William R. Heineman. Cyclic voltammetry. *Journal of Chemical Education*, 60(9):702, 1983.

[48] Kenneth A Kuhn. Sallen-Key Low-pass Filter Sallen-Key Low-pass Filter. (1):1–9, 2016.

[49] Roger C H Kwan, Phoebe Y T Hon, Karen K W Mak, and Reinhard Renneberg. Amperometric determination of lactate with novel trienzyme/poly(carbamoyl) sulfonate hydrogel-based sensor. *Biosensors and Bioelectronics*, 19(12):1745–1752, 2004.

[50] Chun Ze Lai, Melissa A. Fierke, Andreas Stein, and Philippe Bühlmann. Ion-selective electrodes with three-dimensionally ordered macroporous carbon as the solid contact. *Analytical Chemistry*, 79(12):4621–4626, 2007.

[51] W. C. Leong, M. Z. Abdullah, and C. Y. Khor. Application of flexible printed circuit board (FPCB) in personal computer motherboards: Focusing on mechanical performance. *Microelectronics Reliability*, 52(4):744–756, 2012.

[52] Fenghua Li, Junjin Ye, Min Zhou, Shiyu Gan, Qixian Zhang, Dongxue Han, and Li Niu. All-solid-state potassium-selective electrode using graphene as the solid contact. *The Analyst*, 137(3):618–623, 2012.

[53] Meng Li, Yuan Ting Li, Da Wei Li, and Yi Tao Long. Recent developments and applications of screen-printed electrodes in environmental assays-A review. *Analytica Chimica Acta*, 734:31–44, 2012.

[54] Wei Jhe Ma, Ching Hsing Luo, Jiun Ling Lin, Sin Houng Chou, Ping Hung Chen, Mei Jywan Syu, Shin Hung Kuo, and Shin Chi Lai. A portable low-power acquisition system with a urease bioelectrochemical sensor for potentiometric detection of urea concentrations. *Sensors (Switzerland)*, 16(4):1–14, 2016.

[55] K. Maeda-Yorita, K. Aki, H. Sagai, H. Misaki, and V. Massey. L-lactate oxidase and L-lactate monooxygenase: Mechanistic variations on a common structural theme. *Biochimie*, 77(7-8):631–642, 1995.

[56] Andrew Mason, Yue Huang, Chao Yang, and Jichun Zhang. Amperometric Readout and Electrode Array Chip for Bioelectrochemical Sensors. *Iee*, pages 3562–3565, 2007.

[57] Rastislav Monošík, Miroslav Streďanský, Gabriel Greif, and Ernest Šturdík. A rapid method for determination of l-lactic acid in real samples by amperometric biosensor utilizing nanocomposite. *Food Control*, 23(1):238–244, 2012.

[58] Boris Murmann. Digitally Assisted Analog Circuits • Digitally Assisted A / D Converters.

[59] Boris Murmann. D Igitally a Ssisted Assisted Analog Circuits Can Exploit Digital Circuits ' High Density. *Ieee Micro*, pages 38–47, 2006.

[60] Rafael M. Nagler, Sophie Lischinsky, Eric Diamond, Ifat Klein, and Abraham Z. Reznick. New insights into salivary lactate dehydrogenase of human subjects. *Journal of Laboratory and Clinical Medicine*, 137(5):363–369, 2001.

[61] Noel Nesakumar, Kavitha Thandavan, Swaminathan Sethuraman, Uma Maheswari Krishnan, and John Bosco Balaguru Rayappan. An electrochemical biosensor with nanointerface for lactate detection based on lactate dehydrogenase immobilized on zinc oxide nanorods. *Journal of Colloid and Interface Science*, 414:90–96, 2014.

[62] Muhammad Noman, Alessandro Sanginario, Pravin Jagdale, Micaela Castellino, Danilo Demarchi, and Alberto Tagliaferro. Pyrolyzed bamboo electrode for electrogenerated chemiluminescence of Ru(bpy)32+. *Electrochimica Acta*, 133:169–173, 2014.

[63] Takeo Oku. World ' s largest Science , Technology & Medicine Open Access book publisher c. *Agricultural and Biological Sciences Grain Legumes*, 2016.

[64] Keith B. Oldham. Fractional differential equations in electrochemistry. *Advances in Engineering Software*, 41(1):9–12, 2010.

[65] U S E Only. Lactate Assay Kit (Colorimetric). *Cell Biolabs, Inc.*, MET-5012, 2017.

[66] Massimo Onor, Stefano Gufoni, Tommaso Lomonaco, Silvia Ghimenti, Pietro Salvo, Fiodor Sorrentino, and Emilia Bramanti. Potentiometric sensor for non invasive lactate determination in human sweat. *Analytica Chimica Acta*, 989:80–87, 2017.

[67] F. Palmisano, R. Rizzi, D. Centonze, and P. G. Zambonin. Simultaneous monitoring of glucose and lactate by an interference and cross-talk free dual electrode amperometric biosensor based on electropolymerized thin films. *Biosensors and Bioelectronics*, 15(9-10):531–539, 2000.

[68] N. G. Patel, A. Erlenkötter, K. Cammann, and G. C. Chemnitius. Fabrication and characterization of disposable type lactate oxidase sensors for dairy products and clinical analysis. *Sensors and Actuators, B: Chemical*, 67(1):134–141, 2000.

[69] Sandra Pérez and Esteve Fàbregas. Amperometric bienzymatic biosensor for l-lactate analysis in wine and beer samples. *The Analyst*, 137(16):3854, 2012.

[70] Sofia Piedade, Martina Odlo˘, M Gabriela Almeida, Alberto N Ara, Cristina M C M Couto, and M Conceic. Application of lactate amperometric sol – gel biosensor to sequential injection determination of l -lactate. 43:1376–1381, 2007.

[71] Pulse Polarography, Differential Pulse, and Anodic Stripping. Comparison of Various Electrochemical Methods Electrodes and Potentiometry Introduction.

[72] Medeya M. Pribil, Gennady U. Laptev, Elena E. Karyakina, and Arkady A. Karyakin. Noninvasive hypoxia monitor based on gene-free engineering of lactate oxidase for analysis of undiluted sweat. *Analytical Chemistry*, 86(11):5215–5219, 2014.

[73] Related Products. Mcp4901/4911/4921. *Technology*, 2010.

[74] William Putzbach and Niina J. Ronkainen. Immobilization techniques in the fabrication of nanomaterial-based electrochemical biosensors: A review. *Sensors (Switzerland)*, 13(4):4811–4840, 2013.

[75] Su-Il Pyun, Heon-Cheol Shin, Jong-Won Lee, and Joo-Young Go. Electrochemistry of Insertion Materials for Hydrogen and Lithium. 2012.

[76] M. M. Rahman, Muhammad J.A. Shiddiky, Md Aminur Rahman, and Yoon Bo Shim. A lactate biosensor based on lactate dehydrogenase/nictotinamide adenine dinucleotide (oxidized form) immobilized on a conducting polymer/multiwall carbon nanotube composite film. *Analytical Biochemistry*, 384(1):159–165, 2009.

[77] Syed Asad Rahman, Nicholas Furnham, Janet M Thornton, and Sergio Martı. Biophysical Perspective The Classification and Evolution of Enzyme Function. 109(September):1082–1086, 2015.

[78] Kavita Rathee, Vikas Dhull, Rekha Dhull, and Sandeep Singh. Biosensors based on electrochemical lactate detection: A comprehensive review. *Biochemistry and Biophysics Reports*, 5:35–54, 2016.

[79] Claudia L Reardon and Robert M Factor. Sport psychiatry: a systematic review of diagnosis and medical treatment of mental illness in athletes. *Sports medicine (Auckland, N.Z.)*, 40(11):961–80, 2010.

[80] Balancing Redox. Fundamental Photographs. 678:678–705, 1986.

[81] RESUMO. Cyclic Voltammetry. *Cyclic Voltammetry*, pages 1–12, 2008.

[82] Marcelo Ricardo Romero, Facundo Ahumada, Fernando Garay, and Ana M. Baruzzi. Amperometric biosensor for direct blood lactate detection. *Analytical Chemistry*, 82(13):5568–5572, 2010.

[83] Daniel P. Rose, Michael E. Ratterman, Daniel K. Griffin, Linlin Hou, Nancy Kelley-Loughnane, Rajesh R. Naik, Joshua A. Hagen, Ian Papautsky, and Jason C. Heikenfeld. Adhesive RFID sensor patch for monitoring of sweat electrolytes. *IEEE Transactions on Biomedical Engineering*, 62(6):1457–1465, 2015.

[84] D. A. Sakharov, M. U. Shkurnikov, M. Yu Vagin, E. I. Yashina, A. A. Karyakin, and A. G. Tonevitsky. Relationship between lactate concentrations in active muscle sweat and whole blood. *Bulletin of Experimental Biology and Medicine*, 150(1):83–85, 2010.

[85] Gabriella Sanzo, Irene Taurino, Giovanni De Micheli, Sandro Carrara, Gabriele Favero, and Franco Mazzei. Highly sensitive electrodic materials based on Pt nanoflowers grown on Pt nanospheres for biosensor development. *IEEE-NANO 2015 - 15th International Conference on Nanotechnology*, pages 1501–1504, 2015.

[86] Seyedeh Sara. Integrated Electronics to Control and Readout Electrochemical Biosensors for Implantable Applications. 6600, 2015.

[87] Benjamin Schazmann, Deirdre Morris, Conor Slater, Stephen Beirne, Cormac Fay, and Dermot Diamond. A wearable electrochemical sensor for the real-time measurement of sweat sodium concentration. pages 1–22.

[88] Takeshi Shimomura, Touru Sumiya, Masatoshi Ono, Tetsuji Ito, and Taka aki Hanaoka. Amperometric l-lactate biosensor based on screen-printed carbon electrode containing cobalt phthalocyanine, coated with lactate oxidase-mesoporous silica conjugate layer. *Analytica Chimica Acta*, 714:114–120, 2012.

[89] Takeshi Shimomura, Touru Sumiya, Masatoshi Ono, and Tetsuji Itoh. An electrochemical biosensor for the determination of lactic acid in expiration. 6:46–51, 2012.

[90] Francesca Stradolini. MEAD Course Report P ractical A spects in M ixed -S ignal IC s. (September), 2017.

[91] Francesca Stradolini, Tamador Elboshra, Armando Biscontini, Giovanni De Micheli, and Sandro Carrara. Simultaneous monitoring of anesthetics and therapeutic compounds with a portable multichannel potentiostat. *Proceedings - IEEE International Symposium on Circuits and Systems*, 2016-July:834–837, 2016.

[92] Irene Taurino, Gabriella Sanzò, Riccarda Antiochia, Cristina Tortolini, Franco Mazzei, Gabriele Favero, Giovanni De Micheli, and Sandro Carrara. Recent advances in Third Generation Biosensors based on Au and Pt Nanostructured Electrodes. *TrAC - Trends in Analytical Chemistry*, 79:151–159, 2016.

[93] Irene Taurino, Gabriella Sanzó, Franco Mazzei, Gabriele Favero, Giovanni De Micheli, and Sandro Carrara. Fast synthesis of platinum nanopetals and nanospheres for highly-sensitive non-enzymatic detection of glucose and selective sensing of ions. *Scientific Reports*, 5(June):1–10, 2015.

[94] J.D.R. Thomas. *The principles of ion-selective electrodes and of membrane transport*, volume 1. 1982.

[95] E C S Transactions and The Electrochemical Society. Point-of-Care Diagnostics with Inkjet-Printed Microchips A. Lesch. 77(7):73–81, 2017.

[96] Beni Valerio. Biosensor : surface functionalisation Integrating the biorecognition elements. *Lecture Note*, 4613286921, 2014.

[97] Rafael Vargas-Bernal, Esmeralda Rodrguez-Miranda, and Gabriel Herrera-Prez. Evolution and Expectations of Enzymatic Biosensors for Pesticides. *Pesticides - Advances in Chemical and Botanical Pesticides*, (June), 2012.

[98] Joseph Wang. Amperometric biosensors for clinical and therapeutic drug monitoring : a review. 19:47–53, 1999.

[99] Wei Song Wang, Hong Yi Huang, Shu Chun Chen, Kuo Chuan Ho, Chia Yu Lin, Tse Chuan Chou, Chih Hsien Hu, Wen Fong Wang, Cheng Feng Wu, and Ching Hsing Luo. Real-time telemetry system for amperometric and potentiometric electrochemical sensors. *Sensors*, 11(9):8593–8610, 2011.

[100] Xuewen Wang, Zheng Liu, and Ting Zhang. Flexible Sensing Electronics for Wearable/Attachable Health Monitoring. *Small*, 13(25):1–19, 2017.

[101] Rachel White, Daniel Yaeger, and Stasinos Stavrianeas. Determination of Blood Lactate Concentration: Reliability and Validity of Lactate Oxidase-Based Method. *Department of Exercise Science, Willamette University, Salem, OR, USA*, 2(2):83–93, 2009.

[102] Fangqiong Wu, Yuming Huang, and Chengzhi Huang. Chemiluminescence biosensor system for lactic acid using natural animal tissue as recognition element. 21:518–522, 2005.

[103] Eugenia I. Yashina, Anastasiya V. Borisova, Elena E. Karyakina, Olga I. Shchegolikhina, Mikhail Yu Vagin, Dmitry A. Sakharov, Alexandr G. Tonevitsky, and Arkady A. Karyakin. Sol-Gel immobilization of lactate oxidase from organic solvent: Toward the advanced lactate biosensor. *Analytical Chemistry*, 82(5):1601–1604, 2010.

[104] M K Zamanova, V N Glotova, T N Izhenbina, D S Krutas, and V T Novikov. Simultaneous HPLC-UV determination of lactic acid , glycolic acid , glycolide , lactide and ethyl acetate in monomers for producing biodegradable polymers. *Procedia Chemistry*, 10:244–251, 2014.

[105] Jichun Zhang, Nicholas Trombly, and Andrew Mason. A Low Noise Readout Circuit for Integrated Electrochemical Biosensor Arrays. pages 36–39, 2004.

[106] Louis Zumbahlen. Staying Well Grounded. *Analog Dialogue*, 46:1–9, 2012.

Appendix A

Some configurations of Operational Amplifiers

A.0.1 Differential Amplifier

A differential amplifier is an electronic device with two input signals (V_+ and V_-). The output (V_o) is the difference of the two inputs (named inverting (-) and non inverting (+) inputs) incresed of an open loop gain (G_o):

$$V_o = G_o \cdot (V_+ - V_-) \tag{A.1}$$

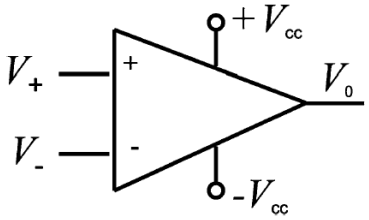

Figure A.1: Differential Amplifier

A.0.2 Operational Amplifier

Operational Amplifier (op-amp) is one type of Differential Amplifier and represents the basic building block of Analog Circuits. It is characterized by ideal characteristics of infinite gain, very high and very low input and output resistance, respectively. The needed of a very high input impedance block the flow current across the op-amp input, and so a zero current is required.

$$G_o \to \infty; \qquad R_i \to \infty; \qquad R_o = 0; \qquad I_{input} = 0. \tag{A.2}$$

A.0.3 Voltage Follower

A voltage follower (Fig. A.2) is an op-amp in which the invertign input is connected to the otuput. The equation A.3 describes this circuit:

$$V_o = V_i \tag{A.3}$$

The voltage follower, also known as Buffer amplifier, does not introduce amplification to the signal, but the output is the input itself. Thanks to a very high input impedance, this configuration is suitable for applications which require not absorb input current.

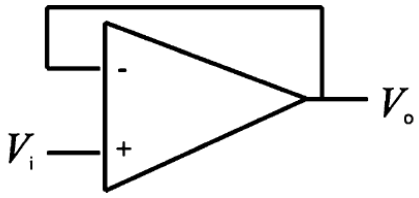

Figure A.2: Voltage Follower

A.0.4 Inverting Amplifier

An Inverting Amplifier (Fig. A.3.**a**) is a type of Differential Amplifier in which the non-inverting input is grounded, while an input voltage (V_i) is applied to the non-inverting input. Besides, a closed loop connects the negative input and the output through two resistors (R_f and R_1).
Remembering that, for an ideal op-amp, $I_{input} = 0$:

$$I_1 = -I_f \qquad and \qquad V_+ = V_- = 0 \tag{A.4}$$

and applying Ohm's law:

$$\frac{V_i}{R_1} = -\frac{V_o}{R_f} \qquad \longrightarrow \qquad V_o = -\frac{R_1}{R_f} \tag{A.5}$$

A.0.5 Non-Inverting Amplifier

On the contrary, a Non-Inverting Amplifier (Fig. A.3.**b**) has an input voltage connected to the positive input (V_i), while the negative one is grounded through a resistor R_1 and connected to the output through the resistor R_f. Applying the same conditions of an ideal op-amp, we have:

$$I_1 = I_f \qquad and \qquad V_+ = V_- = V_i \tag{A.6}$$

and applying Ohm's law:

$$\frac{V_i}{R_1} = \frac{V_o - V_i}{R_f} \qquad \longrightarrow \qquad V_o = \frac{R_1 + R_f}{R_1} \tag{A.7}$$

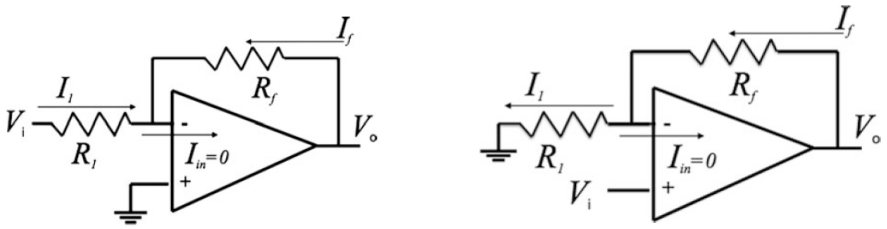

(a) (b)

Figure A.3: **(a)** Inverting Amplifier and **(b)** Non-Inverting Amplifier

A.0.6 Sallen-Key low pass Filter

In general, a Low Pass Filter is a filter used when the considered signal has most of the information in the low frequencies: indeed this filter passes signals with a frequency lower than a certain cutoff frequency and attenuates signals with frequencies higher than the cutoff frequency. Depending on the frequency to cut, different models of LPF can be realized and used: a Sallen-Key low-pass filter belongs to the famlily of Sallen-Key topology and it is a second order active filter with the schematic shown in Figure A.4. In particular, an active filter is a type of electronic filter which uses active componetns, such as amplifier. Instead, a second order filter attenuates the high frequency more steeply than the attenuation due to the first order one.

Applying Kirchhoff's Current Law (KVL) to the circuit, we have:

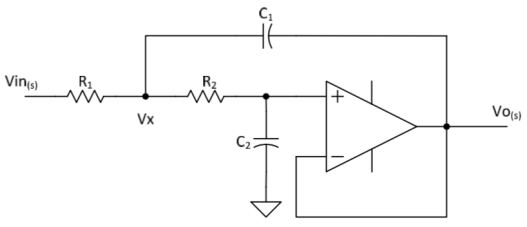

Figure A.4: Sallen-Key unit gain low-pass filter circuit (Reprinted by [48]).

- $\frac{V_{in}-V_x}{R_1} = \frac{V_x-V_{out}}{R_2} + (V_x - V_{out}) \cdot sC_1$
- $\frac{V_x-V_{out}}{R_2} = V_{out} \cdot sC_2$

From these calculations, the tranfer function of the Sallen-Key 2^th order filter is obtained:

$$H(s) = \frac{1}{1 + (R_1 + R_2)C_1 s + R_1 R_2 C_1 C_2 s^2} \tag{A.8}$$